

DISSERTATION

A CONTRIBUTION TO
SELF-EXCITED OSCILLATIONS:
SMOOTH AND NON-SMOOTH
BIFURCATION ANALYSIS IN APPLIED
MECHANICAL SYSTEMS

durchgeführt zum Zwecke der Erlangung des akademischen Grades eines
Doktors der technischen Wissenschaften unter der Leitung von

Prof. Dr. Hans TROGER
E325/A2, Institut für Mechanik und Mechatronik
Abteilung für angewandte Mechanik

eingereicht an der Technischen Universität Wien

Fakultät für Maschinenwesen und Betriebswissenschaften

VON

Andreas TEUFEL
Matrikelnummer 9530299
Hauslabgasse 14/23
1050 Wien

Wien, im Oktober 2007

Andreas Teufel

Zusammenfassung

Der Mechanismus der Selbsterregung ist von großer praktischer Relevanz in technischen schwingungsfähigen Systemen. Als Beispiele, die als übergeordnete Motivation für die vorliegende Arbeit angesehen werden können, seien die Schwingungen von Hochspannungsleitungen in einem Luftstrom oder das Quietschen von Bremsen erwähnt. In mathematisch glatten Systemen wird das Auftreten selbsterregter Schwingungen durch eine Hopf-Verzweigung beschrieben, was am Beispiel synchronisierter Lösungen in mechanischen Systemen gezeigt wird. In zufolge von Reibungseffekten nicht-glatten Systemen liefern neue theoretische Resultate aus dem Bereich der nicht-glatten Verzweigungstheorie wertvolle Impulse zur Beschreibung selbsterregter Reibungsschwingungen.

Synchronisation ist ein Phänomen, das in den unterschiedlichsten Wissenschaftsdisziplinen beobachtbar ist, sobald schwingungsfähige Systeme miteinander interagieren. Das Charakteristikum hierbei ist, dass die Oszillatoren im Verbund eine (gegebenenfalls phasenverschobene) Schwingung mit einer gemeinsamen ("synchronen") Frequenz ausführen, die von den Eigenfrequenzen der isolierten Einzelsysteme abweicht. Als mechanisches Beispiel hierfür werden zwei gekoppelte geringfügig unterschiedlich dimensionierte Pendel betrachtet, die einem Windstrom ausgesetzt sind. Durch die durch die Anströmung bewirkte Energiezufuhr wird das System selbsterregt und durch eine elastische Kopplung zwischen den beiden Pendeln auch synchronisationsfähig. Mathematisch manifestiert sich eine synchronisierte Bewegung im Auftreten eines Grenzyklus im gekoppelten Bewegungsgleichungssystem, welcher im betrachteten Beispiel durch eine Hopf-Verzweigung der Kodimension 2 bei einer kritischen Anströmgeschwindigkeit entsteht. Die Untersuchung dieser Verzweigung hängt wesentlich von den Resonanzeigenschaften der Systemeigenwerte ab:

I. Der Fall nicht resonanter Eigenwerte tritt für starke Koppelung bzw. eine große Eigenfrequenzabweichung der beiden Schwinger ein. Stabilitätsgrenzen für synchronisierte Lösungen können aus den bekannten Methoden der Normalformtheorie einer Hopf-Verzweigung mit zwei unterschiedlichen Paaren rein imaginärer Eigenwerte ermittelt werden. Während für eine starke Kopplung der Pendel erwartungsgemäß stets stabile synchronisierte Lösungen ohne Phasenverschiebung auftreten, kann im Fall der großen Frequenzabweichung eine Schranke für dieselbe in Abhängigkeit der Koppelungsstärke angegeben werden, sodass sich immer synchronisierte Schwingungen einstellen.

II. Im Fall resonanter Eigenwerte, der mechanisch durch eine kleine Abweichung der Eigenfrequenzen der Pendel sowie eine schwache Koppelung hervorgerufen wird, führt hier die Mittelungsmethode zu Amplituden- und Phasengleichungen für die Evolution des Grenzyklus. Synchronisierte Lösungen ergeben sich als stationäre Lösungen der über eine Pendelperiode gemittelten Gleichungen. Durch eine geschickte Variablensubstitution gelingt es eine analytische Stabilitätsuntersuchung der synchronisierten Lösungen durchzuführen und im speziellen Formeln für die Amplituden bzw. die Frequenz des synchronisierten Grenzyklus anzugeben. Insbesondere erlaubt eine einfache graphische Interpretation der synchronisierten Lösungen das Auffinden von Stabilitätsgrenzen in der

von der Frequenzabweichung und der Koppelungsstärke aufgespannten Parameterebene.

Der zweite Themenkomplex, dem sich diese Arbeit zuwenden soll, widmet sich der Entstehung selbsterregter Schwingungen durch Reibung. Da durch die physikalische Natur der Reibung zwangsläufig Unstetigkeiten in den Beschleunigungen auftreten, muss ein besonderes Augenmerk auf die noch im Entwicklungsstadium begriffene Verzweigungstheorie in nicht-glaten Systemen gelegt werden, die hier auf konkrete mechanische Beispiele angewandt werden soll. Reibungsschwinger zählen zu den sogenannten FILIPPOV-Systemen, wo Lösungen an Unstetigkeiten im Phasenraum entlanglaufen können. Für ebene nicht-glatte Systeme des FILIPPOV-Typs sind bereits alle Kodimension-1-Verzweigungen nach KUZNETSOV klassifiziert. Für mechanische Systeme mit einem Freiheitsgrad kann jedoch ein Großteil der möglichen nicht-glaten Verzweigungsarten bereits vorweg ausgeschlossen werden. Ein einfacher Einmassenschwinger auf einem rauhen laufenden Band soll als einführendes Beispiel zur Erklärung nicht-glatter Verzweigungsphänomene dienen. Für eine allgemeine nicht-lineare Abhängigkeit des Reibungskoeffizienten von der Relativgeschwindigkeit kann bereits für den einfachen Reibungsschwinger die Existenz nahezu aller wichtiger nicht-glatter Verzweigungen numerisch nachgewiesen werden, die in mechanischen Systemen mit einem Freiheitsgrad von Relevanz sein können. Mit einer numerischen Fortsetzungsmethode können die Orte der Verzweigungen im Parameterraum verfolgt werden, wobei geometrische Kenngrößen der Reibungskennlinie sowie die Bandgeschwindigkeit als Parameter dienen. Speziell ist hier neben den typischen "stick-slip"-Schwingungen auch das Auftreten von überschwingenden Lösungen zu beobachten, d. h. die Masse bewegt sich in der Bandlaufrichtung kurzzeitig schneller als das Band.

Motiviert durch das Auftreten von Quietschgeräuschen beim Bremsvorgang von Zügen wird in der Folge ein bremsenähnliches kontinuierliches Modell betrachtet, bestehend aus einer auf eine starre Welle aufgeschrumpften elastischen Nabe, wobei die Welle in der Nabe mit konstanter Winkelgeschwindigkeit rotiert. Reduziert man die Bewegungsgleichungen der Nabe in radialer Richtung durch einen eingliedrigen GALERKIN-Ansatz, erhält man ähnliche Gleichungen wie für den einfachen Reibungsschwinger, die nun eine fortlaufende nicht-glatte elastische Welle an der Grenzfläche zwischen der festen Welle und der Nabe beschreiben, wobei durch die hinzutretende Veränderung des Normaldrucks zwischen Welle und Nabe auch Ablöseeffekte auftreten können. Das Auftreten unterschiedlicher Kontaktzonen wie Haften, Gleiten oder Ablösen sind anschauliche Beispiele für Verzweigungen des nicht-glaten Systems, die es gilt numerisch nachzuweisen. Zum Auffinden der Verzweigungskurven im Parameterraum dienen vorrangig der statische Reibungskoeffizient, die Winkelgeschwindigkeit der Welle und das Verhältnis der Radien als Fortsetzungsparameter, während wiederum ein nichtlineares Gesetz für die Abhängigkeit des Reibungskoeffizienten von der lokalen Relativgeschwindigkeit am Wellen-Nabenkontakt angenommen wird. Es wird gezeigt, dass im positiven Umlaufsinn fortlaufende Wellen nur für kleine Nabendurchmesser existieren. Für rückwärtslaufende Wellen ergibt sich ein reiches Verzweigungsverhalten vom Auftreten von "stick-slip"-Wellen, über die Ausbildung von überschwingenden Bereichen (d. h. lokal übersteigt die Tangentialgeschwindigkeit der Nabe die Umfangsgeschwindigkeit der Welle) bis hin zur Entstehung von mehreren Separationszonen. Die erhaltenen Resultate rechtfertigen den Einsatz der nicht-glaten Verzweigungstheorie zum Auffinden der Parameterbereiche qualitativ unterschiedlicher Lösungstypen, die bei einer konventionellen Analyse durch eine Glättung der Unstetigkeiten nicht unterscheidbar wären.

Abstract

The mechanism of self-excitation is of great practical relevance in oscillating technical systems. Oscillating power transmission lines in a wind flow or the squealing noises of brakes serve as examples which may be regarded as a superior motivation for the present thesis. In mathematically smooth systems the onset of self-excited oscillations is described by a Hopf-bifurcation, which will exemplarily be demonstrated for synchronized solutions of a mechanical system. In systems which are non-smooth due to friction effects new theoretical results from non-smooth bifurcation analysis will prove useful for the description of self-excited friction oscillators.

Synchronization is a phenomenon which can be found in many branches of natural sciences, engineering and social life as soon as oscillating systems are interacting. The coupled system may oscillate with a common (“synchronous”) frequency which is different from the eigenfrequencies of the isolated oscillators. Two coupled slightly different pendula which are exposed to a fluid flow shall be considered as a mechanical example. The energy supply due to the fluid flow provides a mechanism of self-excitation and the elastic coupling enables the pendula to synchronize. Mathematically, a synchronized motion manifests itself in the appearance of a limit cycle in the coupled system of the equations of motion. In the considered example, the limit cycle appears by means of a Hopf-bifurcation of codimension 2 at a critical flow velocity. The analysis of the Hopf-bifurcation depends on the resonance properties of the eigenvalues of the system: the eigenvalues are found to be non-resonant for a large frequency detuning and/or a large coupling strength. The stability boundaries of synchronized solutions can be derived from prevailing methods of normal form theory. For a strong coupling the pendula will always perform synchronized motions. If the frequency detuning is assumed to be large it has to be limited by bounds depending on the coupling strength in order to synchronize all solutions.

Resonant eigenvalues are mechanically achieved by a small frequency detuning and a weak coupling of the pendula. In this case the method of averaging is applied in order to obtain equations for the amplitudes and the phase governing the evolution of the limit cycle. Synchronized solutions are found as the stationary solutions of the averaged system. With the aid of a cunning substitution of variables the stability investigations of the synchronized solutions can be performed analytically. In particular, formulas are given for the amplitudes and the frequency of the synchronized limit cycle. Moreover, a simple graphical interpretation of the synchronized solutions facilitates the calculation of stability boundaries in the parameter space spanned by the frequency detuning and the coupling strength.

The second topic, this thesis is devoted to, is concerned with the occurrence of self-excited oscillations due to friction. Because of the physical nature of friction, necessarily a discontinuity is introduced to the system. Thus, special emphasis must be placed upon non-smooth bifurcation theory, which shall be applied to concrete mechanical problems, here. Friction oscillators belong to so-called FILIPPOV-Systems, which are

characterized by the fact that solutions can stay on a discontinuity in the phase space for at least a finite time. All possible codimension-1 bifurcations in planar FILIPPOV-Systems have been classified by KUZNETSOV. In mechanical systems with one degree-of-freedom, however, various types of non-smooth bifurcations may be ruled out from the outset. A simple oscillator consisting of a spring-mass system on a driven belt serves as an example to explain the effect of non-smooth bifurcations. If a general non-linear dependence of the friction coefficient on the relative velocity is assumed, even this simple friction oscillator reveals all major types of non-smooth bifurcations that are expected to appear in general in mechanical systems with one degree-of-freedom. By means of a numerical continuation method these bifurcations are continued in a parameter space, where the geometric quantities of the friction characteristic as well as the band speed serve as continuation parameters. Besides the pertinent “stick-slip” oscillations we also concentrate on finding “overshooting”-solutions where the mass moves in the same direction as the belt but is temporarily faster.

Originating from the problem of squealing noises in breaking trains we consider in the following a brake-like continuous model which consists of a rotating rigid shaft fitted into an elastic bush with a diameter mismatch. The equations of motion of the bush are reduced by a one-mode GALERKIN expansion in the radial direction and thus describe the evolution of non-smooth elastic travelling waves on the shaft-bush interface. The reduced travelling wave equations closely resemble the simple friction oscillator, yet the variation of the normal pressure between the shaft and the bush may additionally cause separation effects. The appearance of different contact regimes, such as sticking, slipping or separating provides a vivid example of non-smooth bifurcations in the considered system, which are calculated numerically. In order to detect the bifurcation curves in the parameter space we predominantly use the static coefficient of friction, the rotation velocity of the shaft and the radial ratio of the bush as continuation parameters. Again, a non-linear friction law depending on the local relative velocity is assumed to hold at the shaft-bush interface. It is shown that waves rotating in the same sense as the shaft only exist for small diameters of the bush. For backward waves rotating in the opposite direction a rich bifurcation scenario is found, yielding pure slip, stick-slip, stick-slip-separation and slip-separation waves. In slip regimes we additionally encounter the emergence of overshooting motions where the tangential velocity of the bush locally exceeds the velocity of the shaft. The obtained results justify the application of non-smooth bifurcation theory in order to find parameter domains of qualitatively different types of solutions which would have been undetected if a conventional strategy was pursued where the discontinuities are avoided using smoothing functions.

Vorwort

Fünf Jahre Arbeit liegen nun hinter mir, in Laufe derer diese Dissertation mit allen Höhen und Tiefen, wie sie in fünf Jahren vorkommen müssen, entstanden ist. Ich war anfangs auf der Suche nach dem Chaos, da bot die offene Stelle am Institut für Mechanik an der TU-Wien eine ideale Gelegenheit. Hin zur Synchronisation von chaotischen Systemen sollte die Richtung zunächst weisen. Das einführende Beispiel geriet aber etwas ausführlicher und schließlich wollte es der Zufall, dass sich durch eine Kooperation mit der französischen Ecole Polytechnique und Prof. Quoc-Son Nguyen ein Umschwenken auf das Gebiet der Reibungsschwingungen und der quietschenden Bremsen anbot. Die Verlockung der Anwendungsorientierung hat also gesiegt. Daher rührt auch die etwas inhomogene Zweiteilung dieser Arbeit, die der Leser unschwer bemerken wird. Vom Chaos ist – abgesehen von meinem Schreibtisch – nicht viel übriggeblieben, dafür ein Eintauchen in das faszinierende Gebiet der Unstetigkeiten wo es durchaus – meiner Meinung nach – lohnen würde, nun aufbauend auf den ersten Resultaten weiterzuarbeiten. Es ist doch wirklich erstaunlich, dass im Zeitalter von Gen-, Nano- und sonstwelchen Technologien immer noch niemand wirklich von Grund auf versteht, warum eine Bremse quietscht, und wie dies zu vermeiden wäre!

An erster Stelle mitverantwortlich für das Zustandekommen dieser Arbeit ist natürlich mein Betreuer, Prof. Hans Troger. Ich bedanke mich bei ihm für all die Freiheiten, die er mir eingeräumt hat, um mein Zweitstudium abzuschließen. Durch seine unbürokratische Denkweise konnte in kleineren Krisen immer wieder eine Lösung gefunden werden. Dem genialen Kopf unseres Institutes, Alois Steindl, sei hier ebenso herzlich gedankt: ohne seine vielen wertvollen mathematischen und numerischen Anregungen würde es so manches Ergebnis dieser Arbeit nicht geben. Herrn Prof. Helmut Springer danke ich für die rasche und unkomplizierte Übernahme des Koreferats. Meinen fluktuierenden Doktoranden-Kolleginnen und -kollegen, Helga Allmer, Bernhard Barkow, Hans Renzeder, Michael Schwarzbart und Amin Chabchoub sage ich danke für die Kaffeerunden, die Mittagessen, die hitzigen Debatten und das eine oder andere Bier auf somancher Tagungsreise. Einer lieben Freundin verdanke ich den letzten entscheidenden Energiestoß, der zum Abschluss dieser Arbeit geführt hat. Und zuallerletzt danke ich meinen Eltern, die meine Vorhaben immer bedingungslos unterstützt haben, mir in harten Zeiten stets ein offenes Ohr und in der ungeplanten Nachspielzeit auch die nötige finanzielle Absicherung geboten haben.

Contents

1	Introduction	9
1.1	Motivation	9
1.2	Selected basics of nonlinear dynamics	10
1.2.1	Dynamical systems	10
1.2.2	Stability, asymptotic stability, superstability	10
1.2.3	Structural stability, topological equivalence and bifurcations	10
1.2.4	Center manifold and Normal Forms	11
1.2.5	The method of averaging	12
1.2.6	Self-excited oscillations	15
2	Synchronization phenomena	16
2.1	Introduction to synchronization phenomena in mechanical systems	16
2.1.1	Synchronized solutions of dynamical systems	17
2.2	Mechanical system and equations of motion	18
2.3	Bifurcation analysis	20
2.3.1	Normal form analysis for a large frequency detuning	20
2.3.2	Small frequency detuning and strong coupling	25
2.3.3	Hopf-bifurcation at 1:1 resonance – small frequency detuning and weak coupling	26
2.4	Discussion and comparison of the results	34
2.5	Conclusion	38
3	Non-smooth bifurcations of mechanical systems with 1-d.o.f involving friction	39
3.1	Introduction to non-smooth systems	40
3.1.1	Filippov Systems	40
3.1.2	Bifurcations in planar Filippov systems	41
3.1.3	Friction oscillators	50
3.1.4	Friction Models	52
3.2	Non-smooth bifurcations of the simple friction oscillator	55
3.2.1	Linear Stability analysis	56
3.2.2	The simple friction oscillator in the context of Filippov systems	57
3.2.3	Numerical Results and discussion	62
4	Non-smooth bifurcations of travelling waves	71
4.1	Motivation	71
4.2	Mechanical model of a brake-like system	71
4.3	Stability of the stationary solution	73
4.4	Travelling wave reduction	74

Contents

4.5	Non-smooth solutions and bifurcations of travelling waves	76
4.5.1	Equilibria and tangent points	76
4.5.2	Numerical Procedure	79
4.5.3	The case $c < 0$	81
4.5.4	The case $c > 0$	95
4.6	Numerical Results	99
4.6.1	Backward waves ($c < 0$)	99
4.6.2	Forward waves ($c > 0$)	101
4.6.3	A note on stability investigations	103
4.7	Conclusions and Outlook	111

1 Introduction

‘Wissenschaft lehrt nicht zu antworten, sie lehrt zu fragen.’
Erwin CHARGAFF, 1905-2002, Austrian/American Biochemist.

1.1 Motivation

The study of self-excited oscillations in mechanical engineering in general and mechanics in particular is steeped in tradition. Yet, it is a field of research that never ceases from being up to date. Self-excited oscillations may be highly desirable such as in everyday applications like pendulum clocks or violin strings. On the other hand the onset of oscillations due to an instability in technical applications may cause severe damage, material fatigue or is simply physiologically annoying. Oscillating electric power lines in a wind flow or squealing brakes may serve as examples. The latter examples can already be regarded as a superior motivation for the present thesis: the major problems under consideration will be self-excited oscillations due to a fluid flow in Chapter 2 and due to friction in Chapters 3 and 4.

The vast development of numerical methods and computing power has very successfully boosted the investigations of complex systems in engineering sciences. Finite element tools are nowadays a standard application in industry and serve very well for numerical experiments. However, because of the complexity of the systems we sometimes lose sight of the basic mechanisms that are responsible for a certain system behavior. One of the basic concerns of this work, thus, shall be rather to scrutinize a problem profoundly and accept the drawback of seemingly too simple models as a necessity. Bifurcation theory shall provide the major mathematical tool and a special emphasis will be placed upon the application of recent advances in the theory of non-smooth bifurcations to applied mechanical problems. Though often neglected, bifurcation theory proves to be very valuable for engineers in applied sciences since it allows to answer fundamental questions like: which problem parameters produce which type of system behavior. It is felt that only the synthesis of the “bottom-up” strategy followed here with the fashionable “top-down” approach by direct numerical simulation can yield results that are valuable, both, for the development of more sophisticated theoretical concepts on the one hand as well as innovative engineering solutions on the other.

All phenomena studied throughout this thesis are due to nonlinearities in the respective mechanical models. It has therefore to be opened with a short summary of important notions of the theory of nonlinear dynamical systems. The examples treated in the remainder are chosen such that the mechanical setting is conceptually simple. The study of flow excited oscillators will lead to the investigation of coupled Van-der-Pol equations, the results thus might be carried over to multiple technical applications exceeding mechanics. The examples of friction oscillators can be reproduced by anybody opening

a bottle of wine and turning the cork within the bottleneck. Despite the simplicity of the model the problem will turn out to be mathematically and mechanically so intricate that a complete understanding of the underlying mechanisms seems out of reach for the time being. In view of the preceding quotation, however, we will obtain a glimpse into a new non-smooth world that offers still vast lands to explore for future pioneers.

1.2 Selected basics of nonlinear dynamics

The available literature on nonlinear dynamics is abundant and it is not the scope of this work to recompile a textbook on this subject. However, the need is felt to prepend here some basic terminologies and definitions with an emphasis on an application oriented viewpoint. We take the liberty of picking out single issues that will be of crucial importance in the course of this thesis. For a complete treatise it is referred to GUCKENHEIMER & HOLMES [1983], ARNOLD [1983], TROGER & STEINDL [1991], KUZNETSOV [1995], SHILNIKOV ET AL. [1998] and SHILNIKOV ET AL. [2001].

1.2.1 Dynamical systems

It suffices here to define a dynamical system as the system of ordinary autonomous differential equations

$$\frac{d\mathbf{x}}{dt} := \dot{\mathbf{x}} = \mathbf{f}(\mathbf{x}, \boldsymbol{\mu}) \quad (1.1)$$

where $\mathbf{x} = \mathbf{x}(t) \in \mathbb{R}^n$ is a solution of (1.1), \mathbf{f} is a vector valued function, $\mathbf{f} : \mathbb{R}^n \rightarrow \mathbb{R}^n$ defining a vector field on \mathbb{R}^n depending on a parameter vector $\boldsymbol{\mu}$; t is an independent variable, usually identified with time. In the sequel we cannot in general require \mathbf{f} to be continuous and smooth. While this will hold true for Chapter 2, the essential results of Chapters 3 and 4 are due to a discontinuity of \mathbf{f} .

1.2.2 Stability, asymptotic stability, superstability

Of course we use the common concept that a solution $\mathbf{x}_0(t)$ of (1.1) is said to be *stable* if a trajectory starting in a neighborhood V of \mathbf{x}_0 it remains in a neighborhood $V_1 \subset V$ for all times; $\mathbf{x}_0(t)$ is *asymptotically stable* if \mathbf{x}_0 is approached asymptotically as $t \rightarrow \infty$. Moreover we introduce the term *superstability* (cf. e. g. KUZNETSOV ET AL. [2003]) if a trajectory starting near \mathbf{x}_0 coincides “exactly” with \mathbf{x}_0 after a finite time. This will frequently appear in the non-smooth examples discussed in Chapters 3 and 4. We note already here that the Poincare map of a superstable periodic trajectory always has a zero eigenvalue.

1.2.3 Structural stability, topological equivalence and bifurcations

The vector field \mathbf{f} in (1.1) is *structurally stable* if all sufficiently small perturbations \mathbf{f}_ϵ of \mathbf{f} are *topologically equivalent* to \mathbf{f} , i. e. there exist homeomorphisms that take orbits of \mathbf{f}_ϵ onto orbits of \mathbf{f} . Usually a *bifurcation* occurs by definition if at a critical parameter value $\boldsymbol{\mu} = \boldsymbol{\mu}^*$ the vector field $\mathbf{f}(\mathbf{x}, \boldsymbol{\mu}^*)$ is not structurally stable. In fact we use this notion of a bifurcation throughout this work. However, it is remarked that in particular

for the non-smooth examples this definition will contradict the intuition that at a bifurcation a “new” solution branches off. LEINE [2000] recommends to use a definition of a bifurcation proposed by SEYDEL [1994], namely: “a bifurcation point is a solution where the number of fixed points or (quasi-)periodic solutions changes when μ passes μ^* .” It is already anticipated here that almost all non-smooth bifurcations that will be discussed in Chapters 3 and 4 would not comply with this definition. Indeed, in the examples that will be considered solutions in a neighborhood of a bifurcation value will be topologically non equivalent. Though, no additional solution will branch off at the bifurcation value. LEINE [2000] suggested to use the term *topological transition* instead to describe this behavior. Again, we emphasize that we stick to the classical definition. Besides, it is also employed by KUZNETSOV ET AL. [2003] whereupon the non-smooth analysis presented here is rooted.

The loci of all bifurcation values μ^* associated with a certain type of bifurcation in the parameter space is called a *bifurcation set*. The visualization of the bifurcation sets in the parameter space will be called a *stratification of the parameter space*. A bifurcation may be classified by the codimension of its bifurcation set in the parameter space.

A bifurcation is *local* if it involves only a sufficiently small neighborhood of a given point in the phase space of (1.1). For smooth systems local bifurcations typically occur for equilibria of (1.1) if the real part of at least one eigenvalue of the Jacobian of (1.1) becomes zero. For non-smooth systems (Chapter 3) there are multiple mechanisms of local bifurcations, such as e. g. the collision of an equilibrium with a discontinuity. A bifurcation is called *global* if the topological change involves the whole phase space. Bifurcations of periodic orbits are generally global but may be described as local bifurcations in a reduced system, such as a Poincare map or a normal form on a center manifold.

1.2.4 Center manifold and Normal Forms

The center manifold theorem proves the existence of an invariant manifold in a neighborhood of an equilibrium of (1.1), which is tangent to the critical subspace of the Jacobian $\partial \mathbf{f} / \partial \mathbf{x}$, spanned by the eigenvectors belonging to the eigenvalues on the imaginary axis. The dimension of the center manifold thus is equal to the number of eigenvalues with zero real part. Assuming that the remaining eigenvalues all have a negative real part every trajectory will be attracted to this center manifold. Thus, the dynamics near the equilibrium and especially the stability behavior can be studied from the dynamics on the center manifold which allows to reduce a system of arbitrary dimension to the dimension of the center manifold.

The reduced system in this sense will in general still be nonlinear, so it would be desirable to choose coordinates on the center manifold that at least make the nonlinearities as simple as possible. This is done by a sequence of coordinate transformations which are consolidated in *normal form theory*. The goal is to eliminate as much low powers in the Taylor series expansion of the nonlinearities as possible. This procedure of calculating a reduced normal form will be exemplarily outlined in Section 2.3.1.

1.2.5 The method of averaging

The *method of averaging* provides another widespread and useful tool in the simplified qualitative analysis of nonlinear dynamical systems. Roughly speaking, a system of differential equations is simplified by averaging all occurring quantities over a certain fast varying variable. Although this notion might be conceptually clear, its theoretical foundation is rather sophisticated. In view of further application to the determination of so-called synchronized solutions (see Section 2.1.1) it shall be referred here to KIRCHGRABER & STIEFEL [1978] who embeds the averaging method into the framework of perturbation theory. In the following the basics as far as necessary for the understanding of subsequent applications will be outlined here in slightly more detail.

Let a system of autonomous ordinary differential equations depending on an external small parameter ϵ take the form

$$\dot{\mathbf{x}} = \mathbf{f}_0(\mathbf{x}) + \epsilon \mathbf{f}_1(\mathbf{x}, \epsilon) \quad (1.2)$$

where $\mathbf{x} \in \mathbb{R}^n$ and \mathbf{f}_i ($i = 0, 1$) are vector valued functions $\mathbf{f}_i : \mathbb{R}^n \times \mathbb{R} \rightarrow \mathbb{R}^n$. If the solution of the unperturbed equation

$$\dot{\mathbf{x}}_0 = \mathbf{f}_0(\mathbf{x}_0) \quad (1.3)$$

has either periodic or quasi-periodic solutions, i. e. \mathbf{x}_0 can be written as $\mathbf{x}_0 = \boldsymbol{\varphi}_0(\boldsymbol{\omega}_0 t)$ where $\boldsymbol{\omega}_0$ is some vector, possibly of dimension 1, then a transformation \mathbf{U} , defined by

$$\mathbf{x} = \mathbf{U}(\boldsymbol{\phi}, \boldsymbol{\Omega}, \mathbf{a}) \quad (1.4)$$

may be applied to (1.2), called an *element transformation* of (1.2). \mathbf{U} has to be 2π periodic in $\boldsymbol{\phi}$ and $\boldsymbol{\Omega}$ and applied to (1.2) yields

$$\begin{aligned} \dot{\boldsymbol{\phi}} &= \boldsymbol{\omega}(\mathbf{a}) + \epsilon \mathbf{R}(\boldsymbol{\phi}, \boldsymbol{\Omega}, \mathbf{a}) \\ \dot{\boldsymbol{\Omega}} &= \epsilon \mathbf{S}(\boldsymbol{\phi}, \boldsymbol{\Omega}, \mathbf{a}) \\ \dot{\mathbf{a}} &= \epsilon \mathbf{T}(\boldsymbol{\phi}, \boldsymbol{\Omega}, \mathbf{a}). \end{aligned} \quad (1.5)$$

Herein \mathbf{R} , \mathbf{S} and \mathbf{T} are vector valued functions also 2π -periodic in $\boldsymbol{\phi}$ and $\boldsymbol{\Omega}$, the vector $\boldsymbol{\omega}$ is constant or may depend on \mathbf{a} . $\boldsymbol{\phi}$ is called a *fast angular variable*, $\boldsymbol{\Omega}$ a *slow angular variable*, the components of \mathbf{a} will be called *amplitudes*. For the moment, the dimensions of the vectors $\boldsymbol{\phi}$, $\boldsymbol{\Omega}$ and \mathbf{a} are arbitrary, yet for practical purposes one would strive for a transformed system (1.5) which does not exceed the dimension of the original equation (1.2). It shall be remarked that in many applications (see e. g. KIRCHGRABER & STIEFEL [1978] or Chapter 2) the element transformation \mathbf{U} (1.4) is a formal formulation of performing a variation of the constants of integration that might appear in the solution of the unperturbed problem (1.3).

The system (1.5) now defines a differential equation on an l -torus \mathbb{T}^l where $l = \dim(\boldsymbol{\phi}) + \dim(\boldsymbol{\Omega})$ the phase space of which is $\mathbb{R}^k \times \mathbb{T}^l$ with $k = \dim(\mathbf{a})$ (cf. SHILNIKOV ET AL. [1998], ARNOLD [1983]). Moreover, (1.5) is suitable for an *averaging operation*, which shall be motivated in the sequel. Allowing a more concise presentation, the quantities occurring in (1.5) shall be formally collected in sets,

$$\mathcal{Q} = \{\boldsymbol{\phi}, \boldsymbol{\Omega}, \mathbf{a}\}, \quad \mathcal{N} = \{\boldsymbol{\omega}, \mathbf{0}, \mathbf{0}\} \quad \text{and} \quad \mathcal{R} = \{\mathbf{R}, \mathbf{S}, \mathbf{T}\}. \quad (1.6)$$

1 Introduction

Equations (1.5) again constitute a perturbation problem of the form (1.2) and may in view of (1.6) be put down in writing

$$\dot{\mathbf{y}}_i = \boldsymbol{\nu}_i(\mathbf{a}) + \varepsilon \mathbf{g}_i(\mathcal{Q}) \quad (1.7)$$

where

$$\mathbf{y}_i \in \mathcal{Q}, \quad \boldsymbol{\nu}_i \in \mathcal{N}, \quad \mathbf{g}_i \in \mathcal{R}$$

and the index i addresses the i -th element of the respective set in (1.6). To each element $\mathbf{y}_i \in \mathcal{Q}$ in (1.7) now a *near identity transformation* is applied, i. e.

$$\mathbf{y}_i = \bar{\mathbf{y}}_i + \varepsilon \mathbf{h}_i(\bar{\mathcal{Q}}), \quad (1.8)$$

where the generating functions \mathbf{h}_i inherit the periodicity properties of the of the functions contained in \mathcal{R} . Substitution of (1.8) into (1.5) yields after some straightforward manipulations equations for the new variables $\bar{\mathbf{y}}_i \in \bar{\mathcal{Q}} = \{\bar{\boldsymbol{\phi}}, \bar{\boldsymbol{\Omega}}, \bar{\mathbf{a}}\}$ of the type

$$\dot{\bar{\mathbf{y}}}_i = \boldsymbol{\nu}_i + \varepsilon \left(\mathbf{g}_i(\bar{\mathcal{Q}}) - \frac{\partial \mathbf{h}_i}{\partial \bar{\boldsymbol{\phi}}} \boldsymbol{\omega} \right) + O(\varepsilon^2). \quad (1.9)$$

The functions \mathbf{h}_i will have to be determined such that equations (1.9) become as simple as possible. It would be desirable that the terms of first order in ε do not depend on $\bar{\boldsymbol{\phi}}$ since then equations (1.5)_{2,3} would by means of (1.8) decouple from the equation for $\bar{\boldsymbol{\phi}}$ (1.5)₁. This requirement may be formulated as a partial differential equation for \mathbf{h}_i ,

$$\mathbf{g}_i(\bar{\mathcal{Q}}) - \frac{\partial \mathbf{h}_i}{\partial \bar{\boldsymbol{\phi}}} \boldsymbol{\omega} = \bar{\mathbf{g}}_i(\bar{\boldsymbol{\Omega}}, \bar{\mathbf{a}}). \quad (1.10)$$

Due to the periodicity of \mathbf{g}_i and \mathbf{h}_i solutions of (1.10) may be sought in terms of Fourier series, viz.

$$\mathbf{g}_i = \sum_{\mathbf{n} \in \mathbb{Z}^d} \mathbf{G}_{i,\mathbf{n}}(\bar{\boldsymbol{\Omega}}, \bar{\mathbf{a}}) e^{i(\mathbf{n} \cdot \bar{\boldsymbol{\phi}})}, \quad \mathbf{h}_i = \sum_{\mathbf{n} \in \mathbb{Z}^d} \mathbf{H}_{i,\mathbf{n}}(\bar{\boldsymbol{\Omega}}, \bar{\mathbf{a}}) e^{i(\mathbf{n} \cdot \bar{\boldsymbol{\phi}})}, \quad (1.11)$$

where the sum is taken over all integer vectors \mathbf{n} of dimension $d = \dim \boldsymbol{\phi}$. KIRCHGRABER & STIEFEL [1978] have proved, albeit in a more general context, that \mathbf{h}_i is a solution of (1.10) that complies with (1.11) if the Fourier coefficients $\mathbf{G}_{i,\mathbf{n}}$ and $\mathbf{H}_{i,\mathbf{n}}$ are related by

$$\mathbf{H}_{i,\mathbf{n}} = -\frac{i\mathbf{G}_{i,\mathbf{n}}}{\mathbf{n} \cdot \boldsymbol{\omega}} \quad \forall \mathbf{n} \in \mathbb{Z}^d \setminus \{\mathbf{0}\}, \quad \mathbf{H}_{i,\mathbf{0}} := \mathbf{0} \quad (1.12)$$

and if we let

$$\bar{\mathbf{g}}_i(\bar{\boldsymbol{\Omega}}, \bar{\mathbf{a}}) = \mathbf{G}_{i,\mathbf{0}}, \quad (1.13)$$

which can easily be verified by substituting (1.11) into (1.10). The latter relation (1.13) describes an averaging operation of the respective quantity $\mathbf{g}_i \in \mathcal{Q}$, which alternatively may be expressed as

$$\bar{\mathbf{g}}_i(\bar{\boldsymbol{\Omega}}, \bar{\mathbf{a}}) = \frac{1}{2\pi^d} \int_0^{2\pi} \cdots \int_0^{2\pi} \mathbf{g}_i(\bar{\boldsymbol{\phi}}, \bar{\boldsymbol{\Omega}}, \bar{\mathbf{a}}) d\bar{\phi}_1 \cdots d\bar{\phi}_d.$$

By virtue of this averaging procedure the original system (1.5) is simplified to

$$\begin{aligned} \dot{\bar{\boldsymbol{\phi}}} &= \boldsymbol{\omega}(\bar{\mathbf{a}}) + \varepsilon \bar{\mathbf{R}}(\bar{\boldsymbol{\Omega}}, \bar{\mathbf{a}}) \\ \dot{\bar{\boldsymbol{\Omega}}} &= \varepsilon \bar{\mathbf{S}}(\bar{\boldsymbol{\Omega}}, \bar{\mathbf{a}}) \\ \dot{\bar{\mathbf{a}}} &= \varepsilon \bar{\mathbf{T}}(\bar{\boldsymbol{\Omega}}, \bar{\mathbf{a}}) \end{aligned} \quad (1.14)$$

and equations (1.14)_{2,3} now may be solved separately from (1.14)₁.

Clearly, it follows from (1.12) that the Fourier coefficients of \mathbf{h}_i may only be calculated if the scalar product $\mathbf{n} \cdot \boldsymbol{\omega} = \sum_j n_j \omega_j$ does not vanish except for $\mathbf{n} = \mathbf{0}$. Vectors $\boldsymbol{\omega}$ satisfying this condition are called *non resonant*. It shall be remarked here that in (1.12) a problem of small denominators occurs if $\boldsymbol{\omega}$ is close to a resonance which leads to a weak convergence of the fourier series (1.11). Since this is most commonly the case in synchronization problems (cf. Chapter 2) where ω_j will correspond to the natural frequencies of a given oscillating system which might be close to each other, albeit not equal. Let us consider an exemplary case where two frequencies ω_j and ω_k , say, are close to each other, thus we may write $\omega_j - \omega_k = O(\varepsilon)$. An integer vector \mathbf{n} satisfying $\mathbf{n} \cdot \boldsymbol{\omega} = O(\varepsilon)$ is $\mathbf{n} = (0, \dots, 0, 1, -1, 0, \dots, 0)$ with 1 and -1 at the j -th and k -th positions, respectively. If so, however, a new quantity $\Omega_l := \phi_j - \phi_k$, $\dot{\Omega}_l = \omega_j - \omega_k + \varepsilon(R_j - R_k) = O(\varepsilon)$ may be defined which is taken as an additional slow angular variable and appended to $\boldsymbol{\Omega}$ while one of the components, ϕ_j or ϕ_k , is dropped from $\boldsymbol{\phi}$.

Returning to the original Equation (1.5) a solution of first order in ε has now been found, namely

$$\begin{aligned}\boldsymbol{\phi}(t) &= \bar{\boldsymbol{\phi}}(t) + \varepsilon \mathbf{h}_1(\bar{\boldsymbol{\phi}}(t), \bar{\boldsymbol{\Omega}}(t), \bar{\mathbf{a}}(t)) , \\ \boldsymbol{\Omega}(t) &= \bar{\boldsymbol{\Omega}}(t) + \varepsilon \mathbf{h}_2(\bar{\boldsymbol{\phi}}(t), \bar{\boldsymbol{\Omega}}(t), \bar{\mathbf{a}}(t)) , \\ \mathbf{a}(t) &= \bar{\mathbf{a}}(t) + \varepsilon \mathbf{h}_3(\bar{\boldsymbol{\phi}}(t), \bar{\boldsymbol{\Omega}}(t), \bar{\mathbf{a}}(t)) .\end{aligned}\tag{1.15}$$

By substituting (1.15) into (1.4) a first order approximation of (1.2) reads

$$\mathbf{x} = \mathbf{U}(\bar{\boldsymbol{\phi}} + \varepsilon \mathbf{h}_1, \bar{\boldsymbol{\Omega}} + \varepsilon \mathbf{h}_2, \bar{\mathbf{a}} + \varepsilon \mathbf{h}_3)\tag{1.16}$$

which can be expanded into a Taylor series of first order in ε as follows,

$$\mathbf{x} = \mathbf{U}(\bar{\boldsymbol{\phi}}, \bar{\boldsymbol{\Omega}}, \bar{\mathbf{a}}) + \varepsilon \left[\frac{\partial \mathbf{U}}{\partial \boldsymbol{\phi}} \mathbf{h}_1 + \frac{\partial \mathbf{U}}{\partial \boldsymbol{\Omega}} \mathbf{h}_2 + \frac{\partial \mathbf{U}}{\partial \mathbf{a}} \mathbf{h}_3 \right] + O(\varepsilon^2).\tag{1.17}$$

In (1.17) the square brackets contain Fourier harmonics of higher order, of which the average over one period in $\bar{\boldsymbol{\phi}}$ is zero. Therefore, we are satisfied with a “mean” solution for \mathbf{x} , given by

$$\mathbf{x}_m = \mathbf{U}(\bar{\boldsymbol{\phi}}, \bar{\boldsymbol{\Omega}}, \bar{\mathbf{a}}).\tag{1.18}$$

Some comments still have to be made regarding the validity of the approximation (1.14) for (1.5) in the time t . In general it can be proven that a solution $\bar{\mathbf{y}}_i(t)$ of the averaged system remains close to a solution $\mathbf{y}_i(t)$ of the original system (i. e. $\bar{\mathbf{y}}_i(t) - \mathbf{y}_i(t) = O(\varepsilon)$) in a time interval proportional to ε^{-1} (ARNOLD [1983], VERHULST [1990], SETHNA [1967]). However, a periodic solution of (1.5) remains in a neighborhood of an equilibrium solution of (1.14) for *all* times $t \geq 0$. If the equilibrium of the averaged equation is asymptotically stable for $t \rightarrow \infty$ then so is the periodic solution in the original system (VERHULST [1990], SANDERS & VERHULST [1985]). The latter statements will justify the application of the averaging method for synchronization problems discussed in Chapter 2.

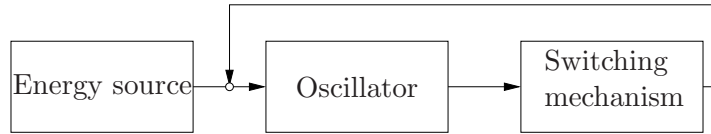


Figure 1.1: Principal scheme of a self excited oscillator.

1.2.6 Self-excited oscillations

The main subject of interest in the present work are self-excited oscillators. A comprehensive introduction can be found in MAGNUS & POPP [2002]. In contrast to free oscillators self oscillating systems are equipped with an energy source. If the energy supply by the energy source is balanced with the amount of dissipation during one oscillation period a periodic motion will set in exhibiting its own specific natural frequency. Thus, a further distinction has to be made from a forced oscillator, where an oscillating system takes over the frequency from the forcing.

We want to employ the notion of MAGNUS & POPP [2002] that a self excited oscillator has three components, namely an energy source an oscillator and a switching mechanism which controls the energy supply from the source to the oscillator (Figure 1.1). In the following we will investigate three different self-sustained oscillators, which are mainly distinguished by the type of the switching mechanisms gathered in Table 1.1.

System	Energy Source	Oscillator	Switching mechanism	Chapter
Flow excited pendula	fluid flow	pendula	nonlinear damping characteristic of the fluid force	2
Simple friction oscillator	driving band	spring-mass	decreasing friction law	3
Shaft-bush problem	rotating shaft	elastic bush	decreasing friction law and vanishing normal pressure	4

Table 1.1: Types of self-excited oscillators that are going to be investigated

2 Synchronization phenomena

The following chapter will be devoted to an investigation of *synchronous* motions (i. e. oscillations with a common frequency) of two weakly or, respectively, strongly coupled mechanical self-sustained oscillators, that would in the absence of an interaction perform self-excited oscillations of different frequencies. After an explanatory introduction to the subject in Section 2.1 the effect of synchronization is defined mathematically in Section 2.1.1. The following sections will consider the case of 1:1 frequency synchronization of two coupled fluid-excited pendula with different natural frequencies, an example which is simple enough such that almost all calculations can be performed analytically and hence a very thorough discussion of the phenomenon can be given. We investigate weak and strong coupling, comparing different approaches in order to find synchronized regimes. Basically, these two cases can be classified as resonant and non-resonant Hopf bifurcations, where in the latter case, which still is rather neglected in the literature on synchronization theory (BLEKHMANN [1988], PIKOVSKY ET AL. [2001]), well-known results of normal form theory will permit a comprehensive description of synchronized motions. The case of weak coupling is studied with the aid of averaging and we finally obtain a descriptive graphical interpretation of synchronized solutions and analytical results for the corresponding amplitudes and frequencies.

2.1 Introduction to synchronization phenomena in mechanical systems

The prevailing historical introduction found in the literature on the phenomenon of synchronization are Huygen's clocks: in 1665 he observed that two pendulum clocks mounted on a beam start to oscillate with a common frequency after some time and the ticks are heard simultaneously. He cunningly perceived that this synchronization is due to the weak coupling because of the elastic beam connecting the clocks. In the 1870s Rayleigh observed the mutual synchronization of slightly detuned organ pipes and discovered the effect of oscillation quenching, when the coupling results in a suppression of the oscillations of interacting systems. In the 20th century, synchronization effects were observed in machine dynamics, if unbalanced rotors are mounted on a common base-plate. More recently self-excited wind-induced vibrations of power transmission lines have been studied by KERN & MAITZ [1998], a system which likewise permits the occurrence of synchronized motions. The spacers within a conductor bundle provide the essential elastic coupling. The big field of chaotic synchronization has to be left out here, since its main application is found in particular in biology, chemistry and electrical engineering. The fascination of the synchronization phenomenon itself shall justify to scrutinize an elementary mechanical example in the following (BLEKHMANN [1988], PIKOVSKY ET AL. [2001]). Mechanically, the striking phenomenon of synchronization may be subsumed in such a way that a (very) weak coupling suffices to synchronize

different oscillators with a *new* synchronous frequency. In this sense synchronized oscillations have to be strictly distinguished from forced oscillations. Mathematically, the effect of synchronization will be explained as the occurrence of a limit cycle in a system of coupled self-sustained oscillators that typically arises by means of a Hopf-bifurcation.

2.1.1 Synchronized solutions of dynamical systems

Although the notion of synchronization as described above seems to be intuitively clear, mathematically exact definitions of synchronization are yet rather scarce, in particular if it comes to the phenomenon of synchronization of non-periodic motions. BLEKHMANN ET AL. [1997] give a most comprehensive definition of synchronized solutions of a set of given dynamical systems which is more vividly explained in BLEKHMANN [2000]. In short, a number of, say, k general *processes*, the states of which are denoted by some time dependent vector $\mathbf{x}_i(t)$, ($i = 1, \dots, k$), are called *synchronized* if for a certain functional $\mathcal{C}[t, \mathbf{x}_i(t)]$, describing some characteristic properties of \mathbf{x}_i at time t , the relation

$$\mathcal{C}[t, \mathbf{x}_1(t + \tau_1)] \equiv \dots \equiv [t, \mathbf{x}_k(t + \tau_k)] \quad (2.1)$$

holds true for some *phase shifts* τ_1, \dots, τ_k . The case where (2.1) is fulfilled for all $t > t_0 \in \mathbb{R}^+$ is referred to as *full synchronization* and *approximate synchronization* occurs if (2.1) just holds approximately. If the limit $t \rightarrow \infty$ yields (2.1) we are facing *asymptotic synchronization*. A mechanical example of the above mentioned process might preferably be a periodic motion of an oscillating body described by some coordinates $\mathbf{x}_i(t)$ and \mathcal{C} can be defined as an integer fraction of the frequency¹ ω_i of the i -th body, viz. $\mathcal{C}[t, \mathbf{x}_i(t)] := \omega_i/n_i$, $n_i \in \mathbb{Z}$. With that (2.1) is identically satisfied if $\omega_i = n_i\omega_s$, which means that the considered bodies are shifted in their phases² but oscillate with frequencies commensurate or possibly equal to a common frequency ω_s , called *synchronous frequency*. This example has accordingly been termed *frequency synchronization* by BLEKHMANN ET AL. [1997] and shall be presented more precisely in the following.

Let a dynamical system be represented by k autonomous ordinary differential equations

$$\dot{x}_i = f_i(x_i), \quad i = 1, \dots, k, \quad (2.2)$$

where $x_i \in \mathbb{R}^1$. Following BLEKHMANN [1988] a solution

$$x_i = m_i\omega_s t + \Phi_i(n_i\omega_s t), \quad m_i, n_i \in \mathbb{Z} \quad (2.3)$$

of (2.2) is called *synchronous* with a common *synchronous frequency* ω_s if each Φ_i is a periodic function in time with period $T_i = 2\pi/n_i\omega$. If one of the integers m_j and n_j is zero for a coordinate x_j the corresponding quantity is called *rotational* ($n_i = 0$) or *oscillating* ($m_i = 0$), respectively. An example for the latter case will be discussed in Section 2.2. Mechanical systems where rotational coordinates are present are discussed e. g. in BLEKHMANN [1988].

¹Of course, a definition of what is meant by a frequency has to be available in the considered example.

²Again, a definition is needed for what is meant by a phase.

In view of the following example a slightly less strict definition of synchronized solutions in connection with the method of averaging, sketched in Section 1.2.5, shall be formulated. Bearing in mind that the fundamental phenomenon discussed here is the appearance of synchronized motions in weakly coupled systems as mentioned before it should be possible to formulate the synchronization problem (2.2) in terms of a perturbation problem, such as (1.2) which can be approximated by means of the averaging method with a system of equations for the phases and amplitudes (1.14). We may look for stationary solutions $\bar{\Omega}_0$ and $\bar{\mathbf{a}}_0$ of (1.14)_{2,3} which satisfy

$$\begin{aligned}\bar{\mathbf{S}}(\bar{\Omega}_0, \bar{\mathbf{a}}_0) &= \mathbf{0}, \\ \bar{\mathbf{T}}(\bar{\Omega}_0, \bar{\mathbf{a}}_0) &= \mathbf{0}.\end{aligned}$$

A solution $\bar{\phi}_0(t)$ on the surface $\bar{\Omega} = \bar{\Omega}_0, \bar{\mathbf{a}} = \bar{\mathbf{a}}_0$ is given by

$$\bar{\phi}_0(t) = [\boldsymbol{\omega}(\bar{\mathbf{a}}_0) + \varepsilon \bar{\mathbf{R}}(\bar{\Omega}_0, \bar{\mathbf{a}}_0)] t,$$

and the original system (2.2) in the form of (1.2) has the mean solution in the sense of Section 1.2.5

$$\mathbf{x}_m(t) = \mathbf{U} [(\boldsymbol{\omega}_0 + \varepsilon \bar{\mathbf{R}}_0) t, \bar{\Omega}_0, \bar{\mathbf{a}}_0] + O(\varepsilon), \quad (2.4)$$

where $\boldsymbol{\omega}_0$ and $\bar{\mathbf{R}}_0$ denote $\boldsymbol{\omega}$ and $\bar{\mathbf{R}}$, respectively, evaluated at $\bar{\Omega} = \bar{\Omega}_0$ and $\bar{\mathbf{a}} = \bar{\mathbf{a}}_0$. Clearly, $\mathbf{x}_m(t)$ is a synchronized solution in compliance with (2.3) if the “frequency” $\boldsymbol{\omega}_0 + \varepsilon \bar{\mathbf{R}}_0$ in (2.4) can be represented as

$$\boldsymbol{\omega}_0 + \varepsilon \bar{\mathbf{R}}_0 \equiv \mathbf{n}\omega_s \quad (2.5)$$

for some integer vector \mathbf{n} and a scalar constant ω_s , the synchronous frequency. It is pointed out, however, that since the solution (2.4) represents only an approximation of first order in ε modulo the fast oscillating terms (cf. Section 1.2.5) the criterion for synchronization (2.5) only holds for small values of ε and is only first order accurate. Hence we are facing the case of approximate synchronization as mentioned above. If the periodic solution \mathbf{x}_m (2.4) is asymptotically stable in the sense of Lyapunov, furthermore the synchronized regime will be reached asymptotically for $t \rightarrow \infty$. Consequently, the problem of finding frequency-synchronized solutions of a given dynamical system has in fact reduced to the determination of the periodic solutions and their stability.

2.2 Mechanical system and equations of motion

We consider two down-hanging rigid pendula, connected by a linear spring (spring constant c) and a linear damping element (damping constant k_{12}) performing planar oscillations in the same plane (see Figure 2.1). Friction at the hinges is taken into account by additional damping elements (k). The system has two degrees of freedom φ_1 and φ_2 and is exposed to a steady fluid flow of uniform velocity U perpendicular to the plane of oscillation of the pendula. For non-circular cross sections of the pendula *galloping (flutter) instabilities* (BLEVINS [1977]) are possible if U is increased beyond a certain critical value U_c . The aerodynamic force f_i acting per unit length on the i -th pendulum due to the fluid flow is given by (BLEVINS [1977])

$$f_i = \frac{1}{2} \rho_F U^2 D_i \left[a_1 \frac{v_i}{U} - a_2 \left(\frac{v_i}{U} \right)^3 \right], \quad (2.6)$$

2 Synchronization phenomena

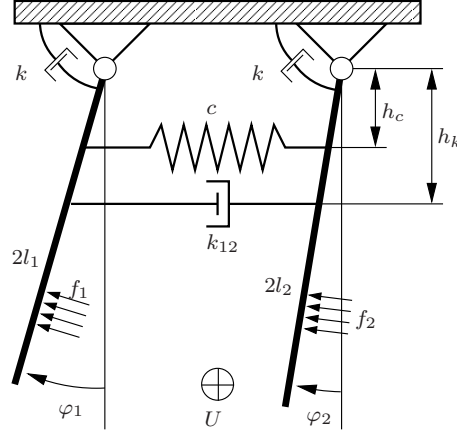


Figure 2.1: Mechanical system consisting of a flow excited double pendulum.

where ρ_F denotes the fluid density, v_i the velocities of the pendula, D defines some characteristic diameter of the cross-sections and the non-dimensional coefficients a_1 and a_2 have to be determined experimentally, depending on the cross-section of the body. We obtain two nonlinear ordinary differential equations for φ_1 and φ_2 which are, under the restriction of small amplitude oscillations $|\varphi_i| \ll 1$,

$$\begin{aligned}\ddot{\varphi}_1 &= -\omega_1^2 \varphi_1 - \beta_1(\varphi_1 - \varphi_2) - \gamma_1(\dot{\varphi}_1 - \dot{\varphi}_2) + (\mu_1 - \alpha_1 \dot{\varphi}_1^2) \dot{\varphi}_1, \\ \ddot{\varphi}_2 &= -\omega_2^2 \varphi_2 + \beta_2(\varphi_1 - \varphi_2) + \gamma_2(\dot{\varphi}_1 - \dot{\varphi}_2) + (\mu_2 - \alpha_2 \dot{\varphi}_2^2) \dot{\varphi}_2.\end{aligned}\quad (2.7)$$

Being most descriptive, the pendula are supposed to be homogeneous rigid rods (area of cross section A) of the same material (density ρ_P) differing solely in their lengths l_i , which after integrating the fluid force (2.6) over the lengths of the pendula leads to the following expressions for the parameters introduced in (2.7):

$$\begin{aligned}\omega_i^2 &= \frac{3g}{4l_i}, \quad \beta_i = \frac{3ch_c^2}{4\rho_P A l_i^3}, \quad \gamma_i = \frac{3k_{12}h_k^2}{4\rho_P A l_i^3}, \\ \mu_i &= \frac{3\rho_F U D}{4\rho_P A l_i} a_i - \frac{3k}{4\rho_P A l_i^3} := \tilde{\mu}_i - \tilde{k}_i, \quad \alpha_i = \frac{3\rho_F D l_i}{2\rho_P A U} a_i.\end{aligned}\quad (2.8)$$

By means of the variable transformation (LANDA [2001])

$$\dot{\varphi}_i = x_i / \sqrt{3} \quad (2.9)$$

we transform the Rayleigh equations (2.7) into a first order system of linearly coupled *Van-der-Pol equations*

$$\begin{aligned}\dot{x}_1 &= y_1, \quad \dot{y}_1 = -\omega_1^2 x_1 - \beta_1(x_1 - x_2) - \gamma_1(y_1 - y_2) + (\mu_1 - \alpha_1 x_1^2) y_1, \\ \dot{x}_2 &= y_2, \quad \dot{y}_2 = -\omega_2^2 x_2 + \beta_2(x_1 - x_2) + \gamma_2(y_1 - y_2) + (\mu_2 - \alpha_2 x_2^2) y_2.\end{aligned}\quad (2.10)$$

in the new variables x_i and their derivatives y_i defining the vector field $\mathbf{F}(x_1, x_2, y_1, y_2) : \mathbb{R}^4 \rightarrow \mathbb{R}^4$. In PIKOVSKY ET AL. [2001] and ARONSON ET AL. [1990] the terms associated with β_i are named *reactive* and those related to γ_i *diffusive* coupling. Two coupled Van-der-Pol oscillators of the form (2.10) with distinct natural frequencies ω_1 and ω_2 but equal parameters β_i , γ_i , μ_i and α_i have been studied in RAND & HOLMES

[1980] and ARONSON ET AL. [1990]. The latter particularly focuses the diffusive case $\beta_i = 0$, which for our model is coupling by damping only. In STORTI & RAND [1982] and CHAKRABORTY & RAND [1988] weakly detuned oscillators similar to the case currently under consideration are discussed for $\gamma_i = 0$ and also for strong and weak coupling, respectively. Particularly for the case of weak coupling explicit analytical representations of some bifurcation sets, which are referred to in Section 2.3.3, are presented in CHAKRABORTY & RAND [1988]. In ARONSON ET AL. [1987] two identical oscillators are examined and beneficial use is made of the additional reflectional symmetry of the vector field defined by (2.10) occurring in that case. In LANDA [2001] two different coupled Van-der-Pol oscillators are discussed in the context of synchronization theory by means of approximative methods. More recently, numerical studies detecting even chaotic behavior were published in LOW ET AL. [2003]. Here, we specifically want to focus our attention on a comprehensive mechanical explanation of the peculiarities of coupled Van-der-Pol equations from a more engineering oriented point of view.

2.3 Bifurcation analysis

In the following we will step through the customary stages of a nonlinear bifurcation analysis (GUCKENHEIMER & HOLMES [1983], TROGER & STEINDL [1991]) starting with the calculation of the critical parameter value (flow speed) by means of a linearized stability analysis. In the sequel, the Hopf bifurcations occurring for large and small frequency detunings and weak and strong coupling, respectively, are investigated.

2.3.1 Normal form analysis for a large frequency detuning

To start with, we want to employ some restrictions on the parameters in (2.10), namely

$$\beta_1 = \beta_2, \quad \gamma_1 = \gamma_2, \quad \alpha_1 = \alpha_2, \quad \mu_1 = \mu_2 - \varepsilon. \quad (2.11)$$

In view of (2.8), it is hard to imagine a mechanical oscillator that fulfills restrictions (2.11). However, since (2.11) is commonly assumed in the literature (LANDA [2001], PIKOVSKY ET AL. [2001]) these restrictions shall be discussed here, though. Physically this can be considered as the case of a large frequency detuning between the oscillators (TEUFEL ET AL. [2003]).

In the neighborhood of the equilibrium position $\mathbf{x} = (x_1, x_2, y_1, y_2) = \mathbf{0}$ system (2.10) can be written in the form $\dot{\mathbf{x}} = \mathbf{J}\mathbf{x} + \mathbf{N}(\mathbf{x})$, $\mathbf{N}(\mathbf{x}) = (0, 0, \alpha_1 x_1^2 y_1, \alpha_2 x_2^2 y_2)$, with the Jacobian matrix

$$\mathbf{J} = \begin{pmatrix} 0 & 0 & 1 & 0 \\ 0 & 0 & 0 & 1 \\ -\beta - \omega_1^2 & \beta & -\gamma - \mu & \gamma \\ \beta & -\beta - \omega_2^2 & \gamma & -\gamma + \varepsilon + \mu \end{pmatrix}, \quad (2.12)$$

The eigenvalues λ of \mathbf{J} obey the characteristic equation

$$\begin{aligned} P(\lambda, \boldsymbol{\mu}) &= \lambda^4 + \lambda^3 (2\gamma - \varepsilon - 2\mu) + \lambda^2 (2\beta - \gamma\varepsilon + (\varepsilon - 2\gamma\varepsilon)\mu + \mu^2 + \Omega) + \\ &\lambda (-\beta\varepsilon - \mu(2\beta + \Omega) + \gamma\Omega - \varepsilon\omega_1^2) + \beta\Omega + \frac{1}{4}(\Omega^2 - \Delta^2) = 0 \end{aligned} \quad (2.13)$$

where use is made of the expressions

$$\Omega = \omega_1^2 + \omega_2^2, \quad \Delta = \omega_1^2 - \omega_2^2, \quad \boldsymbol{\mu} = (\mu, \varepsilon, \gamma)$$

For $\gamma = \varepsilon = 0$ equation (2.13) can be simplified to

$$(\lambda^2 - \lambda\mu + \omega_1^2)(\lambda^2 - \lambda\mu + \omega_2^2) + \beta(2\lambda^2 - 2\lambda\mu + \Omega) = 0 \quad (2.14)$$

which can easily be solved with the aid of the substitution $\nu^2 = \lambda^2 - \lambda\mu$ yielding the eigenvalues λ_i , ($i = 1, \dots, 4$),

$$\lambda_{1,2,3,4} = \frac{\mu}{2} \pm \sqrt{\frac{\mu^2}{4} - \nu_{1,2}^2}, \quad \nu_{1,2}^2 = \frac{1}{2} \left(\Omega + 2\beta \mp \sqrt{4\beta^2 + \Delta^2} \right). \quad (2.15)$$

Clearly, ν_1 and ν_2 are real for $\Omega > 0$ and $\beta > 0$ and thus the zero solution is stable for $\mu < 0$. At $\boldsymbol{\mu} = \mathbf{0}$ a *Hopf-bifurcation* of codimension two (GUCKENHEIMER & HOLMES [1983]) at two pairs of imaginary conjugate eigenvalues occurs. The definition of μ , (2.8)₄, yields a relation for the critical velocity U_c of the flow at which the down-hanging equilibrium position of the pendula becomes unstable. Assuming $k_1 \approx k_2 = k$ and replacing the length l_i of the respective pendulum in (2.8)₄ by some average value \bar{l} we obtain

$$U_c = k / (2a_1 \rho D \bar{l}^2)$$

In order to scrutinize this bifurcation equation (2.10) may be rewritten at $\boldsymbol{\mu} = \mathbf{0}$ in terms of new complex variables \boldsymbol{w} by virtue of the linear transformation $\boldsymbol{x} = \mathbf{T}\boldsymbol{w}$ yielding the bifurcation equation

$$\dot{\boldsymbol{w}} = \mathbf{D}\boldsymbol{w} + \mathbf{G}(\boldsymbol{w}), \quad \boldsymbol{w} = (w_1, w_2, \bar{w}_1, \bar{w}_2) \quad (2.16)$$

where \mathbf{D} is the diagonal matrix containing the eigenvalues of \mathbf{J} and \mathbf{T} is constructed from the eigenvectors of \mathbf{J} at $\boldsymbol{\mu} = \mathbf{0}$, viz.

$$\mathbf{D} = \begin{pmatrix} i\nu_1 & 0 & 0 & 0 \\ 0 & -i\nu_1 & 0 & 0 \\ 0 & 0 & i\nu_2 & 0 \\ 0 & 0 & 0 & -i\nu_2 \end{pmatrix}, \quad \mathbf{T} = \begin{pmatrix} 1 & 1 & 1 & 1 \\ \frac{A+\Delta}{2\beta} & \frac{A+\Delta}{2\beta} & -\frac{A-\Delta}{2\beta} & -\frac{A-\Delta}{2\beta} \\ i\nu_1 & -i\nu_1 & i\nu_2 & -i\nu_2 \\ i\frac{(A+\Delta)\nu_1}{2\beta} & -i\frac{(A+\Delta)\nu_1}{2\beta} & -i\frac{(A-\Delta)\nu_2}{2\beta} & i\frac{(A-\Delta)\nu_2}{2\beta} \end{pmatrix}. \quad (2.17)$$

The abbreviation A stands for $A = \sqrt{4\beta^2 + \Delta^2}$. The nonlinear vector function \mathbf{G} has to be calculated from

$$\mathbf{G}(\boldsymbol{w}) = \mathbf{T}^{-1}\mathbf{N}(\mathbf{T}\boldsymbol{w}), \quad (2.18)$$

its components G_i being homogeneous polynomials of degree 3 in \boldsymbol{w} , viz.

$$G_i(w_1, w_2, \bar{w}_1, \bar{w}_2) = \sum_{\substack{k,l,m,n \\ k+l+m+n=3}} a_{i,klmn} w_1^k w_2^l \bar{w}_1^m \bar{w}_2^n =: \sum_{|\mathbf{m}|=3} a_{i,\mathbf{m}} \boldsymbol{w}^{\mathbf{m}}, \quad (2.19)$$

where $\mathbf{m} := (k, l, m, n)$ and $|\mathbf{m}| := k + l + m + n$. The complex coefficients $a_{i,\mathbf{m}}$ can be derived from the relation

$$a_{i,klmn} = \frac{1}{k! l! m! n!} \frac{\partial^{k+l+m+n} G_i}{\partial w_1^k \partial w_2^l \partial \bar{w}_1^m \partial \bar{w}_2^n}. \quad (2.20)$$

2 Synchronization phenomena

A further reduction of the nonlinear terms in (2.16) by means of normal form theory now depends on the resonance properties of the eigenvalues $\pm i\nu_i$. It is known from the POINCARÉ-DULAC theorem (see e. g. ARNOLD [1983], SHILNIKOV ET AL. [1998]) that a change of variables

$$\mathbf{w} = \mathbf{z} + \mathbf{h}(\mathbf{z}), \quad \mathbf{z} = (z_1, z_2, \bar{z}_1, \bar{z}_2) \quad (2.21)$$

will transfer (2.16) to

$$\dot{\mathbf{z}} = \mathbf{D}\mathbf{z} + \mathbf{R}(\mathbf{z}). \quad (2.22)$$

The polynomials R_i will contain only those powers $\mathbf{z}^{\mathbf{m}}$ where the exponents satisfy the resonance condition

$$k\nu_1 - l\nu_1 + m\nu_2 - n\nu_2 = \nu_i. \quad (2.23)$$

If the ratio ν_1/ν_2 is irrational solutions k, l, m, n for (2.23) are called trivial resonances (SHILNIKOV ET AL. [2001]). Additionally, non-trivial resonances occur if $\nu_1/\nu_2 = M/N$, $M, N \in \mathbb{N}$. Non-trivial resonances are commonly neglected, if N is greater than the order of the lowest trivial resonance, i. e. $N > |\mathbf{m}|$, which is referred to as *weak resonance* and will be treated in the following.

In view of the eigenvalues (2.36) it is evident that for sufficiently large frequency detunings Δ or coupling strength β we avoid being close to the 1:1 resonance where $\nu_1 - \nu_2 = O(\epsilon)$. Synchronized regimes in the instance of non-resonant eigenvalues can most easily be studied from the *normal form* (2.22) of a Hopf-bifurcation of codimension two at two imaginary pairs of eigenvalues without low order resonances (TAKENS [1974], HOLMES [1980] and GUCKENHEIMER & HOLMES [1983]). The normal form in the considered case reads

$$\begin{aligned} \dot{z}_1 &= i\nu_1 z_1 + a_{1,2100} z_1^2 \bar{z}_1 + a_{1,1011} z_1 z_2 \bar{z}_2, \\ \dot{z}_2 &= i\nu_2 z_2 + a_{2,0021} z_2^2 \bar{z}_2 + a_{2,1101} z_1 \bar{z}_1 z_2, \end{aligned} \quad (2.24)$$

or, respectively, in polar coordinates, $z_1 = R_1 e^{i\phi_1}$, $z_2 = R_2 e^{i\phi_2}$,

$$\begin{aligned} \dot{R}_1 &= -R_1 (b_{11}^R R_1^2 + b_{12}^R R_2^2), & \dot{R}_2 &= -R_2 (b_{21}^R R_1^2 + b_{22}^R R_2^2), \\ \dot{\phi}_1 &= \nu_1 + b_{11}^I R_1^2 + b_{12}^I R_2^2, & \dot{\phi}_2 &= \nu_2 + b_{21}^I R_1^2 + b_{22}^I R_2^2, \end{aligned} \quad (2.25)$$

where the coefficients b_{ij}^R and b_{ij}^I are the real and imaginary parts, respectively, of $a_{i,klmn}$ occurring in (2.24). The considered example permits an analytical computation of b_{ij} , namely

$$\begin{aligned} b_{11}^R &= a_{1,2100} = \frac{\alpha(A + \Delta)(2\beta^2 + \Delta^2)}{16A\beta^2}, & b_{12}^R &= a_{1,1011} = \frac{\alpha(A - \Delta)}{4A}, \\ b_{21}^R &= a_{2,1101} = \frac{\alpha(A + \Delta)}{4A}, & b_{22}^R &= a_{2,2100} = \frac{\alpha(A - \Delta)(2\beta^2 + \Delta^2)}{16A\beta^2}, \\ b_{11}^I &= b_{12}^I = b_{21}^I = b_{22}^I = 0. \end{aligned} \quad (2.26)$$

Scaling the amplitudes R_1 and R_2 by

$$R_1 = \frac{\bar{R}_1}{\sqrt{b_{11}^R}}, \quad R_2 = \frac{\bar{R}_2}{\sqrt{b_{22}^R}},$$

and embedding (2.25) as usual into a two-parameter family (GUCKENHEIMER & HOLMES [1983]) yields the simplified amplitude equations

$$\begin{aligned}\dot{\bar{R}}_1 &= \eta_1 \bar{R}_1 - \bar{R}_1(\bar{R}_1^2 + \kappa \bar{R}_2^2), & \dot{\phi}_1 &= \nu_1 + \xi_1, \\ \dot{\bar{R}}_2 &= \eta_2 \bar{R}_2 - \bar{R}_2(\bar{R}_2^2 + \kappa \bar{R}_1^2), & \dot{\phi}_2 &= \nu_2 + \xi_2.\end{aligned}\quad (2.27)$$

η_i and ξ_i being the real and imaginary parts of the unfolding parameters, respectively (TROGER & STEINDL [1991]). The coefficient κ can be calculated analytically using the formula

$$\kappa = 2 \frac{\partial^3 G_2}{\partial w_1 \partial \bar{w}_1 \partial w_2} \left(\frac{\partial^3 G_1}{\partial w_1^2 \partial \bar{w}_1} \right)^{-1}, \quad (2.28)$$

where G_i is given by (2.19). A relation between the unfolding parameters η_i, ξ_i and the physical quantities μ, ε and γ is established from the Taylor series expansion of the eigenvalues (TROGER & STEINDL [1991]),

$$\eta_i + i\xi_i = \left. \frac{\partial \lambda}{\partial \boldsymbol{\mu}} \right|_{\substack{\boldsymbol{\mu}=\mathbf{0} \\ \lambda=i\nu_i}} \cdot \boldsymbol{\mu} = - \frac{1}{\partial P / \partial \lambda} \left. \frac{\partial P}{\partial \boldsymbol{\mu}} \right|_{\substack{\boldsymbol{\mu}=\mathbf{0} \\ \lambda=i\nu_i}} \cdot \boldsymbol{\mu}. \quad (2.29)$$

Evaluating (2.28) and (2.29) using (2.17), (2.18) and the characteristic equation (2.13) yields the results

$$\kappa = \frac{2}{1 + \frac{\Delta^2}{2\beta^2}}, \quad \eta_{1,2} = \frac{\mu}{2} + \left(1 \mp \frac{\Delta}{A}\right) \frac{\varepsilon}{4} - \left(1 \mp \frac{2\beta}{A}\right) \frac{\gamma}{2}, \quad \xi_{1,2} = 0. \quad (2.30)$$

The phase portraits of (2.27) are elaborated for a more general case in GUCKENHEIMER & HOLMES [1983]. In the context of aerodynamically excited mechanical oscillations, similar to the case discussed here, in STRIBERSKY & TROGER [1987] the same type of bifurcation was studied numerically. We shall interpret some major results here within the framework of synchronization theory.

System (2.27) has four stationary solutions, denoted by S_0, \dots, S_3 , namely

$$\begin{aligned}S_0 : \quad \bar{R}_1^* &= 0, \bar{R}_2^* = 0, & S_1 : \quad \bar{R}_1^* &= \sqrt{\eta_1}, \bar{R}_2^* = 0, \\ S_2 : \quad \bar{R}_1^* &= 0, \bar{R}_2^* = \sqrt{\eta_2}, & S_3 : \quad \bar{R}_1^* &= \sqrt{\frac{\kappa\eta_2 - \eta_1}{\kappa^2 - 1}}, \bar{R}_2^* = \sqrt{\frac{\kappa\eta_1 - \eta_2}{\kappa^2 - 1}}.\end{aligned}$$

Reestablishing relations between the quantities R_1, R_2, ϕ_1 and ϕ_2 in (2.27) and the original deflection angles φ_i yields

$$\begin{aligned}\varphi_1(t) &= \frac{1}{\sqrt{3}} \left[\frac{R_1}{\nu_1} \sin \nu_1 t + \frac{R_2}{\nu_2} \sin \nu_2 t \right] + Q_1^{(3)}(R_1, R_2, \nu_1 t, \nu_2 t), \\ \varphi_2(t) &= \frac{1}{2\beta\sqrt{3}} \left[(A - \Delta) \frac{R_1}{\nu_1} \sin \nu_1 t - (A + \Delta) \frac{R_2}{\nu_2} \sin \nu_2 t \right] + Q_2^{(3)}(R_1, R_2, \nu_1 t, \nu_2 t),\end{aligned}\quad (2.31)$$

where the higher order terms $Q_i^{(3)}$ are homogeneous functions in R_1 and R_2 of third degree and higher, quasi-periodic in the time t with periods $2\pi/\nu_1$ and $2\pi/\nu_2$. Evaluated at the stationary values $R_1 = \bar{R}_1^*/\sqrt{b_{11}^R}, R_2 = \bar{R}_2^*/\sqrt{b_{22}^R}$, the form of solution (2.31) is

2 Synchronization phenomena

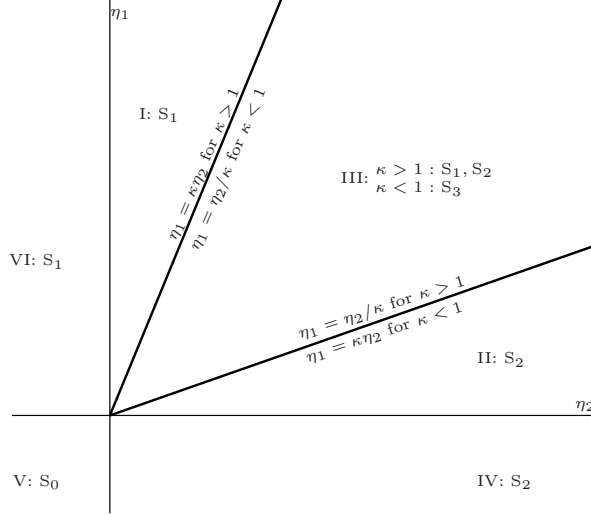


Figure 2.2: Stratification of the parameter plane (η_1, η_2) and the corresponding stable stationary solutions.

similar to the general relation (1.17) discussed in Section 1.2.5, where the amplitude vector $\bar{\mathbf{a}}$ is identified with $\bar{\mathbf{a}} = (R_1, R_2)$, the phases $\bar{\phi}$ are $\nu_1 t$ and $\nu_2 t$ and $\bar{\Omega}$ has zero dimension. The solution (2.31) suggests the following interpretation of the stationary solutions $S_1 \dots S_3$:

- *In-phase synchronization* with the common frequency ν_1 appears at S_1 where the oscillations of the pendula are described by

$$\varphi_1(t) = \frac{1}{\nu_1} \sqrt{\frac{\eta_1}{3b_{11}^R}} \sin \nu_1 t + O(\eta_1^{3/2}), \quad \varphi_2(t) = \frac{A - \Delta}{2\beta\nu_1} \sqrt{\frac{\eta_1}{3b_{11}^R}} \sin \nu_1 t + O(\eta_1^{3/2}).$$

- *Anti-phase synchronization* with the common frequency ν_2 appears at S_2 where the oscillations of the pendula are described by

$$\varphi_1(t) = \frac{1}{\nu_1} \sqrt{\frac{\eta_2}{3b_{22}^R}} \sin \nu_2 t + O(\eta_2^{3/2}), \quad \varphi_2(t) = -\frac{A + \Delta}{2\beta\nu_2} \sqrt{\frac{\eta_2}{3b_{22}^R}} \sin \nu_2 t + O(\eta_2^{3/2}).$$

- At S_3 we obtain the full quasi-periodic motion on a 2-Torus with two distinct frequencies ν_1 and ν_2 described by (2.31)

The conditions for the existence of the fixed points S_1, \dots, S_3 partition the parameter space (η_1, η_2) into six segments I...VI as depicted in Figure 2.2. The stability can easily be checked by linearizing (2.27) (see GUCKENHEIMER & HOLMES [1983]). Obviously, the system will in general tend to synchronize if $\kappa > 1$ regardless of the other parameters which with the aid of (2.30)₁ results in the condition

$$-\sqrt{2}\beta < \Delta < \sqrt{2}\beta. \quad (2.32)$$

In regions I and VI in-phase synchronization is stable contrary to regions II and IV where the anti-phase solutions are attracting. In region III both, in-phase and anti-phase regimes are stable and thus the long-term behavior depends only on the initial conditions.

If $\kappa < 1$ synchronization occurs merely in regions I, II, IV and VI whereas in the segment III we are facing the case of quasi-periodic oscillations. Using (2.30)₂ we arrive at the conditions for in- and anti-phase synchronization, respectively,

$$\begin{aligned} (6\beta^2 + \Delta^2)(4\beta\gamma - \Delta\varepsilon) - A(2\beta^2 - \Delta^2)(2\gamma - \varepsilon - 2\mu) &> 0 && \text{(in-phase),} \\ (6\beta^2 + \Delta^2)(4\beta\gamma - \Delta\varepsilon) + A(2\beta^2 - \Delta^2)(2\gamma - \varepsilon - 2\mu) &< 0 && \text{(anti-phase).} \end{aligned}$$

For the special case of similar oscillators without damping, i. e. $\varepsilon = 0$, $\gamma = 0$ and consequently $\eta_1 = \eta_2 = \mu/2$ we obtain a picture that is qualitatively similar to region III in Figure 2.2. Thus again, the motions of the pendula will synchronize if the parameters β and Δ satisfy the inequality (2.32).

2.3.2 Small frequency detuning and strong coupling

For the mechanical problem, it seems practically more plausible to emphasize the case of zero damping ($\gamma_i = 0$) and identical oscillators, but to consider unfoldings for a small length deviation $(l_2 - l_1)/l_1 = \varepsilon$ and a small damping γ (TEUFEL ET AL. [2006b]). Taking ε as a small parameter reveals the dependencies

$$\begin{aligned} \omega_2^2 &= \omega_1^2(1 - \varepsilon), & \beta_2 &= \beta_1(1 - 3\varepsilon), & \gamma_2 &= \gamma_1(1 - 3\varepsilon), \\ \mu_2 &= \mu_1(1 - \varepsilon) + 2\tilde{k}_1\varepsilon, & \alpha_2 &= \alpha_1(1 + \varepsilon). \end{aligned} \quad (2.33)$$

In the sequel we will for simplicity drop the indices of $\beta_1, \gamma_1, \mu_1, \tilde{k}_1, \alpha_1$. Discussing the case of weak coupling in Section 2.3.3, we will take advantage of the fact that the deviations (2.33) may be of second order in ε if the coupling parameters are assumed to be small themselves.

The Jacobian matrix of system (2.10) is now given by

$$\mathbf{J} = \begin{pmatrix} 0 & 0 & 1 & 0 \\ 0 & 0 & 0 & 1 \\ -\beta - \omega_1^2 & \beta & -\gamma + \mu & \gamma \\ \beta(1 - 3\varepsilon) & -\beta(1 - 3\varepsilon) - \omega_1^2(1 - \varepsilon) & \gamma(1 - 3\varepsilon) & 2\tilde{k}_1\varepsilon - \gamma(1 - 3\varepsilon) + \mu(1 - \varepsilon) \end{pmatrix}, \quad (2.34)$$

with the characteristic equation

$$\begin{aligned} P(\lambda, \boldsymbol{\mu}) &= -\beta(1 - 3\varepsilon)(\beta + \gamma\lambda) + [\beta + \omega_1^2 + \lambda(\gamma + \lambda - \mu)] \times \\ &\quad [\beta(1 - 3\varepsilon) + \omega_1^2(1 - \varepsilon)] - \lambda[\gamma(1 - 3\varepsilon)(\beta + \gamma\lambda) - \\ &\quad (\gamma(1 - 3\varepsilon) + \lambda - \mu(1 - \varepsilon) - 2\tilde{k}_1\varepsilon)(\beta + \omega_1^2 + \lambda(\gamma + \lambda - \mu))] \end{aligned} \quad (2.35)$$

which for $\gamma = 0$ and $\varepsilon = 0$ straightforwardly yields the eigenvalues $\lambda_1, \dots, \lambda_4$,

$$\lambda_{1,2,3,4} = \frac{\mu}{2} \pm \sqrt{\frac{\mu^2}{4} - \nu_{1,2}^2}, \quad \nu_1^2 = \omega_1^2, \quad \nu_2^2 = \omega_1^2 + 2\beta. \quad (2.36)$$

At the critical parameter vector $\boldsymbol{\mu} = (\mu, \varepsilon, \gamma) = \mathbf{0}$ again a Hopf-bifurcation of codimension two occurs. The 1:1 resonance can be avoided only for a sufficiently large coupling

strength β here. The computation of the POINCARÉ-DULAC normal form was outlined in Section 2.3.1. Only the transformation matrix \mathbf{T} must be adapted to,

$$\mathbf{T} = \begin{pmatrix} 1 & 1 & 1 & 1 \\ 1 & 1 & -1 & -1 \\ i\nu_1 & -i\nu_1 & i\nu_2 & -i\nu_2 \\ i\nu_1 & -i\nu_1 & -i\nu_2 & i\nu_2 \end{pmatrix}, \quad (2.37)$$

which affects the unfolding parameters and the coefficient κ in (2.27). Evaluating (2.28) and (2.29) using (2.37), (2.18) and (2.35) gives

$$\begin{aligned} \kappa = 2, \quad \eta_1 &= \frac{1}{2} (\mu + \tilde{k}\varepsilon), & \xi_1 &= -\varepsilon \frac{\nu_1}{4} \\ \eta_2 &= \frac{1}{2} (\mu + \tilde{k}\varepsilon) - \gamma, & \xi_2 &= -\varepsilon \left(\frac{\nu_2}{4} + \frac{\beta}{\nu_2} \right). \end{aligned} \quad (2.38)$$

In Section 2.3.1, where a large frequency detuning between the oscillators was still permitted, we have explained that the stationary solution of (2.27) where $\bar{R}_1^* = 0, \bar{R}_2^* = \sqrt{\eta_2}$ corresponds to an anti-phase synchronized motion, while that with $\bar{R}_1^* = \sqrt{\eta_1}, \bar{R}_2^* = 0$ causes in-phase synchronization with frequencies $\nu_2 + \xi_2$ or $\nu_1 + \xi_1$, respectively. Moreover it is known that a quasi-periodic two frequency regime is only stable if $\kappa < 1$ which is ruled out by (2.38), here. Thus, in the considered example the in- and anti-phase motions of two coupled *identical* pendula (ARNOLD [1978]) are preserved with small frequency shifts ξ_i for a small difference of their lengths ε and a small damping γ . If η_1 and η_2 are negative the origin is the only stable solution, which permits to calculate the critical flow velocity U_c beyond which the pendula start oscillating from $\mu + \tilde{k}\varepsilon = 0$; using the definition (2.8)₄ of μ gives $U_c = k(1 - \varepsilon)/\rho_F D l_1 a_1$.

2.3.3 Hopf-bifurcation at 1:1 resonance – small frequency detuning and weak coupling

The derivation of the normal form (2.27) in the previous subsection was based upon the requirement that the eigenvalues at the Hopf bifurcation $\pm i\nu_1$ and $\pm i\nu_2$ be non-resonant due to strong coupling. In this work, we shall put the emphasis however on the case of weak coupling where actually synchronization is the more striking phenomenon. We start again with equations (2.10) for zero damping $\gamma = 0$ and a small detuning of the natural frequencies $\omega_2 = \omega_1(1 - \varepsilon/2)$ due to a small relative length difference of the pendula ε . Furthermore, in view of (2.33) we now express the smallness of the coefficients β, μ and α by the notations

$$\begin{aligned} \beta_1 &= \beta := \varepsilon\beta', & \mu_1 &= \mu := \varepsilon\mu', & \alpha_1 &= \alpha := \varepsilon\alpha', \\ \beta_2 &= \beta + O(\varepsilon^2), & \mu_2 &= \mu + O(\varepsilon^2), & \alpha_2 &= \alpha + O(\varepsilon^2), \end{aligned} \quad (2.39)$$

In order to obtain the normal form of (2.10) up to order ε in the resonant case we use a direct averaging approach (SETHNA [1995]). Inserting (2.39) into (2.10) yields a perturbation problem suitable for averaging where the unperturbed system is a simple harmonic oscillator with frequency ω_1 . Introducing the element transformation (KIRCH-

GRABER & STIEFEL [1978])

$$\mathbf{x} = \begin{pmatrix} x_1 \\ x_2 \\ y_1 \\ y_2 \end{pmatrix} = \begin{pmatrix} A_1 \cos \phi \\ A_2 \cos(\phi + \psi) \\ \omega_1 A_1 \sin \phi \\ \omega_2 A_2 \sin(\phi + \psi) \end{pmatrix} = \mathbf{U}(\mathbf{y}), \quad \mathbf{y} := (A_1, A_2, \phi, \psi), \quad (2.40)$$

which is widely used to derive amplitude equations for Van-der-Pol oscillators (LANDA [2001], PIKOVSKY ET AL. [2001], RAND & HOLMES [1980]) we formally obtain averaged equations for \mathbf{y} from

$$\dot{\bar{\mathbf{y}}} = \int_0^{2\pi} \frac{\partial \mathbf{U}^{-1}}{\partial \mathbf{y}} \mathbf{F}(\mathbf{U}(\mathbf{y})) d\phi, \quad (2.41)$$

where the bar indicates averaged quantities. Up to order ε , the result of (2.41) reads

$$\begin{aligned} \dot{\bar{A}}_1 &= (1 - \bar{A}_1^2) \bar{A}_1 - \tilde{\beta} \bar{A}_2 \sin \bar{\psi}, & \dot{\bar{\psi}} &= \tilde{\Delta} + \tilde{\beta} \left(\frac{\bar{A}_1}{\bar{A}_2} - \frac{\bar{A}_2}{\bar{A}_1} \right) \cos \bar{\psi}, \\ \dot{\bar{A}}_2 &= (1 - \bar{A}_2^2) \bar{A}_2 + \tilde{\beta} \bar{A}_1 \sin \bar{\psi}, & \dot{\bar{\phi}} &= -\tilde{\omega}_1 - \tilde{\beta} \left(1 - \frac{\bar{A}_2}{\bar{A}_1} \cos \bar{\psi} \right), \end{aligned} \quad (2.42)$$

where the amplitudes as well as the time have been scaled by

$$\bar{A}_1 \rightarrow 2\sqrt{\frac{\mu}{\alpha}} \bar{A}_1, \quad \bar{A}_2 \rightarrow 2\sqrt{\frac{\mu}{\alpha}} \bar{A}_2, \quad t \rightarrow \frac{2}{\mu} t, \quad (2.43)$$

and the parameters are given by³

$$\tilde{\Delta} = \varepsilon \frac{\omega_1}{\mu} = \frac{\Delta}{\mu}, \quad \tilde{\beta} = \varepsilon \frac{\beta'}{\mu \omega_1}, \quad \tilde{\omega}_1 = \frac{2\omega_1}{\mu}. \quad (2.44)$$

where the frequency detuning $\Delta = \omega_1 - \omega_2$ has been introduced. Apparently, at stationary solutions $\dot{\bar{A}}_1 = \dot{\bar{A}}_2 = \dot{\bar{\psi}} = 0$ of (2.42), both pendula oscillate with different amplitudes \bar{A}_1^* and \bar{A}_2^* , with a constant phase shift $\bar{\psi}^*$ and a common frequency ω_s , given by the solution of (2.42)₄ on the manifold $\{\bar{A} = \bar{A}_1^*, \bar{A}_2 = \bar{A}_2^*, \bar{\psi} = \bar{\psi}^*\}$, viz.

$$\bar{\phi}^*(t) = -\omega_s t, \quad \text{where} \quad \omega_s = \omega_1 + \frac{1}{2} \mu \tilde{\beta} \left(1 - \frac{\bar{A}_2^*}{\bar{A}_1^*} \cos \bar{\psi}^* \right). \quad (2.45)$$

With the phase ϕ given by (2.45) a solution \mathbf{x} of (2.10) given in the form of (2.40) complies with the definition (2.3) where the periodic functions Φ_i are now identified with the components of the transformation \mathbf{U} . Thus a stationary solution of (2.42) is naturally frequency synchronized. We want to stress the point that the transformation (2.40) permits a direct calculation of the synchronous frequency ω_s avoiding the ad-hoc assumption that $\omega_s = (\omega_1 + \omega_2)/2$, which is used in LANDA [2001] and PIKOVSKY ET AL. [2001]. In order to find the solutions $(\bar{A}_1^*, \bar{A}_2^*, \bar{\psi}^*)$ and in particular domains for the parameters $\tilde{\Delta}$ and $\tilde{\beta}$ where these solutions exist and are stable, two different approaches are compared in the following. One is to solve (2.42) by means of a perturbation expansion for small $\tilde{\beta}$. The other is based upon a graphical interpretation of the stationary solutions.

³Note that by definitions (2.43)₃ and (2.44) we restrict ourselves to the case $\mu \neq 0$.

A perturbation expansion

A perturbation expansion to (2.42) has been applied in RAND & HOLMES [1980] and shall briefly be sketched here for review purposes. For $\tilde{\beta} = 0$, equations (2.42)_{1,2} have a stationary solution⁴ $A_1^* = 1, A_2^* = 1$ and ψ is a time-like variable $\psi = \tilde{\Delta}t$. Thus, for small $\tilde{\beta}$ we may seek solutions using an expansion

$$A_1(\psi) = 1 + \tilde{\beta}A_{11}(\psi) + O(\tilde{\beta}^2), \quad A_2(\psi) = 1 + \tilde{\beta}A_{21}(\psi) + O(\tilde{\beta}^2), \quad (2.46)$$

which if substituted into (2.42)_{1,2} yields linear ordinary differential equations for A_{11} and A_{21} by comparing the coefficients of $\tilde{\beta}$, namely

$$\begin{aligned} \Delta \frac{dA_{11}}{d\psi} &= -2A_{11} - \sin \psi, \\ \Delta \frac{dA_{21}}{d\psi} &= -2A_{21} + \sin \psi, \end{aligned} \quad (2.47)$$

Using (2.46) in the equation for $\dot{\psi}$ (2.42)₃ and expanding the right-hand-side in a Taylor series in $\tilde{\beta}$ yields

$$\dot{\psi} = \tilde{\Delta} + \tilde{\beta}^2(2A_{11} - 2A_{21}) \cos \psi + O(\tilde{\beta}^4). \quad (2.48)$$

A solution of (2.47) modulo exponentially decaying terms is easily found to be

$$A_{11}(\psi) = \frac{1}{2\sqrt{1 + (\tilde{\Delta}/2)^2}} \cos(\psi + \theta), \quad \text{where } \theta = \arctan \frac{2}{\tilde{\Delta}}, \quad (2.49)$$

and furthermore $A_{21} = -A_{11}$ holds true. Taking this into account and besides assuming that $\tilde{\Delta} \ll 1$ (i. e. $\theta \approx \pi/2$) we obtain from (2.48) together with (2.49) a simple o.d.e. involving only the phase difference, which is

$$\dot{\psi} = \tilde{\Delta} - \tilde{\beta}^2 \sin 2\psi. \quad (2.50)$$

In a synchronized regime the phase difference ψ^* is constant ($\dot{\psi}^* = 0$) and thus given by

$$2\psi_s^* = \arcsin \frac{\tilde{\Delta}}{\tilde{\beta}^2}, \quad 2\psi_u^* = \pi - \arcsin \frac{\tilde{\Delta}}{\tilde{\beta}^2}. \quad (2.51)$$

The subscripts s and u indicate that (2.51)₁ is stable in contrast to (2.51)₂ which is easy to check by calculating $\partial\dot{\psi}/\partial\psi$ from (2.50). Moreover, it is obvious that solutions (2.51) exist only if the inequality

$$-\tilde{\beta}^2 \leq \tilde{\Delta} \leq \tilde{\beta}^2 \quad (2.52)$$

holds which defines a domain bounded by two parabolas in the $(\tilde{\Delta}, \tilde{\beta})$ -space. This domain is an approximation of the parameter region where synchronized solutions are stable..

⁴The bars for A_1, A_2 and ψ are in the following dropped for simplicity.

A graphical approach

Now we will go straightway about finding stationary solutions for (2.42) and consider the algebraic system of equations

$$\mathbf{f}(\mathbf{A}; b) = \begin{pmatrix} (1 - A_1^2)A_1 - bA_2 \\ (1 - A_1^2)A_1 + bA_2 \end{pmatrix} = \mathbf{0}, \quad \tilde{\Delta} + c(\mathbf{A})\sqrt{\tilde{\beta}^2 - b^2} = 0, \quad (2.53)$$

where the following substitutions have been performed:

$$\mathbf{A} = (A_1, A_2), \quad b = \tilde{\beta} \sin \psi, \quad c(\mathbf{A}) = \frac{A_1}{A_2} - \frac{A_2}{A_1}. \quad (2.54)$$

If A_1 , A_2 and $\tilde{\Delta}$ are regarded as variables depending on the parameters b and $\tilde{\beta}$, (2.53)₁ can be solved uncoupled from (2.53)₂ by virtue of some cunning algebraic manipulations laid down in the following.

Solutions of (2.53)₁ may be visualized as the intersection points of two curves, σ_1 and σ_2 , defined by

$$\sigma_1 = \{\mathbf{A} : (A_1^2 + A_2^2) - (A_1^4 + A_2^4) = 0\}, \quad \sigma_2 = \{\mathbf{A} : A_2 = \frac{1}{b}(A_1 - A_1^3)\}, \quad (2.55)$$

and plotted in Figure 2.3a. It is evident that there will in general be two such intersection points, denoted by $\mathbf{A}_1^*(b)$ and $\mathbf{A}_2^*(b)$ depending solely on b . We proceed to derive from (2.53) together with the definition of c , (2.54)₂, on σ_1 the identities

$$A_1^2 + A_2^2 \equiv (2 + c^2)A_1^2A_2^2 \equiv 2 + bc. \quad (2.56)$$

Furthermore, a formula for the derivative of c with respect to b on the curve σ_1 is given by

$$\left. \frac{dc}{db} \right|_{\sigma_1} = \left. \frac{dc}{d\mathbf{A}} \cdot \frac{d\mathbf{A}}{db} \right|_{\sigma_1} = - \left. \frac{dc}{d\mathbf{A}} \cdot \begin{pmatrix} \frac{\partial \mathbf{f}}{\partial \mathbf{A}}^{-1} \frac{\partial \mathbf{f}}{\partial b} \end{pmatrix} \right|_{\sigma_1}. \quad (2.57)$$

All derivatives in (2.57) are easily calculated from (2.54)₃ and (2.53) unless $\partial \mathbf{f} / \partial \mathbf{A}$ is singular, namely at the point of tangency of σ_1 and σ_2 . Thus, it suggests itself to introduce the determinant of the Jacobian of \mathbf{f} by

$$\Theta(A_1, A_2, b) := \det \frac{\partial \mathbf{f}}{\partial \mathbf{A}} = \begin{vmatrix} 1 - 3A_1^2 & -b \\ b & 1 - 3A_2^2 \end{vmatrix} = (1 - 3A_1^2)(1 - 3A_2^2) + b^2 \quad (2.58)$$

and we remark that $\Theta(A_1, A_2, b_c) = 0$. If additionally relation (2.55) is taken into account the evaluation of (2.57) results in the expression

$$\left. \frac{dc}{db} \right|_{\sigma_1} = -2 \frac{(A_1^2 + A_2^2)^2}{A_1^2 A_2^2} \frac{1}{\Theta} = -2(2 + bc)(2 + c^2) \frac{1}{\Theta} = -2(4 + c^2) \frac{1}{\Theta}, \quad (2.59)$$

where in the last two steps again repeated use has been made of (2.56) and (2.55). Relation (2.59) conspicuously reveals that c has to obey the identity $(2 + bc)(2 + c^2) \equiv (4 + c^2)$ for all b , or more concisely $c(bc^2 + c + 2b) \equiv 0$ with the non-trivial solutions

$$c_1(b) = \frac{1}{2b}(-1 + \sqrt{1 - 8b^2}), \quad c_2(b) = -\frac{1}{2b}(1 + \sqrt{1 - 8b^2}). \quad (2.60)$$

Apparently, c_1 and c_2 are real if

$$b \in \left[-\frac{1}{2\sqrt{2}}, \frac{1}{2\sqrt{2}} \right] \quad (2.61)$$

and thus the critical value $b_c = 1/2\sqrt{2}$ has been found below which (2.53) possesses both solutions, \mathbf{A}_1^* and \mathbf{A}_2^* . The result (2.60) is of crucial importance since all quantities dealt with in the subsequent analysis will be educible in terms of $c_i(b)$. In particular, we obtain expressions for the components of $\mathbf{A}_i^* = (A_{1,i}, A_{2,i})$ from solving (2.56),

$$A_{1,i}^2(b) = \frac{4 + c_i^2 - |c_i| \sqrt{4 + c_i^2}}{4 + 2c_i^2}, \quad A_{2,i}^2(b) = \frac{4 + c_i^2 + |c_i| \sqrt{4 + c_i^2}}{4 + 2c_i^2}, \quad (2.62)$$

and for the determinant $\Theta_i(b) = \Theta(A_{1,i}, A_{2,i}, b)$ from (2.59)

$$\Theta_i(b) = -2(4 + c_i^2)/c_i', \quad (2.63)$$

where a prime $(\cdot)'$ is used to indicate differentiation with respect to b . The functions c_i ($i = 1, 2$) correspond to $c(\mathbf{A})$ evaluated at \mathbf{A}_i^* , i. e. $c_i(b) = c(\mathbf{A}_i^*(b))$.

For stationary (i. e. synchronized) solutions of the original system (2.42) it is still required that there exist frequency detunings $\tilde{\Delta}_1, \tilde{\Delta}_2$ in compliance with (2.53)₂, namely

$$\tilde{\Delta}_1(\tilde{\beta}, b) = -c_1(b)\sqrt{\tilde{\beta}^2 - b^2} \quad \text{and} \quad \tilde{\Delta}_2(\tilde{\beta}, b) = -c_2(b)\sqrt{\tilde{\beta}^2 - b^2}. \quad (2.64)$$

In the $(\tilde{\Delta}, \tilde{\beta})$ -space, equations (2.64) define two one-parameter arrays of curves depending on b , the graphs of which are shown in Figure 2.3b. The notations \mathbf{S}_1 and \mathbf{S}_2 shall be introduced for the solution triples $\mathbf{S}_1 = (\mathbf{A}_1^*, \tilde{\Delta}_1)$ and $\mathbf{S}_2 = (\mathbf{A}_2^*, \tilde{\Delta}_2)$ of (2.53) indicating synchronized solutions of (2.42) with amplitudes \mathbf{A}_i^* for a frequency detuning $\tilde{\Delta}_i$ given by (2.64). Observing Figure 2.3a we remark that at \mathbf{S}_1 the pendula oscillate with amplitudes of roughly the same order of magnitude ($A_{1,1} \approx A_{2,1} \approx 1$) while at \mathbf{S}_2 the amplitude $A_{1,2}$ would be considerably smaller than $A_{2,2}$ which seems physically not feasible and indeed, the instability of \mathbf{S}_2 -type solutions will be shown in due course. Obviously, the graphs of $\tilde{\Delta}_1(\tilde{\beta}, b)$ and $\tilde{\Delta}_2(\tilde{\beta}, b)$ are dense in the $(\tilde{\Delta}, \tilde{\beta})$ -space (see Figure 2.3b) and thus synchronized solutions exist for all pairs $(\tilde{\Delta}, \tilde{\beta})$ since for any given combination $(\tilde{\Delta}, \tilde{\beta})$ at least one value for $b \in [0, b_c]$ can be found such that either (2.64)₁ or (2.64)₂ holds.⁵ The definition of b , (2.54)₂, then yields the corresponding stationary phase shift ψ . In order to check the stability properties of \mathbf{S}_1 and \mathbf{S}_2 equations (2.42)₁₋₃ are transformed in terms of the variables A_1, A_2 and b defining a new vector field

$$\begin{aligned} \dot{A}_1 &= (1 - A_1^2)A_1 - bA_2, \\ \dot{A}_2 &= (1 - A_2^2)A_2 + bA_1, \\ \dot{b} &= \tilde{\Delta}\sqrt{\tilde{\beta}^2 - b^2} + c(A_1, A_2)(\tilde{\beta}^2 - b^2). \end{aligned} \quad (2.65)$$

to which a linear stability analysis is subsequently applied in the standard fashion. Resorting to the well known Routh-Hurwitz criterion use will be made of the Jacobian

⁵Without loss of generality we confine ourselves to $\tilde{\Delta} > 0$ which is just a matter of renumbering the oscillators.

\mathbf{J}_b of (2.65) evaluated for \mathbf{S}_i , viz.

$$\mathbf{J}_b = \begin{pmatrix} 1 - 3A_{1,i}^2 & -b & -A_{2,i} \\ b & 1 - 3A_{2,i}^2 & A_{1,i} \\ A_{2,i}(2 + c_i^2)(\tilde{\beta}^2 - b^2) & -A_{1,i}(2 + c_i^2)(\tilde{\beta}^2 - b^2) & -bc_i \end{pmatrix}, \quad (2.66)$$

as well as its invariants

$$\begin{aligned} p_i &= -\operatorname{tr} \mathbf{J}_b = 4(1 + bc_i), \\ q_i &= \operatorname{tr}(\mathbf{J}_b)^2 - \operatorname{tr}(\mathbf{J}_b \mathbf{J}_b^T) = \Theta_i + bc_i(4 + 3bc_i) + (4 + c_i^2)B(b), \\ \vartheta_i &= -\det \mathbf{J}_b = bc_i \Theta_i + 2(4 + c_i^2)B(b), \\ \chi_i &= p_i q_i - \vartheta_i = (4 + 3bc_i) [\Theta_i + 4bc_i(1 + bc_i)] + 2(1 + 2bc_i)(4 + c_i^2)B(b), \end{aligned} \quad (2.67)$$

where $\tilde{\beta}^2 - b^2$ has been abbreviated by $B(b) \geq 0$ and (2.56) had to be reapplied repeatedly. Thus p_i, q_i, ϑ_i and χ_i may be interpreted as linear functions in $B(b)$ for a given b . The aforementioned criterion then asserts that all eigenvalues of \mathbf{J}_b have a negative real part if

$$p_i > 0, \quad q_i > 0, \quad \vartheta_i > 0, \quad \text{and} \quad \chi_i > 0. \quad (2.68)$$

If $\chi_i = 0$ ($p_i, q_i, \vartheta_i > 0$) the Jacobian \mathbf{J}_b exhibits a pair of purely imaginary eigenvalues announcing a Hopf bifurcation and if $\vartheta_i = 0$ ($p_i, q_i, \chi_i > 0$) a bifurcation at a single zero eigenvalue occurs. Furthermore, it is easy to verify that the inequalities

$$-2 \leq \Theta_2(b) \leq 0 \leq \Theta_1(b) \leq 4, \quad -1 \leq bc_2(b) \leq -\frac{1}{2} \leq bc_1(b) \leq 0 \quad (2.69)$$

hold for all $b \in [-b_c, b_c]$. We now essentially have the prerequisites at hand in order to prove the stability or instability of the fixed points \mathbf{S}_1 and \mathbf{S}_2 .

Proposition 2.1. *Stationary solutions \mathbf{S}_2 are unstable for all $\tilde{\beta} \geq 0$ and $b \in [-b_c, b_c]$.*

Proof. Avoiding an explicit calculation of (2.67) for (2.60)₂ the instability of \mathbf{S}_2 -solutions follows immediately from (2.69) by virtue of which (2.67)₄ may be written as

$$\chi_2 = -|4 + 3bc_2| (|\Theta_2| + |4bc_2| |1 + bc_2|) - 2|1 + 2bc_2| (4 + c_2^2)B < 0$$

which violates (2.68), since both terms are either negative or zero for all $B \geq 0$, $b \in [-b_c, b_c]$. \square

Proposition 2.2. *The family of curves (2.64)₁ in the parameter plane possesses an envelope e which has the equation in parametric form*

$$\tilde{\beta}_e(b)^2 = \frac{c_1}{c'_1} b + b^2, \quad \tilde{\Delta}_e(b) = -c_1 \sqrt{\tilde{\beta}_e^2 - b^2} = -c_1 \sqrt{\frac{c_1}{c'_1} b}. \quad (2.70)$$

The envelope (2.70) is a bifurcation set where the Jacobian matrix of \mathbf{f}_b has one single zero eigenvalue and there exists a number $b_{00} < b_c$ such that for any given $b \in]-b_{00}, b_{00}[$ the associated synchronized solution \mathbf{S}_1 is stable if $\tilde{\beta} > \tilde{\beta}_e(b)$ and $\tilde{\Delta}_1$ given by (2.64)₁.

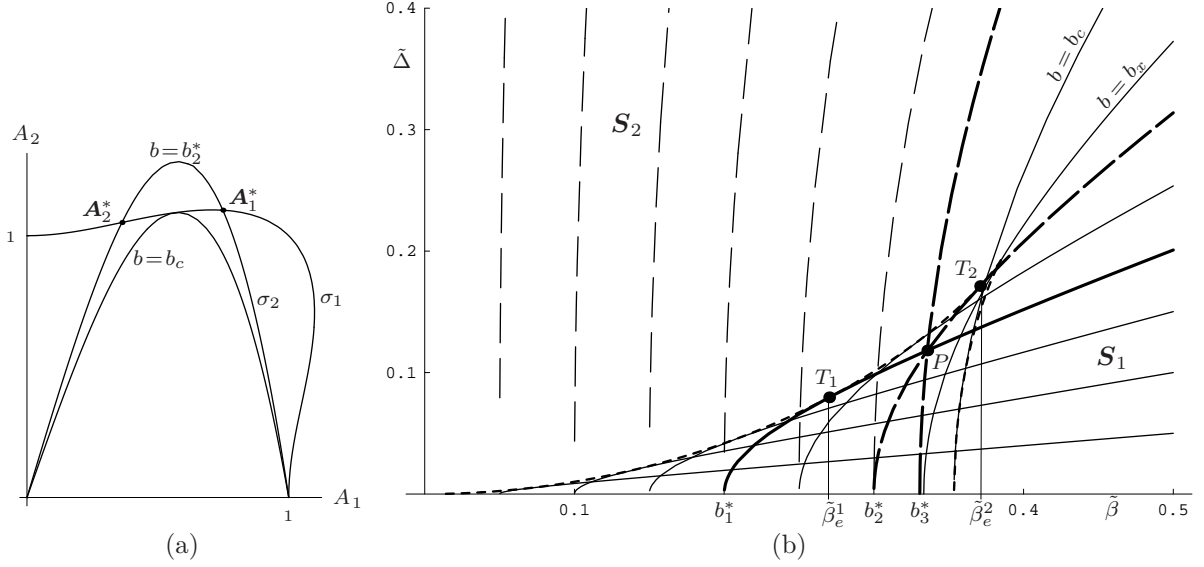


Figure 2.3: (a) Geometrical interpretation of the stationary solutions A_1^* and A_2^* according to equation (2.55). (b) Stratification of the parameter plane, coupling strength $\tilde{\beta}$ versus frequency detuning $\tilde{\Delta}$, into the corresponding synchronized solutions S_1 (solid) and S_2 (dashed). The dotted line indicates the cusp-shaped envelope.

Proof. The representation of the envelope (2.70) is found straightforwardly from solving

$$\tilde{\Delta}_1 + c_1 \sqrt{\tilde{\beta}^2 - b^2} = 0, \quad \frac{\partial}{\partial b} \left(\tilde{\Delta}_1 + c_1 \sqrt{\tilde{\beta}^2 - b^2} \right) = 0,$$

for $\tilde{\Delta}_1$ and $\tilde{\beta}$. Rewriting (2.67)₃ under consideration of (2.63) and solving $\vartheta_1 = 0$ for B immediately yields

$$B|_{\vartheta_1=0} = \tilde{\beta}^2 \Big|_{\vartheta_1=0} - b^2 = \frac{c_1}{c'_1} b$$

which is equivalent to (2.70)₁, i. e. $\tilde{\beta} \Big|_{\vartheta_1=0} = \tilde{\beta}_e$. In order to show that (2.70) is indeed a bifurcation set we have to verify that the remaining invariants are positive for $B(b) = B|_{\vartheta_1=0}$. We observe that p_1 is by (2.69)₂ strictly positive for all $b \in [-b_c, b_c]$; $q_1 > 0$ and consequently $\chi_1 > 0$ holds for $B(b) = B|_{\vartheta_1=0}$ if $2bc_1(4+3bc_1) + \Theta_1(2-bc_1) > 0$, which is obviously fulfilled for $b = 0$ but violated for $b = \pm b_c$. Thus there exists an interval $]-b_{00}, b_{00}[\subset [-b_c, b_c]$ such that $q_1 > 0$ and $\chi_1 > 0$ if $b \in]-b_{00}, b_{00}[$. Using (2.60) as well as (2.63) to replace c_1 and Θ_1 permits a numerical calculation of $b_{00} \cong 0.340089$. Since the coefficients of $B(b)$ in (2.67) are all positive by (2.69), $p_1 > 0, q_1 > 0, \vartheta_1 > 0$ and $\chi_1 > 0$ indeed holds for $B(b) > B|_{\vartheta_1=0}$, i. e. $\tilde{\beta} > \tilde{\beta}_e(b)$, for a given $b \in]-b_{00}, b_{00}[$ and thus S_1 is stable. \square

Proposition 2.3. *The envelope (2.70) exhibits a cusp located at $b_x = 1/3$, $\tilde{\beta}_x = 2/(3\sqrt{3})$, $\tilde{\Delta}_x = 1/(3\sqrt{3})$.*

Proof. The parameter value b_x where the cusp is located can be calculated from the condition that $\partial \tilde{\beta}_e^2 / \partial b = 0$ (which implies that $\partial \tilde{\Delta}_e / \partial b = 0$) at $b = b_x$ yielding

$$3b_x c'_1(b_x)^2 + c_1(b_x)(c'_1(b_x) - b_x c''_1(b_x)) = 0.$$

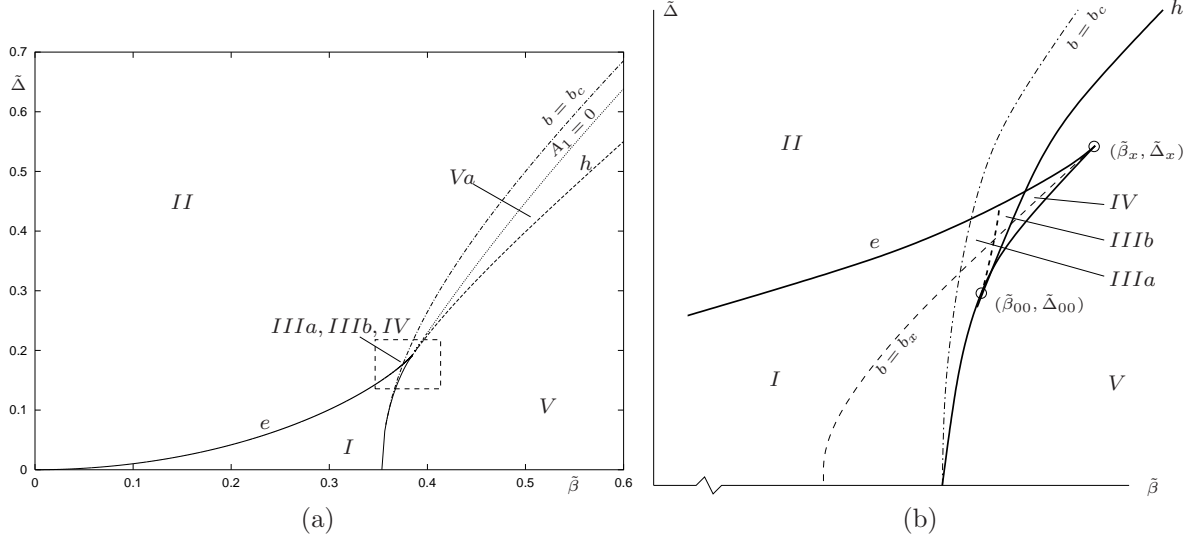


Figure 2.4: (a) A coarse global stratification of the parameter plane including the envelope e and the Hopf bifurcation line h . (b) Enlargement of the frame shown in Figure 2.4a (qualitatively sketched).

After employing $(2.60)_1$ the solution $b_x = 1/3$ may be found analytically together with the associated values $\tilde{\beta}_x = \tilde{\beta}_e(b_x)$ and $\tilde{\Delta}_x = \tilde{\Delta}_e(b_x)$. \square

Proposition 2.4. For $b \in [b_{00}, b_c]$ the curve h , defined by

$$\tilde{\beta}_h(b) = \sqrt{B_h(b) + b^2}, \quad \tilde{\Delta}_h(b) = -c_1(b)\sqrt{B_h(b)}, \quad (2.71)$$

where B_h is given by

$$B_h(b) = -\frac{(4 + 3bc_1)[\Theta_1 + 4bc_1(1 + bc_1)]}{2(1 + 2bc_1)(4 + c_1^2)}, \quad (2.72)$$

defines a bifurcation set where the Jacobian of \mathbf{f}_b has a purely imaginary pair of eigenvalues indicating a Hopf bifurcation. For $\tilde{\beta} > \tilde{\beta}_h(b)$, \mathbf{S}_1 is stable.

Proof. The expression (2.72) is again immediately found from solving $\chi_1 = 0$ in $(2.67)_4$ for B . All further reasoning is similar to the proof of Proposition 2.2 and shall not be repeated. \square

The preceding propositions suggest that codimension 2 singularities will occur at $b = b_x$ as well as at $b = b_{00}$. The first case can intuitively be recognized as a cusp bifurcation (GUCKENHEIMER & HOLMES [1983], TROGER & STEINDL [1991]). In the second case we are facing a double zero eigenvalue since the determinant and the second invariant of \mathbf{J}_b are zero while the trace is still negative. If so, it is well known that the local behavior in a neighborhood of the singular point $\mathbf{A}_1^*(b_{00})$ is governed by the Bogdanov-Takens normal form (GUCKENHEIMER & HOLMES [1983])

$$\dot{z}_1 = z_2, \quad \dot{z}_2 = \eta_1 + \eta_2 z_2 + \kappa_1 z_1^2 + \kappa_2 z_1 z_2, \quad (2.73)$$

where z_1, z_2 are coordinates on a two dimensional center manifold and η_1, η_2 are unfolding parameters. Actually, the task is only to find the coefficients κ_1 and κ_2 in (2.73) which is

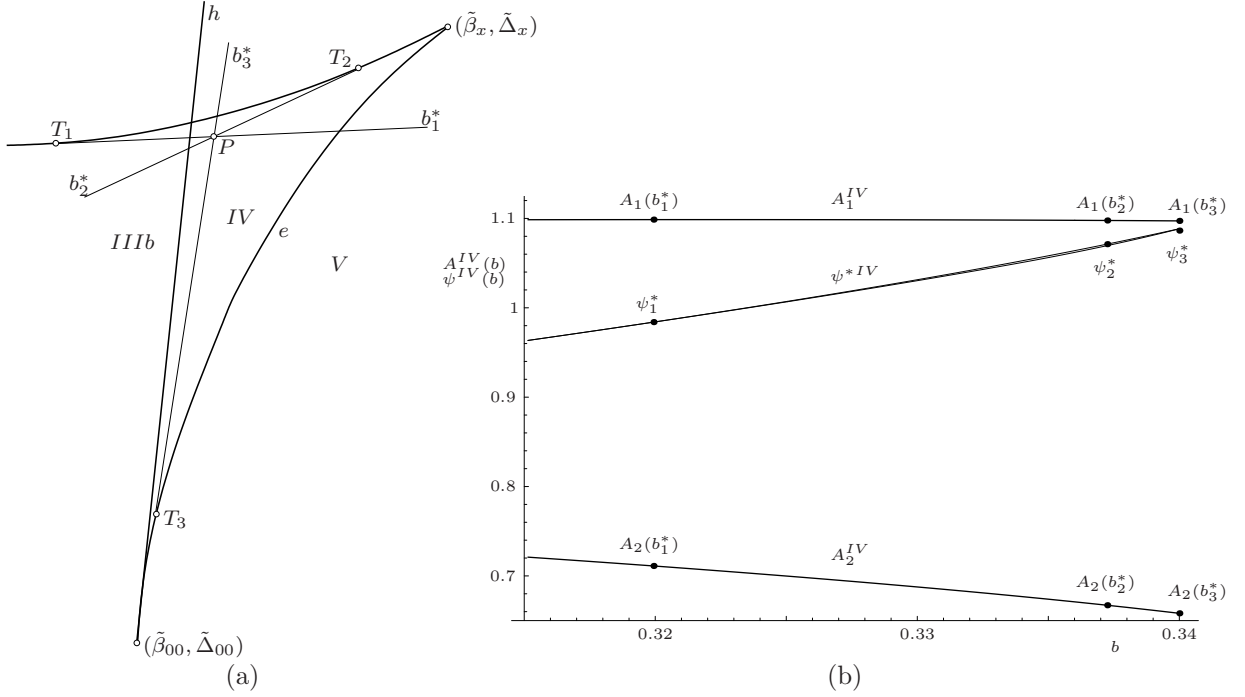


Figure 2.5: (a) Enlargement of region IV in Figure 2.4b. (b) Synchronized amplitudes A^{IV} and phases ψ^{IV} occurring in region IV .

considerably facilitated by the analytical representation (2.62). However, the calculation has to be performed numerically in the standard fashion and we shall be content with stating our results

$$\kappa_1 \cong 0.16670, \quad \kappa_2 \cong -5.48513.$$

Since the topological behavior of (2.73) in fact depends only on the sign of κ_2 we obtain the same type of bifurcations as studied extensively for the periodically driven Van-der-Pol oscillator in HOLMES & RAND [1978]. Comparing their analysis with the results discussed here, obviously the coupling in the considered example plays the role of the driving amplitude of a forced oscillator and the frequency detuning in the coupled system can likewise be identified with the difference between the squares of the eigen-frequency of a single forced oscillator and the frequency of the forcing.

2.4 Discussion and comparison of the results

A qualitative illustration of Propositions 2.2–2.4 in the parameter plane of $\tilde{\beta}$ versus $\tilde{\Delta}$ is drawn in Figure 2.4 and we shall now stress its interpretation with respect to the auxiliary parameter b taking advantage of the curves $b = \text{const.}$ in Figure 2.3b, which will be called b -lines for simplicity.

An arbitrary point $P = (\tilde{\beta}^*, \tilde{\Delta}^*)$ from the domain I in Figure 2.4 can be regarded as the intersection of three distinct b -lines with $b = b_1^*$ and $b = b_2^*$ belonging to different \mathcal{S}_1 -solutions as well as $b = b_3^*$ corresponding to a solution \mathcal{S}_2 (Figure 2.3b). The points of tangency of the curves for b_1^* and b_2^* with the envelope are T_1 and T_2 in Figure 2.3b, where $\tilde{\beta}_e^1 = \tilde{\beta}_e(b_1^*)$ and $\tilde{\beta}_e^2 = \tilde{\beta}_e(b_2^*)$. The values b_i^* then are associated with synchronized

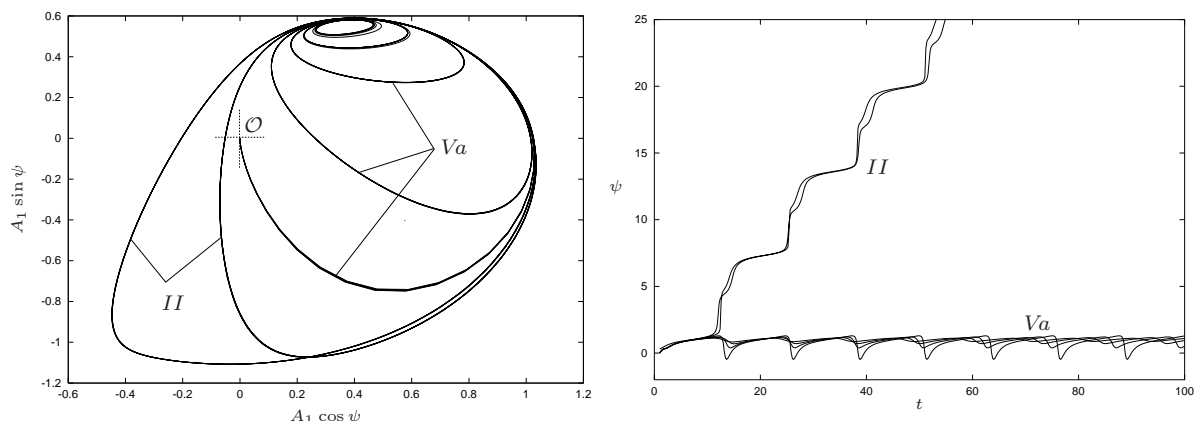


Figure 2.6: Evolution of the limit cycle due to the Hopf bifurcation at h in Figure 2.4a presented in polar coordinates $A_1 \cos \psi$, $A_1 \sin \psi$. Solutions Va are still synchronized with an oscillating but bounded phase shift. The phase starts rotating in region II after the limit cycle has encircled the origin \mathcal{O} .

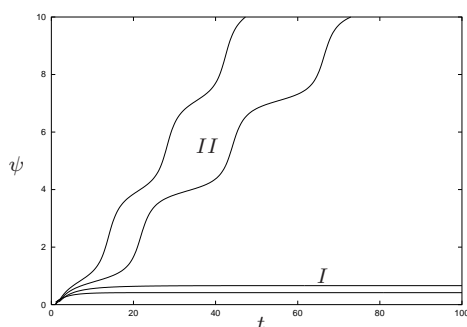


Figure 2.7: Evolution of the phase difference ψ crossing the envelope from region I to II in Figure 2.4a.

phase shifts ψ_i^* whereof $\psi_1^* = \arcsin(b_1^*/\tilde{\beta}^*)$ is the only stable one since $\tilde{\beta}^* > \tilde{\beta}_e^1$ (cf. Proposition 2.2) – sloppily speaking, P lies “beyond” the point of tangency T_1 on a b -line; b_1 thus corresponds to a stable synchronized phase shift close to zero since $b_1^* \ll \tilde{\beta}^*$. The values b_2^* and b_3^* represent unstable synchronized solutions for $\tilde{\beta}^* < \tilde{\beta}_e^2$ and b_3^* is a generally unstable \mathbf{S}_2 -solution. The associated phase shifts ψ_2^*, ψ_3^* will be close to $\pi/2$ since $b_2^*/\tilde{\beta}^* \approx b_3^*/\tilde{\beta}^* \approx 1$.

Similarly, in regions $IIIa$ and $IIIb$ there is still only one stable synchronized solution with the mere difference, that the unstable \mathbf{S}_2 -type solution existing in region I has given way to a third stationary solution of the type \mathbf{S}_1 which is unstable, too. In Region IIb , however, it will be surrounded by a stable limit circle. The homoclinic bifurcation that gives birth to this limit cycle is a distinctive feature of the Bogdanov-Takens bifurcation at b_{00} which is well understood, and for a detailed analysis the reader is again referred to HOLMES & RAND [1978] or GUCKENHEIMER & HOLMES [1983].

It should by now also be clear that in region V there exists only one stable \mathbf{S}_1 -type synchronized motion (cf. Figure 2.3b) with a phase shift close to zero similar as in region I .

Interestingly, two stable synchronized solutions occur in the tiny region IV , and one is tempted to ask whether these are physically pertinent. Applying the same graphical technique as described previously, we obtain for a point P in region IV three intersecting b -lines, b_1^*, b_2^*, b_3^* , among the family of \mathcal{S}_1 -solutions (Figure 2.5a). The line b_1^* corresponds to a stable synchronized solution by Proposition 2.2, the solution associated with b_2^* again is unstable since the point of tangency T_2 of the b -line with the envelope e is located beyond P ; b_3^* is stable either by Proposition 2.2 if $b_3^* < b_{00}$ or otherwise by Proposition 2.4. Clearly, these solutions exist only for those b -lines entering IV which happens for b in the interval $[0.315140, 0.340103]$, obtained numerically. With the aid of (2.62) it is straightforward to compute all possible amplitudes $A_1^{IV}(b)$ and $A_2^{IV}(b)$ accompanied with the phase shifts $\psi^{*IV}(\tilde{\beta}, b)$ appearing in region IV (Figure 2.5b). Comparing the numerical values of $\tilde{\beta}_x$ and $\tilde{\beta}_{00}$ we observe that they differ only by 10^{-3} and thus we may obtain $\psi^{*IV}(\tilde{\beta}, b) \approx \psi^{*IV}(b)$ approximately from $\psi^{*IV}(b) = \arcsin(b/\tilde{\beta}_{00})$ for b in the above interval. Figure 2.5b now demonstrates that the amplitudes as well as the phase shift for the different synchronized solutions in IV are so close to each other that physically, a qualitative difference would not be observable.

Equally as described in PIKOVSKY ET AL. [2001] synchronization is lost crossing the envelope e from I to II by a global saddle-node bifurcation which gives rise to a stable quasi periodic regime where the phase difference increases steadily (Figure 2.7). However, at the Hopf-bifurcation curve h synchronization is still maintained since the phase shift ψ starts oscillating, though, but remains bounded (Figure 2.6b). The solution finally starts drifting if the bifurcating limit cycle hits one of the degenerate singularities at $A_1 = 0$ or $A_2 = 0$, respectively, and thus becomes in fact a homoclinic orbit (Figure 2.6a). This phenomenon was described for periodically driven oscillators in PIKOVSKY ET AL. [2001] and for two coupled Van-der-Pol equations in CHAKRABORTY & RAND [1988]. The bifurcation line where $A_1 = 0$ separating regions II and Va was determined numerically by a straightforward homotopy method and is inserted into the coarse bifurcation diagram Figure 2.4.

Up to now, three results are available regarding the existence and stability of synchronized solutions of two coupled Van-der-Pol equations and in the following we shall relate the outcomes of Sections 2.3.2 and 2.3.3 with the rather comprehensive results of §2.3.3. In Section 2.3.2 we found, that for strong coupling the oscillators are always synchronized similar to the case of identical coupled pendula if the frequency detuning due to the length difference is assumed to be small. This obviously is in compliance with Figure 2.3b, where for sufficiently large $\tilde{\beta}$ synchronized solutions of the \mathcal{S}_1 -type are always found. For large coupling *and* frequency detunings we found in TEUFEL ET AL. [2003] essentially the same result using normal form theory as obtained in STORTI & RAND [1982] by means of more intricate perturbation techniques, namely the synchronization threshold to be $\tilde{\Delta} = \sqrt{2}\tilde{\beta}$. It is easy to verify that this is an asymptote to the Hopf-bifurcation line (2.71) i. e. that $\lim_{b \rightarrow b_c} (\tilde{\Delta}_h/\tilde{\beta}_h) = c_1(b_c) = \sqrt{2}$ which follows from $B_h(b_c) = \infty$. The representation of the envelope (2.70) together with the solution (2.60) permits to calculate a Taylor series expansion for $\tilde{\Delta}_e(\tilde{\beta})$ which takes the form

$$\tilde{\Delta}_e(\tilde{\beta}) = \frac{3}{2\sqrt{2}}\tilde{\beta}^2 + O(\tilde{\beta}^4) \approx 1.06\tilde{\beta}^2. \quad (2.74)$$

2 Synchronization phenomena

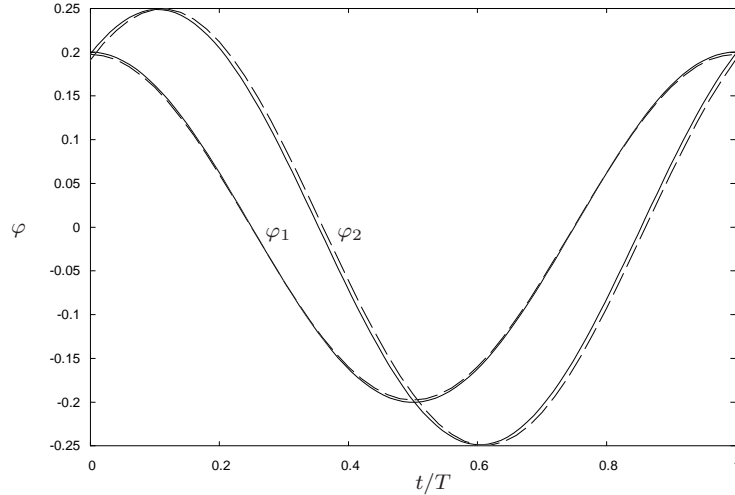


Figure 2.8: Comparison of analytical (solid) and numerical (dashed) results for the original deflection angles φ of the pendula plotted for one period.

This reveals that the perturbation expansion (2.46) in §2.3.3 indeed yields an acceptable approximation to the “exact” result (2.74). Moreover, it can be shown that the bifurcation sets (2.70) and (2.71) coincide with the representations presented in CHAKRABORTY & RAND [1988] if the parameter b is eliminated.

A remark on in- and anti-phase synchronization

Note, that the transformation (2.54) is only unique for $-\pi/2 \leq \psi \leq \pi/2$. For $\pi/2 < \psi < 3\pi/2$ we have to change the $+$ sign in (2.53)₂ since the cosine function then is negative. However, the vector field defined by the averaged equations (2.42)₁₋₃ is equivariant under the symmetry transformation $A_1 \rightarrow A_2$, $A_2 \rightarrow A_1$, $\psi \rightarrow \psi + \pi$ (TROGER & STEINDL [1991]). Therefore, any stationary phase shift ψ found in §2.3.3 can be rotated by π without altering the results but swapping the roles of A_1 and A_2 . Thus the stability of an anti-phase regime $\psi + \pi$ is carried over to the associated in-phase regime ψ and the occurrence of in- or anti-phase synchronization is a matter of initial conditions.

Numerical verification

In order to demonstrate practically the procedure of calculating synchronized solutions, an exemplary case shall now be worked out. Choose for instance

$$b = 0.2, \quad \tilde{\beta} = 0.33,$$

corresponding roughly to the point P in Figure 2.3. Then (2.64)₁ yields the frequency detuning $\tilde{\Delta} = 0.115087$ which produces a stable synchronized regime. Selecting furthermore $\mu = 0.4$, $\alpha = 0.1$ and $\omega_1 = 10$ permits to calculate β and ω_2 from (2.44), $\omega_2 = 9.953$, $\beta = 1.32$. The values of the amplitudes A_1^* , A_2^* are calculated from formulas (2.62), as well as the phase shift ψ^* from (2.54)₂ and the synchronous frequency ω_s from (2.45), which yields

$$A_1^* = 1.07745, \quad A_2^* = 0.86684, \quad \psi^* = 0.65110, \quad \omega_s = 10.000747. \quad (2.75)$$

After reapplying the transformations (2.43), (2.40) and (2.9), the analytical approximation of the synchronized vibration modes in terms of the angles of the pendula is found to be

$$\varphi_1(t) = \frac{2A_1^*}{\omega_s} \sqrt{\frac{\mu}{3\alpha}} \sin(\omega_s t) + \text{h.o.t.}, \quad \varphi_2(t) = \frac{2A_2^*}{\omega_s} \sqrt{\frac{\mu}{3\alpha}} \sin(\omega_s t - \psi^*) + \text{h.o.t.},$$

which is illustrated in Figure 2.8 in comparison with the numerical result. Numerically, for the parameter values given above and $\gamma = 0$ the synchronized periodic solution was obtained straightforwardly from solving (2.7) complemented by the trivial equation for the period $\dot{T} = 0$ as a boundary value problem using a multiple shooting method implemented in the software package BOUNDSCO (OBERLE ET AL. [1985]). If the time is scaled by T the boundary conditions take the form $\varphi_i(0) = \varphi_i(1)$, $\dot{\varphi}_i(0) = \dot{\varphi}_i(1)$ and $\varphi_1(0) = \varphi_2(0)$. The numerical computation yields a value for the synchronous frequency as $2\pi/T = 10.00164$ which supports the assertion that the frequency of the synchronous oscillation might well be higher than both natural frequencies of the uncoupled oscillators. Likewise, this is fortified by the analytical result (2.75) and formula (2.45). Thus the prevailing assumption, that the synchronous frequency was the arithmetic mean of the natural frequencies, is neither justified nor necessary.

2.5 Conclusion

It has been shown that two different coupled pendula can be synchronized by a fluid flow in the sense that they oscillate with a common frequency which is different from their natural frequencies. The stationary solutions of the averaged equations of motion are identified with synchronized motions of the coupled system. Conditions have been derived for the existence and stability of these synchronized motions depending on the coupling strength and the frequency detuning. In particular for the case of strong coupling classical normal form theory provided a simple means of interpreting the oscillation modes on a center manifold as in-phase or anti-phase synchronized motions. In the case of weak coupling a graphical interpretation of the synchronized phase shifts was given using an auxiliary parameter in the averaged equations. Remarkably, an analytical solution for the amplitudes as well as the synchronous frequency in the synchronized regime could be found and previous findings could be embedded into the present approach.

3 Non-smooth bifurcations of mechanical systems with 1-d.o.f involving friction

It was in 1785 that Charles Augustin de COULOMB formulated the idea that friction is the force necessary to overcome the asperities of two contacting surfaces in order to initiate slipping. Although this notion is clear from common sense, its deeper mathematical and physical foundations are yet far from being completely settled. Coulomb asserted a linear proportionality between the normal load and the friction force, independent of the sliding velocity. Originating from Coulomb's law an abundance of models have been developed, each aiming for a functional relationship between the applied load and both, the static and the dynamic friction force, depending on various physical parameters, such as the relative velocity of the surfaces in contact, the temperature or the contact time. From a mathematical point of view non-smooth nonlinearities are conceptually induced to the problem due to the obvious distinction of static and dynamic friction. Unlike inertia forces which "smoothly" counteract motion, friction forces are capable of inhibiting motion at all unless a critical load is applied in the "limit of static friction", which merely explains the everyday observation that a body keeps sticking on a surface if the applied forces are small enough. If this critical load is reached and a motion sets in, the friction force acting against the direction of motion typically experiences a sudden "non-smooth" change or even a jump, depending on parameters which appear due to the dynamics of the system, such as typically the relative velocity.

Consequently in a mathematical modeling approach a friction law has to be selected with a minimal set of parameters where mathematical complexity has to be balanced with physical significance. One might be tempted to ask the question the other way around: which friction law is necessary to produce which physical effect? Actually, this shall be the main question during the remainder of this thesis: we stay within the concept of a proportionality between the normal force and the friction force and let the coefficient of proportionality (the "friction coefficient") be mathematically given by a function of the relative velocity, the shape of which is determined by three descriptive geometrical parameters and has both, a decreasing and increasing part depending on the relative velocity (Section 3.1.4).

A widespread mathematical framework to deal with non-smooth systems is *Filippov-Theory*, the foundations of which are explained in Section 3.1.1. For more information the reader is referred to FILIPPOV [1988], LEINE [2000], AWREJCWICZ & LAMARQUE [2003] or KUZNETSOV ET AL. [2003]. It will be shown in Section 3.1.2 that friction oscillators naturally belong to the class of Filippov-systems. The effects of a 3-parameter friction law applied to a simple one degree-of-freedom (1-d.o.f.) friction oscillator are

studied in Section 3.2 which provides a basis for the understanding of the analysis performed in Chapter 4 dealing with friction induced travelling waves.

3.1 Introduction to non-smooth systems

In the following we are concerned with piecewise smooth systems (p.s.s.) which are described by a set of m n -dimensional ordinary differential equations of the form (KUZNETSOV ET AL. [2003])

$$\dot{\mathbf{x}} = \mathbf{f}_i(\mathbf{x}), \quad \mathbf{x} \in S_i \subset \mathbb{R}^n, \quad i = 1, \dots, m. \quad (3.1)$$

We have to be more generous than KUZNETSOV ET AL. [2003] and do not make any restrictions on the dimension of the subregions S_i . We merely require them to be open and non-overlapping (see Chapter 4 for an example). The subregions S_i are delimited by boundaries Σ_j . From a mechanical point of view these discontinuities are typically induced by contact problems possibly involving friction. While friction in systems with one degree of freedom will be the main issue of this chapter an infinite dimensional example will be treated in Chapter 4 where also the loss of contact between two bodies introduces a discontinuity to the system.

A p.s.s. is said to be *continuous* with respect to a boundary Σ_k if $\mathbf{f}_i(\mathbf{x}) = \mathbf{f}_j(\mathbf{x}) \forall \mathbf{x} \in \Sigma_k$ where Σ_k separates S_i from S_j . If a system is not continuous with respect to a discontinuity and thus $\mathbf{f}_i(\mathbf{x}) \neq \mathbf{f}_j(\mathbf{x})$ on Σ_k then we call the system a *Filippov System*. If we address a FILIPPOV system here we always have to refer to a certain boundary since the complete system (3.1) may possess other discontinuities with respect to which it may well be non-Filippov (continuous) as for the example in Chapter 4.

3.1.1 Filippov Systems

In Filippov systems a trajectory has two possibilities to cross a boundary depending on the signs of the transversal components of the adjacent vector fields. Let the discontinuity be described by an equation $\Sigma : \mathbf{H}(\mathbf{x}) = 0$ and let \mathbf{f}_1 denote the vector field in S_1 where per definition $\mathbf{H}(\mathbf{x}) < 0$ and \mathbf{f}_2 denote the vector field in S_2 where $\mathbf{H}(\mathbf{x}) > 0$. The auxiliary quantity $s = (\text{grad } \mathbf{H}(\mathbf{x}) \cdot \mathbf{f}_1(\mathbf{x}))(\text{grad } \mathbf{H}(\mathbf{x}) \cdot \mathbf{f}_2(\mathbf{x})) > 0$ is defined for $\mathbf{x} \in \Sigma_k$ which is positive if \mathbf{f}_1 and \mathbf{f}_2 point in the same direction on Σ_k and negative if they point in the opposite direction. If $s > 0$ a trajectory will cross the boundary and has a discontinuity in its derivative. Otherwise, if $s \leq 0$ trajectories will either be pushed towards Σ from both subdomains S_1 and S_2 or the vector fields, both in S_1 and S_2 , want to tear a point away from Σ . In any case, if a trajectory enters Σ inside a domain where $s \leq 0$ by whatever means it will stay there. Thus, the condition $s \leq 0$ defines a *sticking*¹ set on Σ .

If $\text{grad } \mathbf{H} \cdot \mathbf{f}_1 > 0$ and $\text{grad } \mathbf{H} \cdot \mathbf{f}_2 < 0$ on Σ the sticking set is *attracting*. The sticking region in the phase space of a friction oscillator which mechanically describes

¹In mathematically oriented publications (e. g. KUZNETSOV ET AL. [2003], LEINE [2000], LUO [2004], LUO [2007]) consistently the term *sliding* is used for a solution that stays on Σ . Here, we want to refrain from this expression in order to avoid confusions with its mechanical meaning and, in view of the mechanical applications, use *sticking* instead.

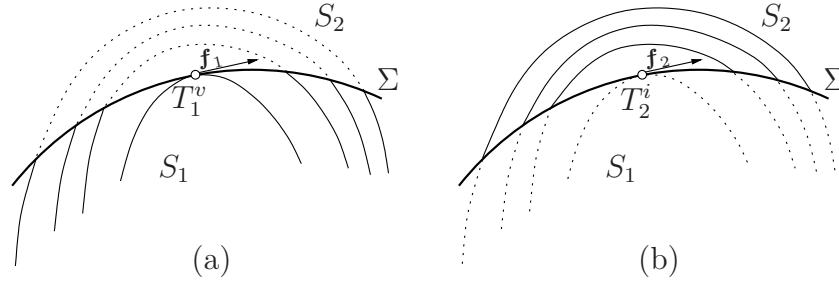


Figure 3.1: Examples of tangent points, (a) Visible tangent point T_1^v of \mathbf{f}_1 , (b) invisible tangent point T_2^i of \mathbf{f}_2 . Dotted curves indicate, respectively, the (invisible) extension of the trajectories to the opposite subdomain.

static friction is a typical example for an attracting sticking set (see Section 3.2).

If $\text{grad } \mathbf{H} \cdot \mathbf{f}_1 < 0$ and $\text{grad } \mathbf{H} \cdot \mathbf{f}_2 > 0$ on Σ , the sticking set is *repelling*. Although a solution that stays on a repelling sticking set is defined by Filippov theory (FILIPPOV [1988], LEINE [2000]) it is not unique. It may stay on Σ but likewise exit to the adjacent domains S_1 or S_2 . This will happen for certain parameter combinations in the shaft-bush problem considered in Chapter 4 (see Figure 4.6).

Yet, a vector field has to be *defined* inside a sticking set on Σ since the \mathbf{f}_i are ambiguous there. A method to define the derivative $\mathbf{g}(\mathbf{x})$ of a sticking motion in the aforementioned sense was given by FILIPPOV [1988] and is such to construct a convex combination of \mathbf{f}_1 and \mathbf{f}_2 , viz.

$$\dot{\mathbf{x}} = \mathbf{g}(\mathbf{x}), \quad \mathbf{g}(\mathbf{x}) = \lambda \mathbf{f}_1(\mathbf{x}) + (1 - \lambda) \mathbf{f}_2(\mathbf{x}), \quad \lambda = \frac{\text{grad } \mathbf{H} \cdot \mathbf{f}_2}{\text{grad } \mathbf{H} \cdot (\mathbf{f}_2 - \mathbf{f}_1)}, \quad (3.2)$$

$$\mathbf{x} \in \Sigma_k, \quad \lambda \in [0, 1].$$

This construction will be demonstrated geometrically for the example of a simple friction oscillator in Section 3.2 and Figure 3.7. Obviously, $\lambda = 0$ if \mathbf{f}_2 is tangent to Σ_k or $\mathbf{f}_2 = \mathbf{0}$ and $\lambda = 1$ if \mathbf{f}_1 is tangent to Σ_k or $\mathbf{f}_1 = \mathbf{0}$. Thus sticking intervals are bounded either by *tangent points* of the vector fields with the discontinuity or by so-called *boundary equilibria* of $(3.2)_1$. Equilibria where $\mathbf{g}(\mathbf{x}) = \mathbf{0}$ inside Σ_k are called *pseudo equilibria*.

A tangent point of a vector field \mathbf{f}_i with Σ may either be *visible* if the trajectory that produces the tangency is visible in S_i . It is called *invisible* if the trajectory containing the tangent point is not visible in S_i . Figure 3.1 shall clarify this notion.

3.1.2 Bifurcations in planar Filippov systems

Considering a p.s.s. of the form (3.1) it is intuitively evident that inside each domain S_i all kinds of different smooth solutions and their bifurcations may appear in the same manner as in smooth systems. However, qualitative changes in the types of solutions are expected if a trajectory interacts with the discontinuities, i. e. eventually crosses or sticks on them. For planar Filippov systems with one discontinuity KUZNETSOV ET AL. [2003] have given a comprehensive listing of all possible codimension-1 bifurcations that stem from the presence of the discontinuity in the phase space. Without repeating

their treatise we give a rough outline of their classification. They distinguish five groups of basic bifurcation mechanisms in Filippov systems:

- (i.) Collisions of equilibria with the discontinuity,
- (ii.) Collisions of tangent points,
- (iii.) Collisions of pseudo equilibria,
- (iv.) Bifurcations of cycles with sticking segments²,
- (v.) Pseudo-homoclinic and pseudo-heteroclinic bifurcations.

Since these types of bifurcations are not yet well established among the engineering community a complete assembly of all the types found by KUZNETSOV ET AL. [2003] shall be given in the following Table 3.1 although we already want to mention that for the examples considered here only a few of them are relevant. Nevertheless short explanations of the mechanisms are given in the table and sketches of the phase portraits are presented from Kuznetsov's paper. Most of the time we stick to their nomenclature, however sometimes different names will be introduced in view of the following applications. For cycles which include sticking segments we will already use the succinct term *stick-slip cycle* which will be explained in Section 3.2.2. For all further details the reader is referred to the original paper. A mathematically more sophisticated approach towards bifurcations in discontinuous dynamical systems is found e. g. in LUO [2004] and LUO [2007].

²Frequently called *sliding bifurcations* (e. g. DI BERNARDO ET AL. [2002])

Table 3.1: Classification of non-smooth bifurcations in a planar Filippov systems following KUZNETSOV ET AL. [2003].

T ... tangent point,
 X ... equilibrium,
 P ... pseudo-equilibrium,
 L ... closed cycle,
 $()_{\alpha}$... generic cases,
 $()_0$... at the bifurcation,
 $()^i$... counters,
 $()^{(i)}$... refers to the i -th subdomain S_i .

Description	Phase-portraits		
	before bifurcation	at bifurcation	after bifurcation
(i.) <i>Collisions of equilibria with the discontinuity</i>			
Boundary focus bifurcations			
BF₁: Collision of T , P and X accompanied by the annihilation of a limit cycle			
BF₂: Collision of T , P and X whereupon P and X are extinguished			
BF₃: Collision of T and X accompanied by the annihilation of a limit cycle and the birth of a stable pseudo-node			
BF₄: Collision of T and X accompanied by the birth of an unstable pseudo-node			

continued on next page

3 Non-smooth bifurcations of mechanical systems with 1-d.o.f involving friction

<p>BF₅: Collision of T, P and X similar to BF₂: except that the sticking segment is repelling.</p>			
<p>Boundary node bifurcations</p>			
<p>BN₁: Collision of T and X giving birth to a pseudo-node</p>			
<p>BN₂: Collision of T, P and X whereupon P and X are extinguished</p>			
<p>Boundary saddle bifurcations</p>			
<p>BS₁: Collision of T, P and X whereupon P and X are extinguished.</p>			
<p>BS₂: Collision of T, P and X whereupon P and X are extinguished. A difference w.r.t BS₁: is found in the slope of the saddle's unstable manifold.</p>			

continued on next page

3 Non-smooth bifurcations of mechanical systems with 1-d.o.f involving friction

<p>BS_3: Collision of T and X: a standard saddle becomes a pseudo-saddle.</p>			
<p>(ii.) <i>Collisions of equilibria with the discontinuity</i></p>			
<p>Double tangency bifurcations</p>			
<p>DT_1: Disappearance of a sticking segment</p>			
<p>DT_2: Closing of a crossing window</p>			

continued on next page

3 Non-smooth bifurcations of mechanical systems with 1-d.o.f involving friction

Collision of two visible tangent points			
<p>VV₁: Closing and reopening of a crossing window</p>			
<p>VV₂: A repelling sticking domain becomes attractive</p>			
Collisions of visible and invisible tangent points			
<p>VI₁: A repelling sticking domain becomes attractive</p>			
<p>VI₂: Collision of a pseudo-saddle with the tangent points accompanied by closing and reopening a crossing window</p>			
<p>VI₃: The collision of an unstable pseudo-node with the tangent points accompanied by closing and reopening a crossing window yields a stable pseudo-node and two tangencies.</p>			

continued on next page

Collisions of two invisible tangent points			
<p>Π_1: Opening and closing of a crossing window</p>			
<p>Π_2: An attracting sticking segment with a pseudo-node becomes repelling.</p>			
(iii.) Collisions of pseudo-equilibria			
Pseudo-saddle-node bifurcation			
<p>PSN: Merger of a pseudo-node with a pseudo-saddle</p>			
(iv.) Bifurcations of cycles with sticking segments			
Grazing (or touching) bifurcations			
<p>GR₁: A stable smooth limit cycle touches the discontinuity and becomes a “stick-slip”-cycle</p>			
<p>GR₂: An unstable smooth limit cycle merges with a non-smooth “stick-slip”-cycle</p>			
Sliding disconnection			

continued on next page

3 Non-smooth bifurcations of mechanical systems with 1-d.o.f involving friction

<p>SD: A “stick-slip”-cycle breaks up after the appearance of a tangency inside the sticking domain.</p>			
Switching bifurcation			
<p>SW: A “stick-slip”-cycle is created with slipping parts in S_1 and S_2.</p>			
Crossing bifurcations			
<p>CR₁: The trajectory in S_2 devours one of two sticking segments. One sticking segment is left.</p>			
<p>CR₂: The trajectory in S_2 devours the only sticking segment which yields a (stable) pure crossing cycle.</p>			

continued on next page

3 Non-smooth bifurcations of mechanical systems with 1-d.o.f involving friction

(v.) Pseudo-homoclinic and pseudo-heteroclinic bifurcations			
Pseudo-homoclinic bifurcations			
<p>HO₁: Bifurcation of a homoclinic orbit to a pseudo-saddle-node</p>			
<p>HO₂: Bifurcation of a sticking homoclinic orbit to a pseudo-saddle</p>			
<p>HO₃: Bifurcation of a sticking pseudo-homoclinic orbit to a saddle accompanied by the annihilation of a limit cycle.</p>			
Pseudo-heteroclinic bifurcations			
<p>HE₁: Bifurcation of a heteroclinic orbit between two pseudo-saddles</p>			
<p>HE₂: Bifurcation of a heteroclinic orbit between a pseudo-saddle and a saddle</p>			

3.1.3 Friction oscillators

Here, we will in the following focus our attention on bifurcations that may occur in mechanical systems involving friction. To this end let us confine our considerations to planar Filippov systems with one discontinuity that stem from the mechanical description of friction oscillators with one degree of freedom. Thus, consider equations of the form

$$\ddot{x} + q(x, \dot{x}) = \text{sgn}(V - \dot{x})p(x, \dot{x}) \quad (3.3)$$

where p and q are smooth functions and the *set valued* sign function is defined by (LEINE [2000])

$$\text{sgn}(v_{rel}) = \begin{cases} -1 & v_{rel} < 0 \\ [-1, 1] & v_{rel} = 0 \\ 1 & v_{rel} > 0 \end{cases} \quad (3.4)$$

x is the degree of freedom of a rigid body which is in frictional contact with a surface moving with velocity V . The r.h.s. of (3.3) models the resulting friction force acting on the body and thus typically is of the form $\mu(v_{rel})F_N(x, \dot{x})$ where F_N is the normal force acting perpendicular to the plane of contact and $\mu(v_{rel})$ models the dynamic coefficient of friction depending on the relative velocity $v_{rel} = V - \dot{x}$ (cf. Section 3.1.4). The function $q(x, \dot{x})$ accounts for all remaining forces acting on the considered body. In the phase plane $(x, y = \dot{x})$ the discontinuity Σ of (3.3) is thus given by the line

$$\Sigma = \{\mathbf{x} = (x, y) \in \mathbb{R}^2 : V - y = 0\}, \quad (3.5)$$

dividing the phase space into the two regions with positive and negative relative velocity, namely

$$S_1 = \{\mathbf{x} \in \mathbb{R}^2 : V - y > 0\}, \quad S_2 = \{\mathbf{x} \in \mathbb{R}^2 : V - y < 0\}. \quad (3.6)$$

The vector fields valid in S_1 and S_2 read

$$\mathbf{f}_1(x, y) = \begin{pmatrix} y \\ -q(x, y) + p(x, y) \end{pmatrix}, \quad \mathbf{f}_2(x, y) = \begin{pmatrix} y \\ -q(x, y) - p(x, y) \end{pmatrix}. \quad (3.7)$$

With the vector fields given by (3.7) it is evident that friction oscillators naturally comply with Filippov's construction of sticking solutions explained in Section 3.1.1 since the x -components of \mathbf{f}_1 and \mathbf{f}_2 are both equal to V on Σ (see Figure 3.7).

The coordinates $(x_T^{(i)}, y_T^{(i)})$ of the tangent points T_i of \mathbf{f}_i delimiting a sticking region on Σ are found from

$$y_T^{(1)} = y_T^{(2)} = V, \quad T_1 : -q(x_T^{(1)}, V) + p(x_T^{(1)}, V) = 0, \quad T_2 : -q(x_T^{(2)}, V) - p(x_T^{(2)}, V) = 0. \quad (3.8)$$

A sticking set may thus be defined on Σ by

$$\Sigma_s = \{\mathbf{x} \in \Sigma : |q(x, V)| \leq p(x, V)\}, \quad (3.9)$$

which includes all points where a trajectory cannot cross the discontinuity. In the planar case the visibility of the tangent points given by (3.8) can be checked by investigating the second derivatives of a trajectory at T_i , which are found to be

$$\left. \frac{d^2y}{dx^2} \right|_{T_1} = \frac{1}{V} \left(\frac{\partial q}{\partial x} - \frac{\partial p}{\partial x} \right) \Big|_{(x_T^{(1)}, V)}, \quad \left. \frac{d^2y}{dx^2} \right|_{T_2} = \frac{1}{V} \left(\frac{\partial q}{\partial x} + \frac{\partial p}{\partial x} \right) \Big|_{(x_T^{(2)}, V)}. \quad (3.10)$$

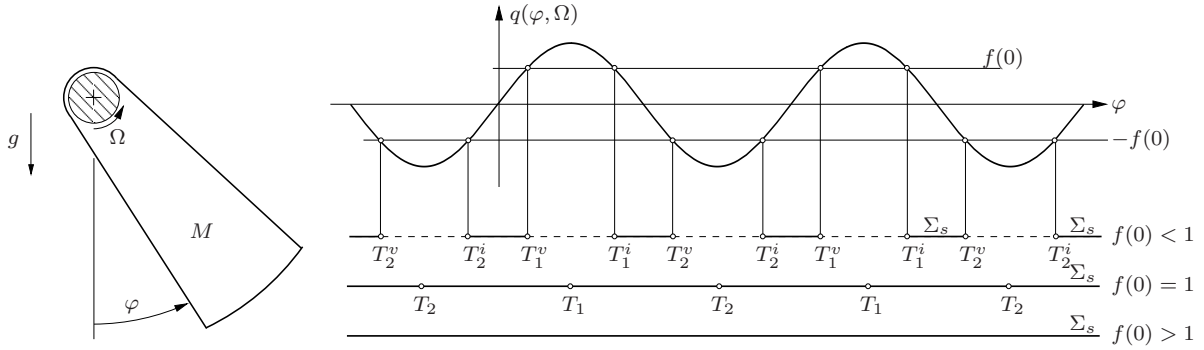


Figure 3.2: Mechanical model of a driven pendulum with friction

Figure 3.3: Construction of visible and invisible tangent points T_i^v , T_i^i and sticking sets Σ_s depending on the friction parameter $f(0)$

A tangent point T_1 is visible if $y''(T_1) < 0$ and invisible if $y''(T_1) > 0$, T_2 is visible if $y''(T_2) > 0$ and invisible if $y''(T_2) < 0$. If $y'' = 0$ the trajectory has a cubic tangency as it is the case for the DT-bifurcations in Table 3.1.

All equilibria (x_0, y_0) of (3.3) fulfill

$$y_0 = 0, \quad q(x_0, 0) = \text{sgn}(V)p(x_0, 0). \quad (3.11)$$

It is easy to check that they are stable if

$$\left(-\frac{\partial q}{\partial y} + \text{sgn}(V)\frac{\partial p}{\partial y} \right) \Big|_{(x_0, 0)} < 0 \quad \text{and} \quad \left(-\frac{\partial q}{\partial x} + \text{sgn}(V)\frac{\partial p}{\partial x} \right) \Big|_{(x_0, 0)} < 0 \quad (3.12)$$

Thus comparing (3.7) with (3.5) reveals that in friction oscillators where the discontinuity is just given by a vanishing relative velocity generally boundary and pseudo equilibria on Σ cannot exist if $V \neq 0$. Obviously, the discontinuity does not cross the x -axis in the phase plane and hence, the cases (i.), (iii.) and (v.) in KUZNETSOV's classification are not applicable for friction oscillators of the form (3.3). If $V = 0$ we are facing a degenerate situation where the sticking domain is filled with infinitely many equilibria. This is mathematically due to the fact that $\text{sgn}(0)$ as defined in (3.4) takes all values from 0 to 1. From a mechanical point of view this is consistent with the notion of static friction. Thus case (i.) is degenerate for friction oscillators and will be illustrated in more detail for the simplest mechanical model – a mass on a driven belt – in Section 3.2 and Figure 3.9. Beyond that, we only expect bifurcations falling in categories (ii.) and (iv.). A mechanical example illustrating the collision of tangent points (ii.) is sketched below without going into details. A concise non-smooth bifurcation analysis will be presented in Section 3.2 for the aforementioned simple friction oscillator, where the possible types of bifurcations of cycles with sticking segments (iv.) will be explained exemplarily.

Example: Sticking set of a Froude -Pendulum

Consider the academic but instructive example of a pendulum (mass M) installed on a shaft which is rotating with angular velocity Ω (Figure 3.2). Gravitation is active and friction shall be present between the pendulum and the shaft (Figure 3.2). With an

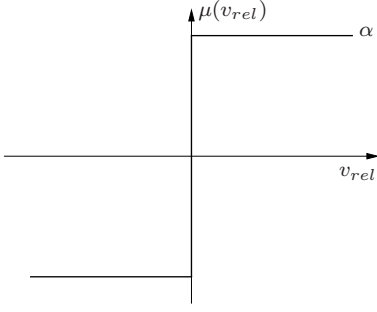


Figure 3.4: Coulomb's friction model

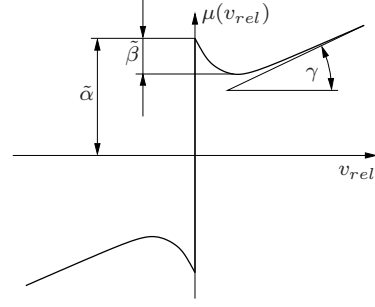


Figure 3.5: General friction law with three parameters.

appropriate scaling the deflection angle φ of the friction-pendulum, known as *Froude-pendulum* obeys the o.d.e.

$$\ddot{\varphi} + \sin \varphi = \operatorname{sgn}(\Omega - \dot{\varphi})f(\Omega - \dot{\varphi}), \quad (3.13)$$

where f incorporates some friction law (see Section 3.1.4). For the construction of the sticking set Σ_s given by (3.9) we compute the tangent points T_1, T_2 by (3.8) and get

$$\dot{\varphi}_T^{(1)} = \dot{\varphi}_T^{(2)} = \Omega, \quad T_1 : \sin(\varphi_T^{(1)}) = f(0), \quad T_2 : \sin(\varphi_T^{(2)}) = -f(0). \quad (3.14)$$

The visibility of the tangent points in (3.14) is determined by (3.10) which applied to the current example yields

$$\left. \frac{d^2 y}{dx^2} \right|_{T_i} = \frac{1}{\Omega} \cos(\varphi_T^{(i)})$$

The solution of (3.14) is finally illustrated graphically in Figure 3.3. The superscripts v and i are used to indicate visible and invisible tangent points. Obviously, for $f(0) < 1$ the sticking domain is composed of an infinite number of sticking intervals bounded by an infinite number of tangent points T_1 and T_2 , respectively. Inbetween the sticking intervals a trajectory can cross the discontinuity. The value $f(0) = 1$ marks a bifurcation point where a visible and an invisible tangent point of each vector field merge, which corresponds to the double tangency bifurcation DT_2 in Table 3.1. At $f(0) = 1$ the sticking set is connected containing cubic tangent points T_i . They disappear for $f(0) > 1$ which yields completely different solution types of (3.13). For $f(0) \geq 1$ a trajectory will stay on the discontinuity forever as soon as it is touched, i. e. the mass keeps sticking for all times. If $f(0) \leq 1$ we expect stick-slip motions and there are windows where the discontinuity may be crossed towards motions with negative relative velocity. A more detailed analysis of this system exceeding the classical literature (KAUDERER [1958], ANDRONOV ET AL. [1966], MAGNUS & POPP [2002]) would be fruitful in the context of Filippov theory but is beyond the scope of this thesis.

3.1.4 Friction Models

It has already been mentioned that an empiric relation describing the friction force depending on the relative velocity has to enter the system (3.3). Typically, normal and tangential forces at the contact area are related by a friction coefficient μ which itself may depend on several parameters and the relative velocity between the two bodies in

contact (IBRAHIM [1994]). Although various formulas for μ are prevalent (LI & FENG [2004], LEINE ET AL. [1998], HETZLER ET AL. [2007]) we shall present only those being of prior importance for the following considerations.

Coulomb's model of dry friction

Albeit abundant in the literature Coulomb's model of dry friction has to be prepeded here merely for review purposes. It assumes a constant coefficient of friction $\mu = \alpha$ independent of the relative velocity of the bodies in contact (Figure 3.4). In the simplest case of an elastically mounted mass on a driven belt (cf. Section 3.2), Coulomb friction would not allow for stick-slip solutions, let alone more complicated non-smooth periodic solutions. However, for more complicated problems Coulomb's friction law is still widely used because of its simplicity (e. g. MOIROT ET AL. [2002]). Alterations to the Coulomb model, such as the introduction of a dynamic coefficient of friction which is still constant but different from the static coefficient of friction effectuate non-Filippov systems and provoke numerical difficulties and thus shall not be considered here. (cf. LEINE [2000], AWREJCEWICZ & LAMARQUE [2003]).

A generalized friction model

Based upon a representation for the friction coefficient μ depending on the relative velocity v_{rel} which is presented in AWREJCEWICZ & LAMARQUE [2003] we propose the model

$$\mu(v_{rel}) = \operatorname{sgn} v_{rel} \left(\eta + \frac{\alpha - \eta}{1 + \delta |v_{rel}|} \right) + \gamma v_{rel}. \quad (3.15)$$

Introducing the scalings

$$v_{rel} = \frac{\tilde{v}_{rel}}{\delta}, \quad \eta = \frac{\tilde{\eta}}{\delta}, \quad \alpha = \frac{\tilde{\alpha}}{\delta},$$

reveals that the parameter δ has a scaling property, namely

$$\mu(v_{rel}) = \frac{1}{\delta} \tilde{\mu}(\tilde{v}_{rel}) = \frac{1}{\delta} \operatorname{sgn} \tilde{v}_{rel} \left(\tilde{\eta} + \frac{\tilde{\alpha} - \tilde{\eta}}{1 + |\tilde{v}_{rel}|} \right) + \gamma \tilde{v}_{rel} = \frac{1}{\delta} \tilde{\mu}(\delta v_{rel}). \quad (3.16)$$

The graph of the friction characteristic given by (3.16) is depicted in Figure 3.5. The parameter $\tilde{\alpha}$ now is a measure for the static coefficient of friction, and the linear term introduced by the coefficient γ describes an asymptotic slope of the friction characteristic for high relative velocities which could be regarded as a model for lubrication (IBRAHIM [1994]). The third parameter $\tilde{\eta}$ is related to the relative minimum of (3.16) where $\tilde{\mu}'(\tilde{v}_{rel}^*) = 0$ at

$$\tilde{v}_{rel}^* = -1 + \sqrt{\frac{\tilde{\alpha} - \tilde{\eta}}{\gamma}}. \quad (3.17)$$

Introducing the descriptive parameter $\tilde{\beta}$ shown in Figure 3.5, which accounts for the maximum drop of the dynamic friction coefficient, by

$$\tilde{\beta} = \tilde{\alpha} - \tilde{\mu}(\tilde{v}_{rel}^*)$$

permits to express the parameter $\tilde{\eta}$ by

$$\tilde{\eta} = \tilde{\alpha} - \left(\sqrt{\tilde{\beta}} + \sqrt{\gamma} \right)^2. \quad (3.18)$$

Inserting (3.18) into (3.16) yields the final representation of the scaled friction law:

$$\tilde{\mu}(\tilde{v}_{rel}) = \text{sgn } \tilde{v}_{rel} \left[\tilde{\alpha} - \left(\sqrt{\tilde{\beta}} + \sqrt{\gamma} \right)^2 \left(1 - \frac{1}{1 + |\tilde{v}_{rel}|} \right) \right] + \gamma \tilde{v}_{rel}, \quad (3.19)$$

which will be used throughout the remainder of this work. The parameters $\tilde{\alpha}$, $\tilde{\beta}$ and γ appearing in (3.19) will act as the main problem parameters in the examples discussed in Section 3.2 and Chapter 4. So we will be able to study the influence of the shape of the friction law on the mechanical behavior of a system.

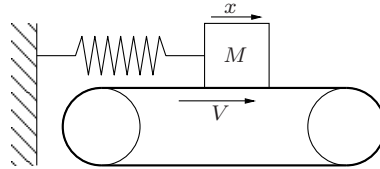


Figure 3.6: Simplest configuration of a mechanical friction oscillator

3.2 Non-smooth bifurcations of the simple friction oscillator

The simplest friction oscillator we can think of is depicted in Figure 3.6 and consists of an elastically mounted mass on a driving belt running at the speed V . The coefficient of friction μ between the mass and the belt shall be modeled by the representation (3.15) which gives the equation of motion

$$\ddot{x} = -\omega^2 x + g\mu(V - \dot{x}), \quad (3.20)$$

where ω is the natural frequency of the oscillator and g is gravity. In view of (3.3) the nonlinear function p is given by $p(x, \dot{x}) = g \operatorname{sgn}(V - \dot{x})\mu(V - \dot{x})$ here. Letting $\dot{x} = y$ and introducing scaled variables

$$\tilde{x} = \omega \delta x, \quad \tilde{y} = \delta y, \quad \tilde{t} = \omega t, \quad \tilde{V} = \delta V, \quad \tilde{\eta} = \frac{g\delta}{\omega} \eta, \quad \tilde{\alpha} = \frac{g\delta}{\omega} \alpha, \quad \tilde{\gamma} = \frac{g}{\omega} \gamma \quad (3.21)$$

yields the simple non-dimensional equations of motion

$$\tilde{x}' = \tilde{y}, \quad \tilde{y}' = -\tilde{x} + \tilde{\mu}(\tilde{V} - \tilde{y}), \quad (3.22)$$

where $\tilde{\mu}$ can be written in the form given in (3.19) with γ substituted by $\tilde{\gamma}$ and $(\cdot)'$ indicates differentiation with respect to the scaled time \tilde{t} . Thus, we end up with a piecewise smooth planar system of o.d.e.'s of the type (3.1) due to the non-smoothness of the function $\tilde{\mu}$ with four problem parameters, namely the driving velocity \tilde{V} of the belt, the static coefficient of friction $\tilde{\alpha}$, the dynamic friction drop $\tilde{\beta}$ and the asymptotic slope of the friction characteristic $\tilde{\gamma}$. The tildes will be dropped for simplicity in the following.

Despite its simplicity, system (3.22) will show a rather rich bifurcation behavior due to the sophisticated friction model. We will find solutions where the mass is stationary slipping on the belt, there might be smooth oscillations and there will be stick-slip cycles, where the mass temporarily sticks to the belt. In particular stick-slip cycles, where for a short period of time the mass moves faster than the belt and in the same direction are found under certain conditions. These motions will be termed “overshooting” in the following. Systems of the form (3.22) with simpler friction laws, especially for Coulomb-friction (cf. Section 3.1.4), are exhaustively examined in the literature (cf. AWREJCEWICZ & LAMARQUE [2003], LEINE [2000]). ELMER [1997] discusses the bifurcation behavior of a simple friction oscillator for a smooth friction law, putting some emphasis on smooth Hopf-bifurcations occurring in this case. GALVANETTO & BISHOP [1999] discuss a non-smooth system with a two-parameter friction law and additional damping and also show the existence of overshooting solutions. LEINE ET AL. [1998]

discuss the effect of different friction models, also considering time-dependent static friction, and compare numerical methods. HETZLER ET AL. [2007] do some analytical stability investigations of the steady state for a friction oscillator with an exponentially decreasing friction law and damping. However, they don't consider overshooting solutions. DERECOLE & KUZNETSOV [2004] discover non-smooth bifurcations in (3.22) for a linearly decreasing friction law. However, their results are to some extent physically infeasible. Here we want to add a concise study of the non-smooth bifurcations in the spirit of DERECOLE & KUZNETSOV [2004] depending on the shape of the friction law and the belt velocity.

3.2.1 Linear Stability analysis

System (3.22) has one fixed point at

$$x_0 = \mu(V), \quad y_0 = 0 \quad (3.23)$$

corresponding to the stationary slipping solution of the mass block on the belt running with velocity V . It is well known (ELMER [1997], HETZLER ET AL. [2007]) and obvious that this stationary solution is stable if $\mu'(V) > 0$ and unstable if $\mu'(V) < 0$ (cf. Section 3.1.2). At the critical value V^* where $\mu'(V^*) = 0$ the stability changes by a Hopf-bifurcation. From (3.17) and (3.18) we know the locus of these Hopf-bifurcations in the parameter space, given by

$$V^* = \sqrt{\beta/\gamma}. \quad (3.24)$$

The stationary solution now is stable for $V > V^*$ and unstable otherwise. In order to examine the nature of the Hopf-bifurcation and the bifurcating smooth limit cycle we compute the normal form (GUCKENHEIMER & HOLMES [1983]) of (3.22) in a neighborhood of (3.23). Introducing the notation $\mathbf{x} = (x, y)$ and likewise $\mathbf{x}_0 = (x_0, y_0)$ small deviations from the stationary solution are measured by

$$\boldsymbol{\xi} = \mathbf{x} - \mathbf{x}_0$$

The transformation

$$\boldsymbol{\xi} = \mathbf{B}\mathbf{z}$$

where \mathbf{z} defines the complex vector $\mathbf{z} = (z, \bar{z})$ and

$$\mathbf{B} = \frac{1}{2} \begin{pmatrix} 1 & 1 \\ i & -i \end{pmatrix}$$

permits to write (3.22) as a series

$$\begin{aligned} \dot{z} = & iz + i\frac{1}{8}\mu''(V^*)(z^2 + \bar{z}^2) - i\frac{1}{4}\mu''(V^*)z\bar{z} + \dots \\ & + \frac{1}{48}\mu'''(V^*)(z^3 - \bar{z}^3) + \frac{1}{16}\mu'''(V^*)(z\bar{z}^2 - z^2\bar{z}) + O(z^4) \end{aligned} \quad (3.25)$$

By means of the normal form reduction process (TROGER & STEINDL [1991]) a successive change of coordinates given by

$$\mathbf{z} = \mathbf{w}_0 + \mathbf{h}_2(\mathbf{w}_0), \quad \mathbf{w}_0 = \mathbf{w} + \mathbf{h}_3(\mathbf{w}),$$

is applied to (3.25) where $\mathbf{w}_0 = (w_0, \bar{w}_0)$, $\mathbf{w} = (w, \bar{w})$ and $\mathbf{h}_{2,3}$ are homogeneous polynomials of degree 2 and 3, respectively, in their arguments. All nonlinear terms in (3.25) except for the term $w^2\bar{w}$ can consequently be eliminated by proper choices of \mathbf{h}_i . The normal form of (3.22) finally takes the form (cf. formulas in TROGER & STEINDL [1991], p. 187)

$$\dot{w} = iw - \frac{1}{48} (3\mu'''(V^*) - i2\mu''(V^*)) w^2\bar{w}. \quad (3.26)$$

Using polar coordinates $w = Re^{i\varphi}$ yields amplitude and phase equations for the bifurcating limit cycle

$$\begin{aligned} \dot{R} &= \kappa R - \frac{3}{48} \mu'''(V^*) R^3, \\ \dot{\varphi} &= 1 - \frac{1}{24} \mu''(V^*) R^2, \end{aligned} \quad (3.27)$$

where the complex unfolding parameter κ has been introduced which can be computed by formula (2.29) and (3.24)

$$\kappa = -\frac{\mu''(V^*)}{2} (V - V^*) = -\frac{(\sqrt{\beta} + \sqrt{\gamma})^2}{(1 + \sqrt{\beta/\gamma})^3} \left(V - \sqrt{\frac{\beta}{\gamma}} \right).$$

Observing the third derivative

$$\mu'''(V^*) = -\frac{6(\sqrt{\beta} + \sqrt{\gamma})^2}{(1 + \sqrt{\beta/\gamma})^4} < 0$$

shows that the Hopf-bifurcation at V^* is always subcritical because the coefficient of R^3 in (3.27) is always positive and hence an unstable limit cycle bifurcates from (3.23).

3.2.2 The simple friction oscillator in the context of Filippov systems

Up until now we have dealt with the smooth properties of the friction oscillator for sufficiently high relative velocities $V - y$. Yet, essential non-smooth features of (3.22) have not been exploited. As explained in Section 3.1.2 the condition of vanishing relative velocity defines a discontinuity boundary Σ in the phase space given by (3.5). Now we cast (3.22) into the form of (3.7) in order to reveal its non-smooth nature:

$$\dot{\mathbf{x}} = \begin{cases} \mathbf{f}_1(\mathbf{x}) & \text{if } \mathbf{x} \in S_1, \\ \mathbf{g}(\mathbf{x}) & \text{if } \mathbf{x} \in \Sigma \text{ and } |x| < \mu(0), \\ \mathbf{f}_2(\mathbf{x}) & \text{if } \mathbf{x} \in S_2, \end{cases} \quad (3.28)$$

where

$$\begin{aligned} \mathbf{f}_1(\mathbf{x}) &= \begin{pmatrix} y \\ -x + \alpha - (\sqrt{\beta} + \sqrt{\gamma})^2 \left(1 - \frac{1}{1 + V - y} \right) + \gamma(V - y) \end{pmatrix}, \\ \mathbf{f}_2(\mathbf{x}) &= \begin{pmatrix} y \\ -x - \alpha + (\sqrt{\beta} + \sqrt{\gamma})^2 \left(1 - \frac{1}{1 - V + y} \right) + \gamma(V - y) \end{pmatrix}, \\ \mathbf{g}(\mathbf{x}) &= \begin{pmatrix} V \\ 0 \end{pmatrix}. \end{aligned} \quad (3.29)$$

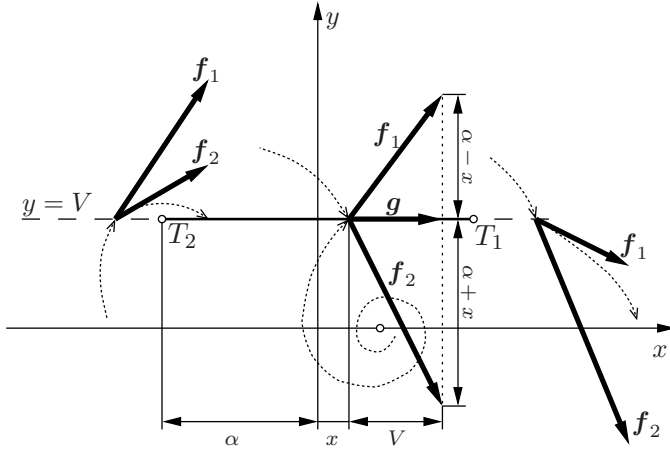


Figure 3.7: Filippov's construction of sticking solutions for the friction oscillator

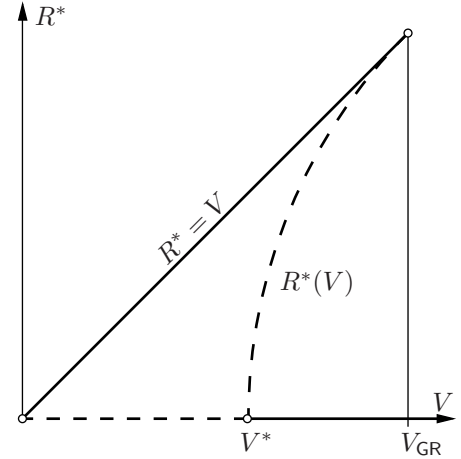


Figure 3.8: Analytical approximation of a bifurcation diagram for the grazing bifurcation

The domains S_1 and S_2 have been defined in (3.6). The trivial vector field $\mathbf{g}(\mathbf{x})$ describes the mass sticking on the belt if the elastic spring force is lower than the static friction force in consistence with the Filippov-construction. (cf. Section 3.1.1, Figure 3.7).

Tangent points

Next we look for points where one of the vector fields \mathbf{f}_1 and \mathbf{f}_2 is tangent to Σ , which means that $y = V$ and $\dot{y} = 0$. Thus, we easily obtain the tangent points

$$T_1 = (\alpha, V), \quad T_2 = (-\alpha, V)$$

for \mathbf{f}_1 and \mathbf{f}_2 , respectively. Inbetween T_1 and T_2 a trajectory that hits Σ from is “forced” to stay on the discontinuity from either side (cf. Figure 3.7), which mechanically causes the sticking motion. Inside the sticking domain

$$\Sigma_s = \{\mathbf{x} \in \Sigma : |x| < \alpha\}$$

the friction force is strong enough to balance the elastic spring force. Outside the sticking region inertia and elastic forces are predominant.

Grazing bifurcations

It suggests itself to ask for which parameter values the bifurcating limit cycle at (3.24) “touches” the discontinuity Σ at the tangent point T_1 . This incident is called a *grazing bifurcation* (KUZNETSOV ET AL. [2003], Table 3.1) which gives rise to a non-smooth stick-slip cycle. Throughout this work we will only be concerned with grazing bifurcations where a smooth and a non-smooth cycle merge which means that one of the bifurcating cycles has to be unstable. In Table 3.1 this corresponds to case GR₂. An approximation for the radius R^* of the bifurcating smooth cycle depending on the parameter V can be obtained from the amplitude equation (3.27) by setting $\dot{R} = 0$, i.

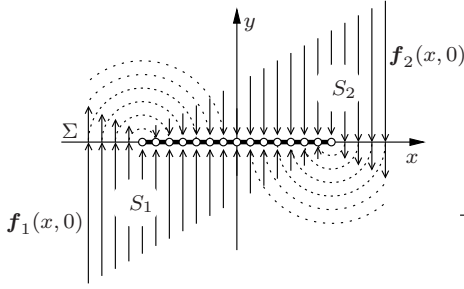


Figure 3.9: Degenerate situation in the phase plane for $V = 0$. Arrows represent the vector fields \mathbf{f}_1 and \mathbf{f}_2 at $y = 0$.

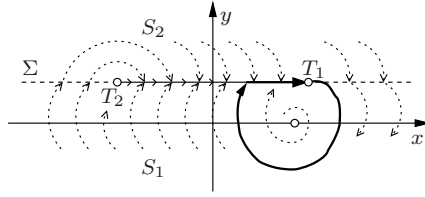


Figure 3.10: Formation of a stick-slip cycle for $V > 0$.

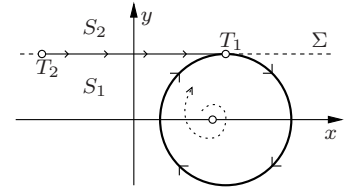


Figure 3.11: Grazing bifurcation: a smooth cycle touches the discontinuity Σ .

e.

$$R^*(V) = \sqrt{\frac{8}{3}(1 + V^*)(V - V^*)}. \quad (3.30)$$

The limit cycle hits the discontinuity if the branch given by (3.30) is tangent to the line $R^* = V$ in the bifurcation diagram plotted in Figure 3.8. The locus of grazing bifurcations in the parameter space spanned by β, γ and V can thus be calculated from the condition

$$\left. \frac{\partial R^*(V)}{\partial V} \right|_{V=V_{gr}} = 1. \quad (3.31)$$

Evaluating (3.31) yields the rough approximation

$$V_{GR} = \frac{1}{3} \left(2 + 5\sqrt{\beta/\gamma} \right) \quad (3.32)$$

for the bifurcation curve, which is of mere qualitative value, though. We remark that by (3.32) and (3.24) for $\gamma = 0$ there are neither grazing nor Hopf bifurcations.

Numerically the loci of grazing bifurcations in the (β, V) plane can be calculated from the boundary value problem (b.v.p.)

$$\begin{aligned} \dot{\mathbf{x}} &= \tau \mathbf{f}_1(\mathbf{x}), & x(0) &= \alpha, & y(0) &= V, \\ \dot{\tau} &= 0, & x(1) &= x(0), & y(1) &= y(0), \end{aligned} \quad (3.33)$$

which can be continued with respect to two problem parameters; τ denotes the period of the grazing cycle.

Stick-slip oscillations

It is well known (cf. GALVANETTO & BISHOP [1999], KUNZE & KÜPPER [1997]) and intuitively obvious that for small driving velocities V instantly a stable limit cycle appears, that has a sticking segment, thus called a *stick-slip cycle*: For $V = 0$, clearly, the discontinuity Σ is given by the line $y = 0$. A continuum of equilibria exists at $y = 0, |x| < \alpha$ (cf. Figure 3.9). For $V > 0$ the continuum of equilibria has bifurcated into the unstable focus discussed in Section 3.2.1 and a surrounding stable non-smooth

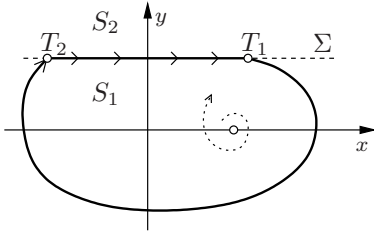


Figure 3.12: Switching bifurcation: a trajectory connects the tangent points T_1 and T_2 .

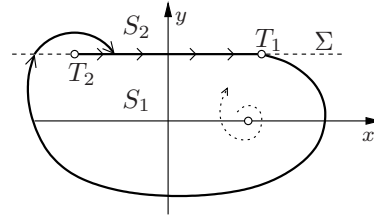


Figure 3.13: Overshooting stick-slip cycle: in S_2 the relative velocity is negative.

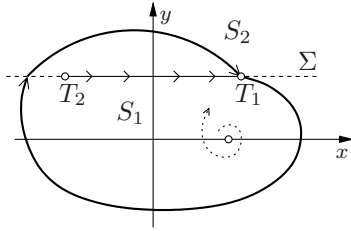


Figure 3.14: Crossing bifurcation: A trajectory leaving Σ at T_1 enters S_1 and returns to T_1 .

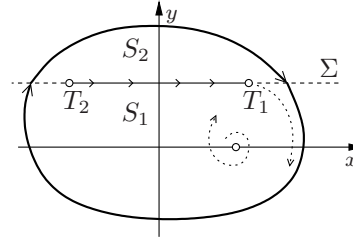


Figure 3.15: Crossing cycle: a limit cycle is composed of two slipping segments in S_1 and S_2 respectively. Sticking does not appear.

stick-slip cycle. The formation of the limit cycle becomes clear since for sufficiently small V and y the trajectories around the unstable focus can be regarded as logarithmic spirals. Therefore a trajectory leaving the sticking domain at the tangent point T_1 will be repelled from the fixed point and hits the discontinuity again in Σ_s (Figure 3.10). For increasing the band velocity V the amplitude of the limit cycle is approximately proportional to V , and thus the line $R^* = V$ may be regarded as a representation for the stick-slip circle in Figure 3.8 which is indeed a schematic bifurcation diagram. The stick-slip cycle merges with the unstable smooth limit cycle at the grazing bifurcation and disappears suddenly for parameter values beyond V_{GR} . The grazing bifurcation thus resembles a non-smooth fold bifurcation (GALVANETTO & BISHOP [1999]).

Stick-slip cycles are calculated numerically by solving the boundary value problem

$$\begin{aligned} \dot{\mathbf{x}} &= \tau_1 \mathbf{f}_1(\mathbf{x}), & x(0) &= \alpha, & y(0) &= V, \\ \dot{\tau}_1 &= 0, & y(1) &= V, \end{aligned} \quad (3.34)$$

which can be continued with respect to one parameter, τ_1 being the period of the slip-segment. The sticking period τ_s is easily found from

$$\tau_s = \frac{\alpha - x(1)}{V}.$$

The period of the stick-slip cycle then is given by $\tau_1 + \tau_s$.

Switching bifurcations

It may happen that for a critical parameter value the stick-slip cycle connects both tangent points T_1 and T_2 (Figure 3.12). In the neighborhood of this value the slip trajectory may “switch” from S_1 to S_2 by crossing the discontinuity outside of Σ_s and a

qualitatively new type of limit cycle is born. This incident is therefore called a *switching bifurcation* (case SW in Table 3.1). Mechanically the slip trajectory in S_2 corresponds to a motion with negative relative velocity, i. e. the mass moves faster than the belt, a phenomenon which will be called *overshooting*. The part of the trajectory lying in S_2 hits Σ_s again and we end up with a stable overshooting stick-slip cycle (Figure 3.13).

The loci of switching bifurcations in the parameter space are found from a numerical two-parameter continuation of the boundary value problem

$$\begin{aligned} \dot{\mathbf{x}} &= \tau_1 \mathbf{f}_1(\mathbf{x}), & x(0) &= \alpha, & y(0) &= V, \\ \dot{\tau}_1 &= 0 & x(1) &= -\alpha, & y(1) &= V. \end{aligned} \quad (3.35)$$

The period of the switching cycle is $\tau_1 + 2\alpha/V$. In order to calculate overshooting cycles the non-smooth system (3.28) is replaced by a composite system of smooth ODEs for \mathbf{x}_1 and \mathbf{x}_2 defined respectively in S_1 and S_2 , namely

$$\begin{aligned} \dot{\mathbf{x}}_1 &= \tau_1 \mathbf{f}_1(\mathbf{x}_1), & \mathbf{x}_1 &\in S_1, & x_1(0) &= \alpha, & y_1(0) &= V, \\ \dot{\mathbf{x}}_2 &= \tau_2 \mathbf{f}_2(\mathbf{x}_2), & \mathbf{x}_2 &\in S_2, & x_2(0) &= x_1(1), & y_2(0) &= y_1(1), \\ \dot{\tau}_1 &= 0, & & & y_1(1) &= V, \\ \dot{\tau}_2 &= 0, & & & y_2(1) &= V, \end{aligned} \quad (3.36)$$

where τ_1 is the slip-period with positive relative velocity and τ_2 measures the duration of overshooting, the overall period thus being $\tau_1 + \tau_2 + (\alpha - x_2(1))/V$.

Crossing bifurcations

Imagine that upon the variation of a problem parameter the overshooting segment in S_2 grows large enough to meet the tangent point T_1 again (Figure 3.14) and thus the stick phase is lost. The following cycle circumvents the sticking domain Σ_s completely and is merely composed by two halves lying in S_1 and S_2 , respectively (Figure 3.15). Since the shape of the limit-cycle has again changed qualitatively from an overshooting stick-slip to an overshooting slip cycle, this event is called a *crossing bifurcation* (case CR₂ in Table 3.1).

The boundary value problem suitable for the continuation of a crossing bifurcation with respect to two parameters is given by

$$\begin{aligned} \dot{\mathbf{x}}_1 &= \tau_1 \mathbf{f}_1(\mathbf{x}_1), & \mathbf{x}_1 &\in S_1, & x_1(0) &= \alpha, & y_1(0) &= V, \\ \dot{\mathbf{x}}_2 &= \tau_2 \mathbf{f}_2(\mathbf{x}_2), & \mathbf{x}_2 &\in S_2, & x_2(0) &= x_1(1), & y_2(0) &= y_1(1), \\ \dot{\tau}_1 &= 0, & & & y_1(1) &= V, & y_2(1) &= V \\ \dot{\tau}_2 &= 0, & & & x_2(1) &= \alpha, \end{aligned} \quad (3.37)$$

where again the non-smooth system has been splitted into the dynamics in S_1 described by \mathbf{x}_1 and S_2 described by \mathbf{x}_2 . The adjacent crossing cycle is likewise calculated from

$$\begin{aligned} \dot{\mathbf{x}}_1 &= \tau_1 \mathbf{f}_1(\mathbf{x}_1), & \mathbf{x}_1 &\in S_1, & y_1(0) &= V, \\ \dot{\mathbf{x}}_2 &= \tau_2 \mathbf{f}_2(\mathbf{x}_2), & \mathbf{x}_2 &\in S_2, & x_2(0) &= x_1(1), & y_2(0) &= y_1(1), \\ \dot{\tau}_1 &= 0, & & & y_1(1) &= V, & y_2(1) &= V \\ \dot{\tau}_2 &= 0, & & & x_2(1) &= x_1(0), \end{aligned} \quad (3.38)$$

the overall period being $\tau_1 + \tau_2$.

3.2.3 Numerical Results and discussion

We subsequently use the software package SLIDECONT provided by DERECOLE & KUZNETSOV [2004] in order to compute the one-parameter continuation of stick-slip, stick-slip-overshooting and overshooting-slip solutions described by b.v.p's (3.34), (3.36) and (3.38) as well as the two-parameter continuation problems for bifurcation points given by (3.33), (3.35) and (3.37). We start with the stratification of the parameter plane (belt velocity V versus friction drop β) for a small asymptotic slope of the friction characteristic ($\gamma = 0.008$) and a fixed value of the static friction coefficient $\alpha = 0.4$ presented in Figure 3.16. The curve of grazing bifurcations is marked by GR, switching bifurcations occur at the curve SW and crossing bifurcations at CR in Figure 3.16. Moreover, there exist two fold-bifurcations of crossing cycles, the loci of which are indicated by "LP". However, we already note here that these fold-bifurcations occur at physically meaningless values of β and hence are of pure mathematical interest. However, we want to point out that in DERECOLE & KUZNETSOV [2004] and ABADI [2003] they find similar folds but did not recognize their physical infeasibility! The curve of Hopf-bifurcations labeled "Ho" is found analytically from (3.24). Figure 3.16 also includes qualitative sketches of the phase portraits associated with the domains resulting from the intersection of bifurcation curves in the parameter plane – irrespective of their physical meaning.

In the sequel we show three examples of bifurcation paths. Figures 3.17-3.21 and Figures 3.22-3.25 show the different solutions occurring for either a low band velocity of $V = 2.5$ or a high band velocity $V = 9$ varying the friction drop β . Technically this parameter study may be interpreted as a change in the surface texture. Figures 3.26-3.28 show the bifurcation scenario for a given friction characteristic increasing the band speed. Finally, parameter studies are performed to reveal the influence of the parameters α and γ on the bifurcation behavior of the friction oscillator.

Bifurcations at constant band velocity

For a given band velocity of $V = 2.5$, static coefficient of friction $\alpha = 0.4$ and fixed $\gamma = 0.008$ we cross the parameter plane in Figure 3.16 on a horizontal path. For a flat friction characteristic (i. e. small β) we start with a single stable equilibrium position (Figure 3.17). After the grazing bifurcation at GR in Figure 3.17 two limit cycles appear suddenly: a stable stick slip cycle and an unstable smooth limit cycle surrounding the yet stable focus (Label 1 in Figure 3.17, Figure 3.18). The smooth limit cycle disappears at the Hopf-bifurcation (Ho), where the stability of the equilibrium position changes. Next, we encounter a switching bifurcation (Mark SW in Figure 3.17) after which an overshooting cycle is born (Label 2 in Figure 3.17, Figure 3.19) where the mass moves faster than the belt for a very short period of time. Proceeding further crossing the CR-curve in Figure 3.16 (Mark CR in Figure 3.17) a crossing cycle that does not enter the sticking domain (Label 2 in Figure 3.17, Figure 3.20) is created by means of a crossing bifurcation.

Here, we do not want to refrain from presenting a physically meaningless but mathematically interesting sequence of fold bifurcations of crossing cycles, occurring for $\beta/\alpha > 1$, which means that the friction force would become negative for a range of relative velocities (Figure 3.21). The fold bifurcations are seen as limit points in the

bifurcation diagram (labels LP in Figure 3.17). The continuation paths of these limit points in the (V, β) -domain are included in Figure 3.16. At LP a stable and an unstable crossing cycle merge and disappear catastrophically. In-between the limit points, three nested crossing cycles coexist (see Figure 3.21).

Choosing a larger band velocity $V = 9$ produces the bifurcation diagram in Figure 3.22. The sequence of grazing, switching, crossing and fold bifurcations is similar to the case discussed before. The evolution of the limit cycles in the phase space is depicted in Figures 3.23-3.25. Yet, the smooth cycle surrounding the stable equilibrium persists for all values of β of physical relevance. In the range between the limit points LP in Figure 3.22 we observe the coexistence of four limit cycles of alternate stability, three of which are non-smooth and cross the discontinuity.

Bifurcations for a given friction law

Practically, it seems to be easier to increase the band speed V for a given friction law, i. e. to choose a vertical path through the parameter plane in Figure 3.16. Performing this experiment numerically one obtains the bifurcation diagram plotted in Figure 3.26. The value of $\beta/\alpha = 0.75$ was chosen such to demonstrate all possible types of bifurcations. For low band velocities we observe the immediate formation of a stick-slip cycle surrounding the unstable focus as explained in Section 3.2.2. After a sequence of switching and crossing bifurcations (Figure 3.27) a crossing cycle is obtained with a short overshooting segment and no stick regime. Increasing V beyond the Hopf-bifurcation (label Ho in Figure 3.26) this progression of non-smooth bifurcations is reversed again. Exemplarily, an overshooting stick-slip cycle and the enclosed unstable smooth cycle are depicted in Figure 3.28. The overshooting and stick regime, however, are considerably smaller than the slip regime with positive relative velocity. At the second switching bifurcation ($V \approx 12.3$) the small overshooting segment vanishes and the resulting standard stick-slip cycle merges at GR with the unstable smooth cycle that has bifurcated at the Hopf-point Ho. The stable focus remains the sole attractor for $V > V_{GR}$.

The Influence of α and γ

Up to now, we kept the static coefficient of friction α and the asymptotic slope γ fixed. In order to reveal the influence of the remaining parameters on the bifurcation scenario the loci of the turning points of the switching curve (SW) and the crossing curve (CR) in the (β, V) -plane have been continued with respect to α and γ . This means that the minimum values of β/α for switching and crossing bifurcations are sought depending on α and γ (Figure 3.29). One observes that grazing and switching bifurcations are shifted towards lower values of β and higher values of V for decreasing α or γ . Projecting these continuation paths into the (β, γ) -plane yields the chart in Figure 3.30 which shows the possibility for overshooting stick-slip oscillations and crossing cycles to occur upon variation of V if a certain combination of γ and β/α is chosen. In domain \mathcal{A} in Figure 3.30 stick-slip oscillations disappear by a grazing bifurcation for rising band velocities. In the domain \mathcal{B} the stick slip cycle starts overshooting in an interval of V , whereas in \mathcal{C} the stick phase vanishes completely and crossing cycles appear in an interval of V . The example shown in Figures 3.26-3.28 belongs to domain \mathcal{C} as indicated in Figure

3.30. Recall that if $\gamma > 0$ for arbitrary β and sufficiently high V the non-smooth cycle will disappear by a grazing bifurcation and the mass will attain the stable equilibrium position.

For the case of $\gamma = 0$ the static equilibrium is always unstable and thus is surrounded by a non-smooth cycle for all physically reasonable combinations of parameter values. Grazing bifurcations do not appear. Figure 3.29 shows the stratification of the (β, V) -plane, including the loci of switching (SW), crossing (CR) and Hopf (Ho) bifurcations in that particular case. Although not proven, the numerical results plotted in Figure 3.30 and Figure 3.31 support the conjecture that for sufficiently high velocities V we always end up with a non-sticking crossing cycle created by a crossing bifurcation. Although physically meaningless it is interesting to mention that for a given velocity ($V = 1.33$ was chosen in Figure 3.32) at $\beta/\alpha = 1$ (LP^∞) an additional unstable crossing cycle of infinite amplitude appears, the radius of which decreases for $\beta/\alpha > 1$. The stable and unstable crossing cycles annihilate each other at the point “LP” above which no stable steady-state solution exists (Figure 3.32).

A note on stability considerations

The stability of the presented solutions was merely checked by, respectively, forward or backward integration of the non-smooth system (3.28) in time. A simple algorithm proposed by LEINE [2000] was used which introduces a small neighborhood of the discontinuity Σ . A trajectory entering this neighborhood is either numerically “pushed” towards the discontinuity or transferred across Σ depending on whether $|x| < \alpha$ or not. The stability investigations, however, are intuitively clear for the simple example considered so far such that no need is felt to strive for more sophisticated methods.

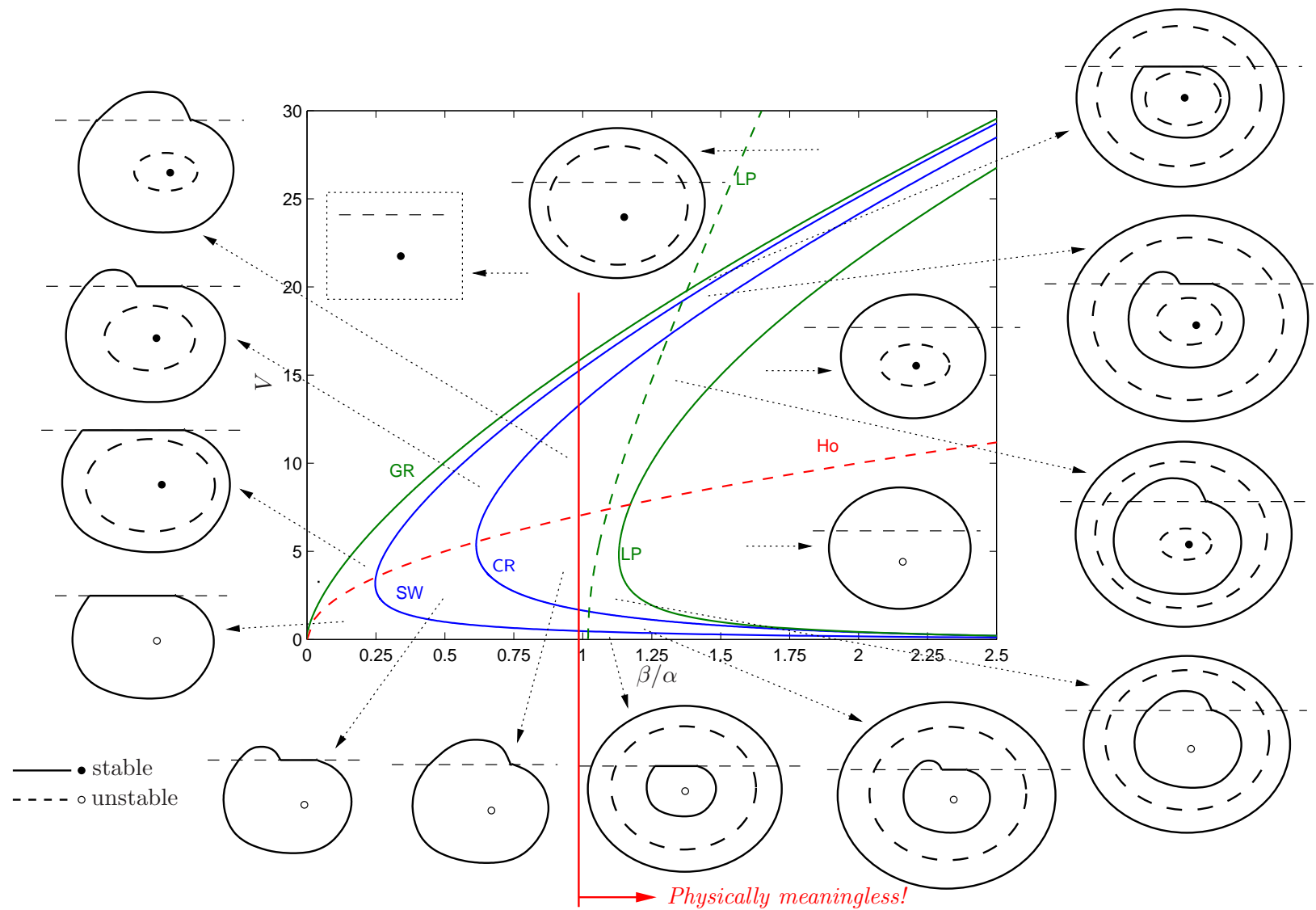


Figure 3.16: Stratification of the parameter plane for $\alpha = 0.4, \gamma = 0.008$ and sketches of the phase portraits with the discontinuity line corresponding to the parameter domains.

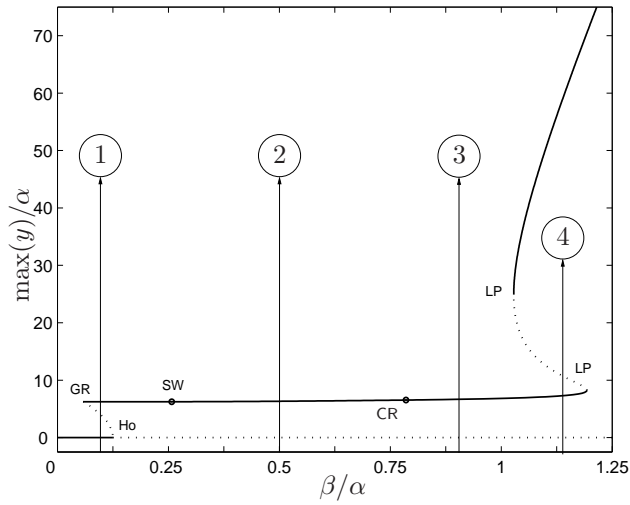


Figure 3.17: Bifurcation diagram depending on the friction drop β for $V = 2.5, \alpha = 0.5, \gamma = 0.008$. Plots of the phase plane corresponding to the marks 1 – 4 are displayed in Figures 3.18-3.21. Solid lines indicate stable, dashed lines unstable solutions.

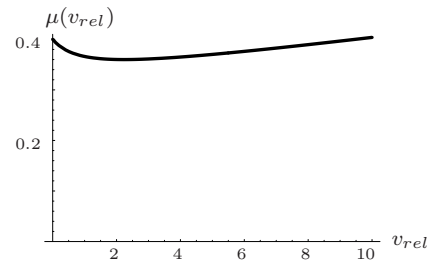
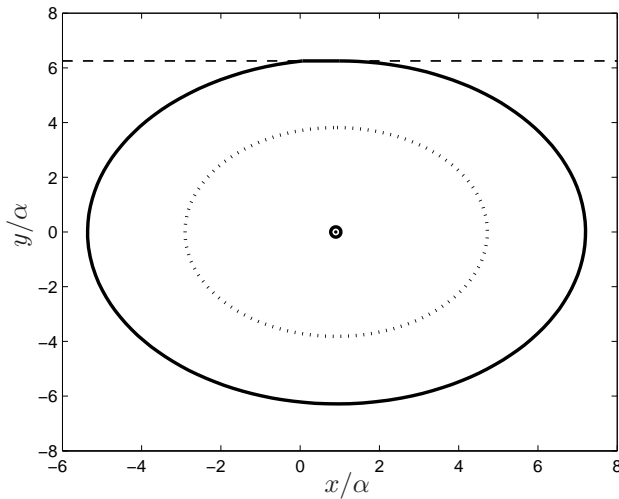


Figure 3.18: Phase portrait of the stick-slip cycle for $\beta = 0.04$ and the corresponding friction characteristic $\mu(v_{rel})$ (above). The stable fixed point is surrounded by an unstable smooth limit cycle.

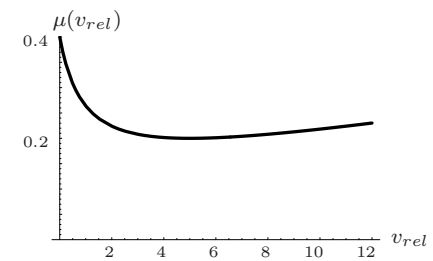
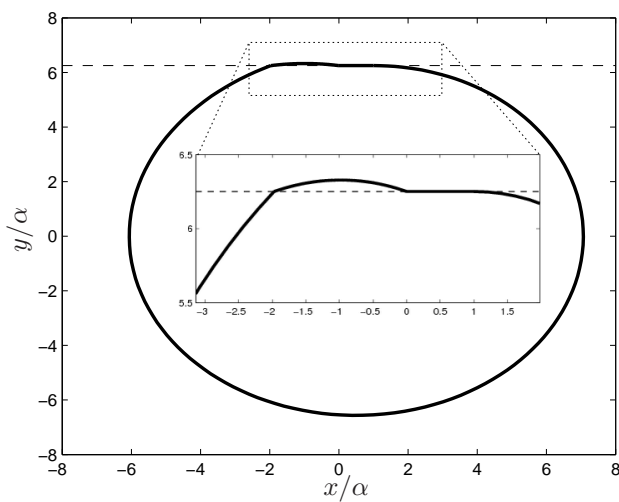


Figure 3.19: Phase portrait of the overshooting stick-slip cycle for $\beta = 0.2$ and the corresponding friction characteristic $\mu(v_{rel})$ above. The overshooting segment is clearly visible in the embedded enlargement.

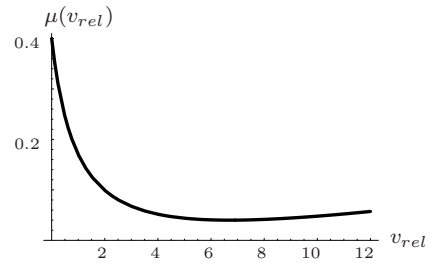
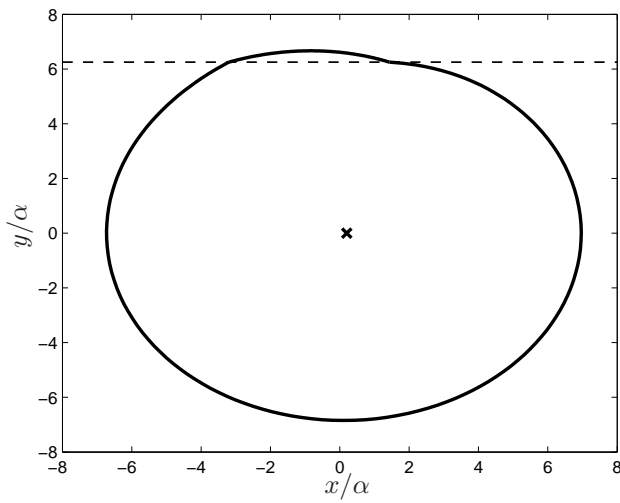


Figure 3.20: Phase portrait of the overshooting slip cycle without sticking for $\beta = 0.36$ and the corresponding friction characteristic $\mu(v_{rel})$ (above).

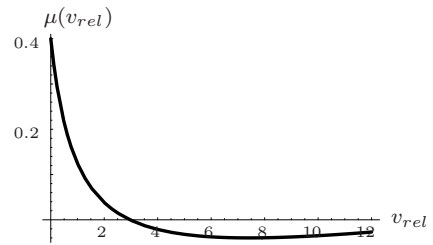
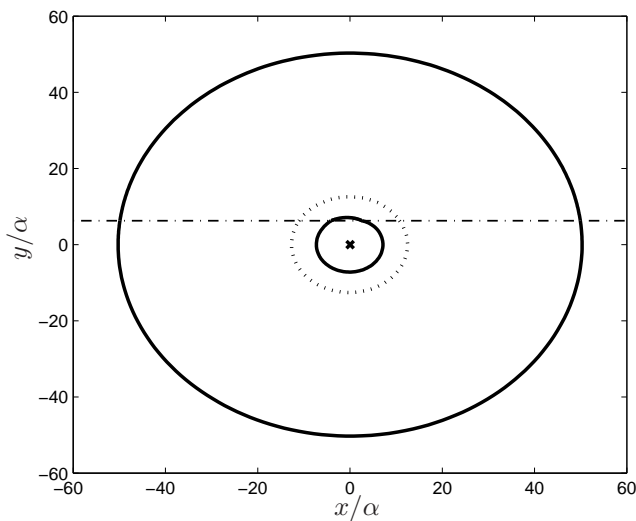


Figure 3.21: Coexistence of 3 crossing cycles for $\beta = 0.44$. The corresponding friction characteristic is physically meaningless since the friction force becomes negative (above).

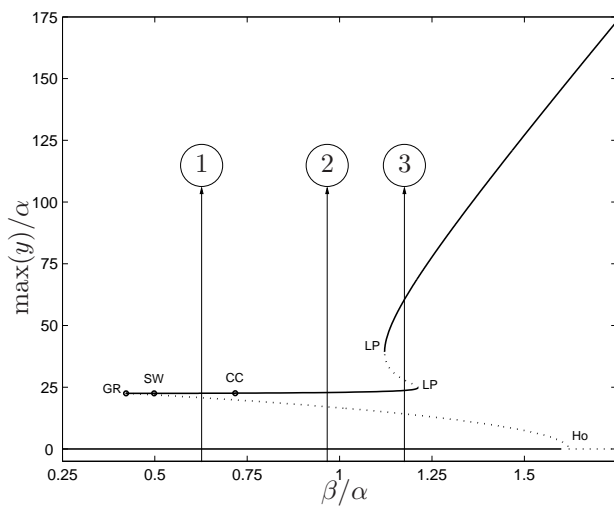


Figure 3.22: Bifurcation diagram depending on the friction drop β for $V = 2.5, \alpha = 0.5, \gamma = 0.008$. Plots of the phase plane corresponding to the marks 1 – 3 are displayed in Figures 3.23-3.25.

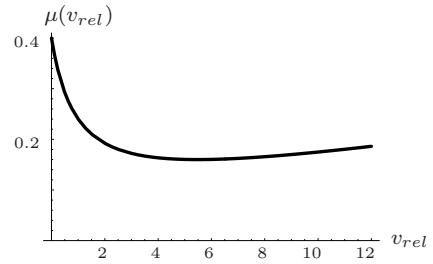
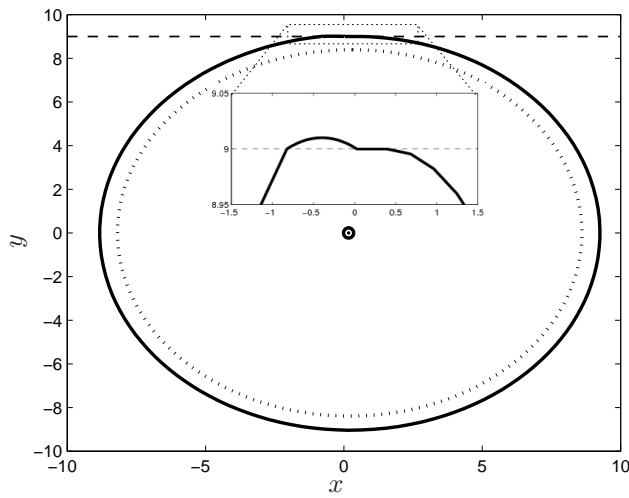


Figure 3.23: Phase portrait of the overshooting stick-slip cycle for $\beta = 0.24$ and the corresponding friction characteristic (above). The overshooting segment is enlarged. An unstable limit-cycle surrounds the stable equilibrium

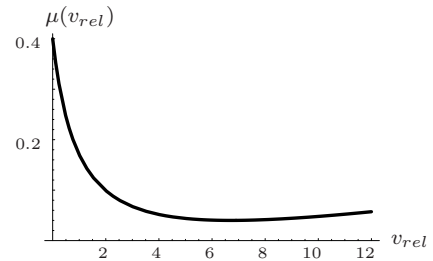
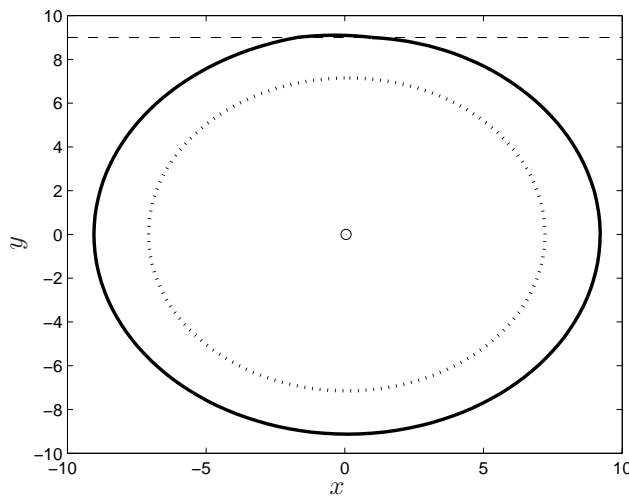


Figure 3.24: Phase portrait of the slip cycle with a small overshooting segment for $\beta = 0.36$ and the corresponding friction characteristic (above). The stable fixed point and the unstable smooth cycle persist.

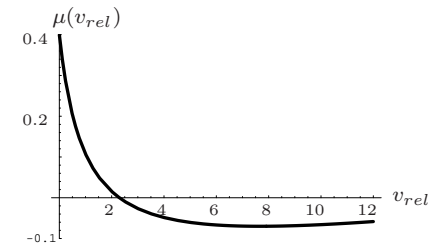
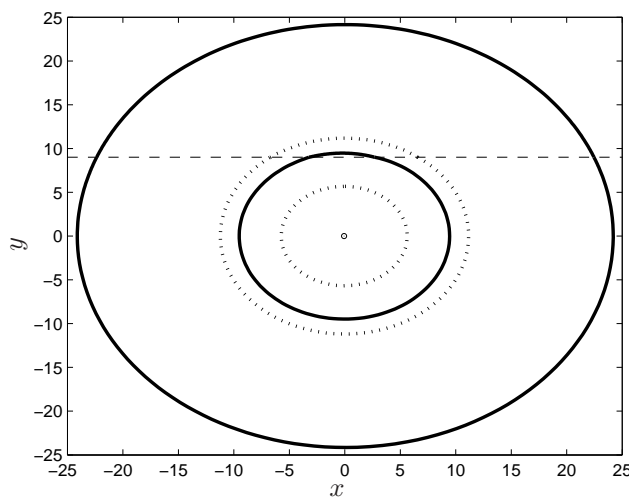


Figure 3.25: Coexistence of 3 crossing cycles for $\beta = 0.47$ with the unstable smooth cycle. The associated friction characteristic (above) is physically meaningless, though.

3 Non-smooth bifurcations of mechanical systems with 1-d.o.f involving friction

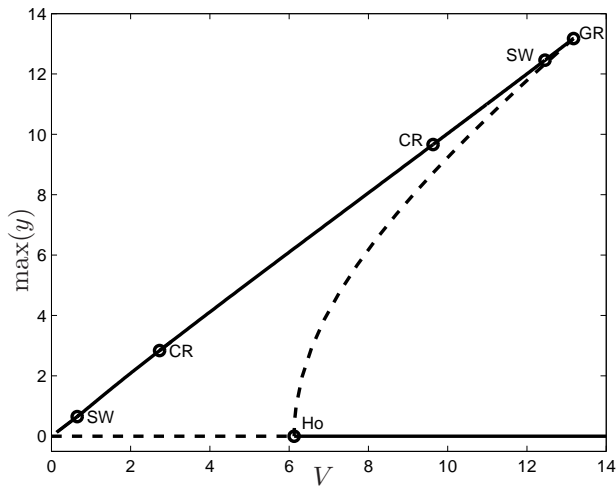


Figure 3.26: Bifurcation diagram depending on the belt velocity V for $\beta/\alpha = 0.75, \gamma = 0.008$. Solid lines indicate stable, dashed lines unstable solutions. Grazing, switching and crossing events of the non-smooth cycle are indicated by “GR”, “SW” and “CR”.

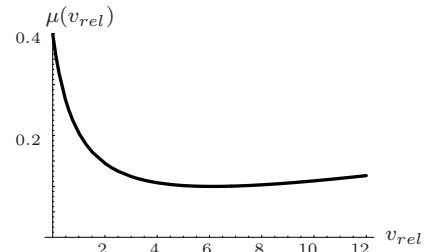
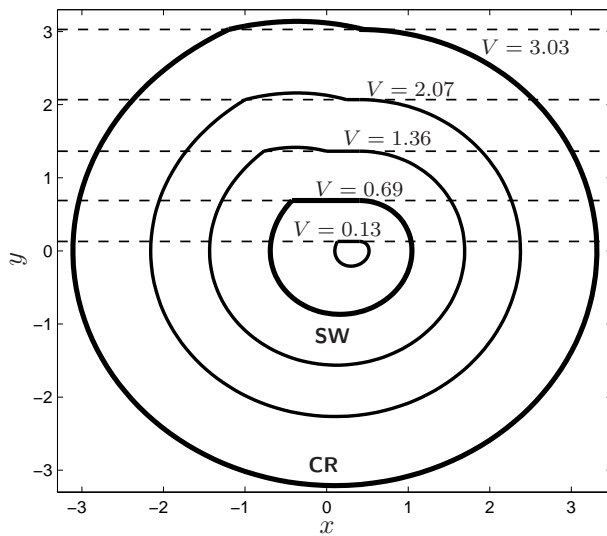


Figure 3.27: Evolution of the stick-slip cycle for increasing driving velocities V . Cycles corresponding to the switching (SW) as well as the crossing bifurcation (CR) are highlighted. The associated friction law is displayed above.

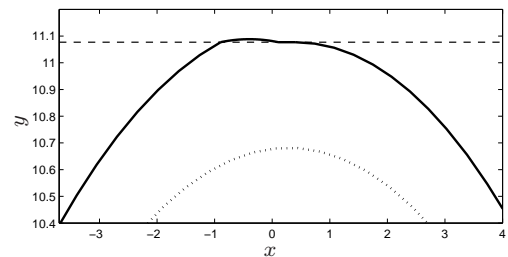
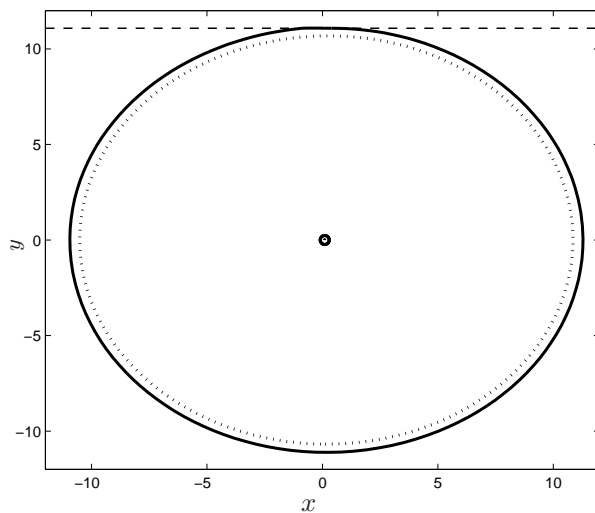


Figure 3.28: Example of an overshooting stick-slip cycle at $V = 11.077$ coexisting with an unstable smooth cycle as well as a stable equilibrium. The overshooting and stick phases are only observable in the enlargement above.

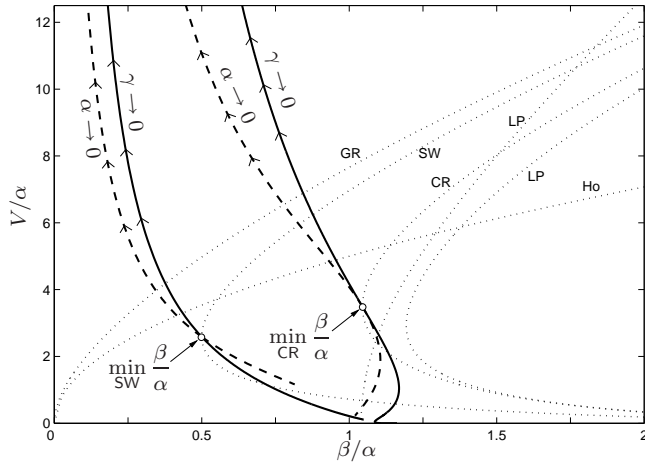


Figure 3.29: Stratification of the parameter plane (β, V) for $\alpha = 0.4, \gamma = 0.1$ including the continuation paths of the turning points for $\alpha \rightarrow 0$ and $\gamma \rightarrow 0$. GR ... grazing bifurcations, SW ... switching bifurcations, CR ... crossing bifurcations, Ho ... Hopf-bifurcations, LP ... fold bifurcations of crossing cycles.

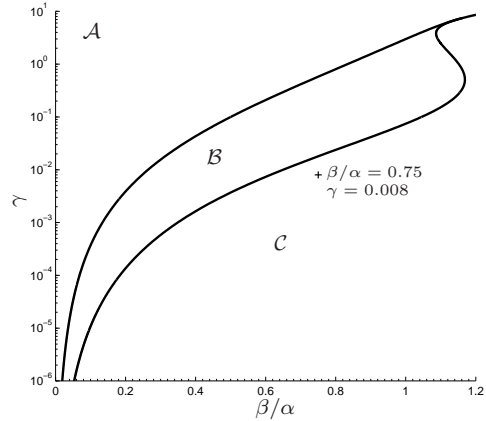


Figure 3.30: Projection of the continuation paths of Figure 3.29 into the (β, γ) -plane; $\alpha = 0.4$ is kept fixed. \mathcal{A} : Stick-slip oscillations disappear by a grazing bifurcation for increasing V , \mathcal{B} : Overshooting stick-slip oscillations exist in an interval of V , \mathcal{C} : Crossing cycles exist in an interval of V . The marker indicates the point corresponding to Figures 3.26-3.28.

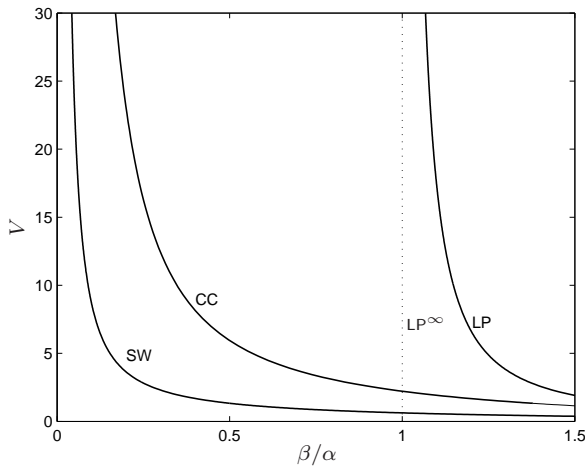


Figure 3.31: Stratification of the parameter plane for $\gamma = 0, \alpha = 0.4$. Beyond LP^∞ two crossing cycles of alternate stability coexist.

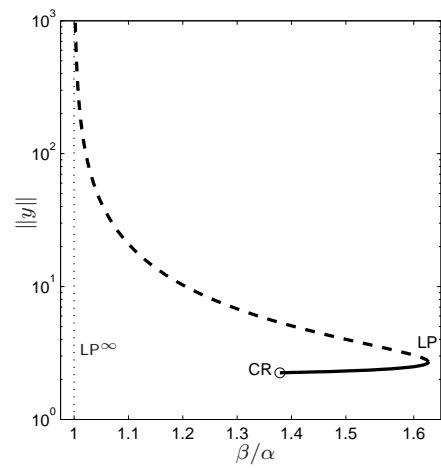


Figure 3.32: Bifurcation diagram for increasing β at $\alpha = 0.4, \gamma = 0, V = 1.33$ beyond the crossing bifurcation at CR. Solid lines indicate a stable crossing cycle, the dashed solution branch is unstable.

4 Non-smooth bifurcations of travelling waves

4.1 Motivation

One of the obvious effects of friction are squealing noises, be it in squeaking doors, in brakes or in the ultimate cultivation the sound of a violin. The problem considered in this chapter was triggered by an investigation of brake squeal noises in disc and drum brakes of the high speed (“TGV”-)train in France performed by Q. S. NGUYEN and his research group (MOIROT ET AL. [2002], NGUYEN [2003], MOIROT & NGUYEN [2002]). In MOIROT ET AL. [2002] they simulated a very simplified brake-like model consisting of a rigid shaft inside an elastic annular bush (Figure 4.1) with a finite element discretization and found rotating waves that exhibit stick, slip and separation zones between the shaft and the bush for certain parameter combinations. A connection of their results to the occurrence of squealing noises remains a conjecture, however. The task was to get a deeper insight into the dynamics of the system using concepts of non-smooth bifurcation theory in order to study the influence of the problem parameters on friction induced waves, in particular on the occurrence of the stick-slip and separation phenomena. While MOIROT ET AL. [2002] stick to a Coulomb-type friction model, here we furthermore want to incorporate the more sophisticated friction model introduced in the previous chapter.

4.2 Mechanical model of a brake-like system

Consider an elastic annular bush fitted to a rigid shaft with a diameter mismatch δ (Figure 4.1). The shaft is rotating with angular velocity Ω . Friction between the rotating shaft and the bush shall be taken into account by a friction coefficient μ depending on the local relative velocity v_{rel} . The bush obeys the standard planar equations of motion of a linear elastic continuum together with the appropriate boundary and contact conditions in polar coordinates (r, θ) (cf. MOIROT ET AL. [2002]),

$$\operatorname{div} \boldsymbol{\sigma} = \ddot{\mathbf{u}}, \quad \boldsymbol{\sigma} = \frac{\nu}{(1+\nu)(1-2\nu)} \operatorname{tr}(\boldsymbol{\varepsilon}) \mathbf{I} + \frac{1}{1+\nu} \boldsymbol{\varepsilon}, \quad \boldsymbol{\varepsilon} = \frac{1}{2} (\nabla \mathbf{u} + \nabla \mathbf{u}^T) \quad (4.1a)$$

$$\mathbf{u}(\xi, \theta, t) = \mathbf{0}, \quad (4.1b)$$

$$\begin{aligned} \sigma_{rr}(1, \theta, t) &= -p(\theta, t), & \sigma_{r\theta}(1, \theta, t) &= -q(\theta, t) \\ u(1, \theta, t) &\geq \delta, & p(u(1, \theta, t) - \delta) &= 0, \end{aligned} \quad (4.1c)$$

$$v_{rel}(\theta, t) = \Omega - \dot{v}(1, \theta, t), \quad |q| \leq \mu(v_{rel})p, \quad v_{rel}(q - \mu(v_{rel})p) = 0 \quad (4.1d)$$

for the stress and strain tensors $\boldsymbol{\sigma}$, $\boldsymbol{\varepsilon}$ and the displacement field $\mathbf{u} = (u, v, w)$; ν denotes the Poisson ratio. The ratio of the radii $\xi = R_o/R_i$, the pressure p and the shear stress

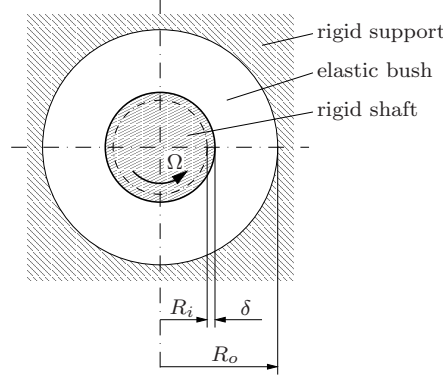


Figure 4.1: Rotating (Ω) rigid shaft (radius $R_s = R_i + \delta$ fitted into an annular bush (radii R_i, R_o) with diameter mismatch δ , i. e. the undeformed inner radius of the bush $R_i < R_s$ by the amount δ .

q have been introduced and the physical quantities have been scaled by¹

$$\mathbf{u} \leftarrow \frac{1}{R_i} \mathbf{u}, \quad \delta \leftarrow \frac{\delta}{R_i}, \quad \boldsymbol{\sigma} \leftarrow \frac{1}{E} \boldsymbol{\sigma}, \quad r \leftarrow \frac{r}{R_i}, \quad t \leftarrow \frac{1}{R_i} \sqrt{\frac{E}{\rho}} t, \quad \Omega \leftarrow R_i \sqrt{\frac{\rho}{E}} \Omega, \quad (4.2)$$

where E and ρ are Young's modulus and the density of the bush. At the outer boundary ($r = \xi$) all displacements are set to zero by (4.1b). Boundary condition (4.1c) describes the possibility of separation between the bush and the shaft: if the bush is in contact with the shaft then $u = \delta$ holds at $r = 1$ and the normal pressure p is nonzero, otherwise $p = 0$ during separation. Boundary condition (4.1d) incorporates the friction law $\mu(v_{rel})$ relating normal and shear stresses at the shaft-bush interface. Again, either the relative tangential velocity at the interface $v_{rel} = 0$ or $q = \mu(v_{rel})p$. Writing out (4.1a) in planar polar coordinates (r, θ) yields linear partial differential equations for the radial and tangential displacements u and v , respectively:

$$\begin{aligned} \frac{\partial^2 u}{\partial r^2} + \frac{1}{r} \frac{\partial u}{\partial r} - \frac{u}{r^2} - (2 - \kappa_1) \frac{1}{r^2} \frac{\partial v}{\partial \theta} + \kappa_1 \frac{1}{r} \frac{\partial^2 v}{\partial r \partial \theta} + (1 - \kappa_1) \frac{1}{r^2} \frac{\partial^2 u}{\partial \theta^2} &= \eta_1 \ddot{u}, \\ \frac{\partial^2 v}{\partial r^2} + \frac{1}{r} \frac{\partial v}{\partial r} - \frac{v}{r^2} + (2 + \kappa_2) \frac{1}{r^2} \frac{\partial u}{\partial \theta} + \kappa_2 \frac{1}{r} \frac{\partial^2 u}{\partial r \partial \theta} + (1 + \kappa_2) \frac{1}{r^2} \frac{\partial^2 v}{\partial \theta^2} &= \eta_2 \ddot{v}, \end{aligned} \quad (4.3)$$

where

$$\kappa_1 = \frac{1}{2(1 - \nu)}, \quad \kappa_2 = \frac{1}{1 - 2\nu}, \quad \eta_1 = \frac{1 - \nu - 2\nu^2}{1 - \nu}, \quad \eta_2 = \frac{2(1 - \nu - 2\nu^2)}{1 - 2\nu}.$$

The non-linearity is introduced to the problem by the non-smooth boundary conditions (4.1c) and (4.1d), written out

$$\begin{aligned} \left[\frac{\partial u}{\partial r} + \frac{\nu}{1 - 2\nu} \left(u + \frac{\partial u}{\partial r} + \frac{\partial v}{\partial \theta} \right) \right] (u - \delta) \Big|_{r=1} &= 0, \\ \left\{ \frac{1}{2(1 + \nu)} \left(\frac{\partial u}{\partial \theta} - v + \frac{\partial v}{\partial r} \right) - \frac{\mu(v_{rel})}{1 + \nu} \left[\frac{\partial u}{\partial r} + \frac{\nu}{1 - 2\nu} \left(u + \frac{\partial u}{\partial r} + \frac{\partial v}{\partial \theta} \right) \right] \right\} (\Omega - \dot{v}) \Big|_{r=1} &= 0, \end{aligned}$$

¹The scalings (4.2) differ from those proposed in MOIROT ET AL. [2002] in order to get hold of Ω as problem parameter

which result from the possibility of separation and the employed friction law. Similar to (3.19) we now use the slightly modified version

$$\mu(v_{rel}) = \alpha \left\{ \text{sgn}(v_{rel}) \left[1 - \hat{\beta} \left(1 - \frac{1}{1 + |v_{rel}|} \right) \right] + \gamma v_{rel} \right\} \quad \text{where} \quad \hat{\beta} = \left(\sqrt{\beta} + \sqrt{\gamma} \right)^2. \quad (4.4)$$

4.3 Stability of the stationary solution

Equations (4.3) have a stationary solution $\mathbf{u}_0 = (u_0, v_0)$ where $\dot{u} \equiv 0, \dot{v} \equiv 0$, given by (MOIROT ET AL. [2002])

$$\begin{aligned} u_0 &= \delta \frac{1}{\xi^2 - 1} \left(\frac{\xi^2}{r} - r \right), & v_0 &= \delta \mu(\Omega) \frac{1}{\xi^2 - 1} \left(\frac{\xi^2}{r} - r \right) \left(1 + \frac{1}{\xi^2(1 - 2\nu)} \right), \\ p_0 &= \delta \frac{1}{\xi^2 - 1} \frac{1}{1 + \nu} \left(\xi^2 + \frac{1}{1 - 2\nu} \right), & q_0 &= \mu(\Omega) p_0 \end{aligned} \quad (4.5)$$

In the vicinity of \mathbf{u}_0 equations (4.3) are linear if separation and sticking is excluded for small disturbances and $\Omega > 0$. We assume the perturbations of u to be negligible and write (cf. CHANDRASEKHAR [1970])

$$u(r, \theta, t) \equiv u_0, \quad v(r, \theta, t) = v_0 + V(r) e^{ik\theta + \lambda t}, \quad (4.6)$$

where k is the wave number of the transversal disturbance. For a stable stationary solution all eigenvalues λ must have a negative real part for all k such that all disturbances decay exponentially in time. Neglecting (4.3)₁ one obtains from (4.3)₂ the eigenvalue problem

$$L[V] := (rV(r))' - s^2 \frac{V(r)}{r} = \eta_2 \lambda^2 r V(r). \quad (4.7)$$

where $s^2 = (k^2(1 + \kappa_2) + 1)$. The corresponding linearized boundary conditions read

$$\begin{aligned} (1 - 2\nu + 2ik\nu\mu(\Omega) + 2p_0\mu'(\Omega)(1 - \nu - 2\nu^2)\lambda) V(1) - (1 - 2\nu)V'(1) &= 0, \\ V(\xi) &= 0. \end{aligned} \quad (4.8)$$

Equation (4.7) is of the Bessel type, the eigenfunctions $V(r)$ are thus represented by the modified Bessel functions of index s , namely $I_s(\sqrt{\eta_2}\lambda r)$ and $K_s(\sqrt{\eta_2}\lambda r)$ (cf. SMIRNOW [1967]). The boundary conditions (4.8) can be written as

$$(a_0 + \epsilon\lambda)V(1) + a_1V'(1), \quad V(\xi) = 0, \quad (4.9)$$

where $a_0, \lambda \in \mathbb{C}, a_1 \in \mathbb{R}$ and $\epsilon = 2p_0\mu'(\Omega)(1 - \nu - 2\nu^2)$ is small which is physically justified since the mismatch δ as well as the slope of the friction characteristic $\mu'(\Omega)$ will be small. If $\epsilon = 0$ (e. g. $\mu'(\Omega) = 0$) the boundary value problem (4.7) and (4.9) is self-adjoint and due to the complex boundary conditions has a skew-symmetric distribution of infinitely many complex eigenvalues, i. e. if λ_0 is an eigenvalue then so is $-\lambda_0$ because the square of λ appears in (4.7). Hence, in contrast to the 1-d.o.f. friction oscillator discussed in Section 3.2 in the present continuous problem the stability of the stationary solution does not change if $\mu'(\Omega) = 0$. For a small perturbation $\epsilon \neq 0$, the eigenvalues λ_1 , say, will remain in a neighborhood of λ_0 and thus we are apt to formulate

Proposition 4.1. *The stationary solution \mathbf{u}_0 given by (4.5) is unstable w.r.t. perturbations (4.6) for all parameter values and ϵ sufficiently small.*

Proof. Let λ_0 and $-\lambda_0$ be eigenvalues of the unperturbed boundary value problem $\epsilon = 0$ and λ_1 be an eigenvalue of the perturbed problem. V_0 and V_1 are the corresponding eigenfunctions. Then use integration by parts to calculate

$$\int_1^\xi (L[V_0]V_1 - L[V_1]V_0) dr = [rV_0'V_1 - rV_1'V_0]_1^\xi = \eta_2 (\lambda_0^2 - \lambda_1^2) \int_1^\xi rV_0V_1 dr. \quad (4.10)$$

Using the boundary relations $V_1'(1) = -(a_0 + \epsilon\lambda_1)V(1)/a_1$ and $V_0'(1) = -a_0V_0(1)/a_1$ in (4.10) yields

$$\lambda_1^2 = \lambda_0^2 + \epsilon \frac{V_0(1)V_1(1)}{a_1\eta_2 \int_1^\xi rV_0V_1 dr} \lambda_1, \quad (4.11)$$

which reveals that both solutions of (4.11) for λ_1 depend smoothly on ϵ . Since either λ_0 or $-\lambda_0$ has a positive real part we will find a λ_1 with $\text{Re}(\lambda_1) > 0$ and thus \mathbf{u}_0 is unstable. \square

4.4 Travelling wave reduction

Following MOIROT ET AL. [2002] we use a Galerkin reduction to simplify the problem. The displacements are sought in the form

$$u = U(\theta, t)X(r), \quad v = V(\theta, t)X(r), \quad (4.12)$$

where the radial distribution $X(r)$ is taken from the static solution (4.5), namely

$$X(r) = \frac{1}{\xi^2 - 1} \left(\frac{\xi^2}{r} - r \right).$$

The quantities U and V thus describe the (nondimensional) displacements of the shaft-bush interface depending on the polar angle θ . Performing the Galerkin reduction of (4.1) employing (4.12) (cf. NGUYEN [2003]) yields the following system of p.d.e's for U and V :

$$\begin{aligned} \ddot{U} - bU'' - dV' + gU &= P \\ \ddot{V} - aV'' + dU' + hV &= Q \\ P \geq 0, \quad U - \delta \geq 0, \quad P(U - \delta) &= 0, \\ |Q| \leq \mu(\Omega - \dot{V})P, \quad Q - \mu(\Omega - \dot{V})P &= 0, \end{aligned} \quad (4.13)$$

where $(\cdot)'$ denotes differentiation with respect to θ . The constants a, b, d, g, h depend on ξ and the Poisson ratio ν and are given by

$$\begin{aligned} a &= \frac{\tilde{a}A}{B}, \quad b = \frac{\tilde{b}A}{B}, \quad d = \frac{aC_1 - bC_2}{A}, \quad g = \frac{2\tilde{a} + 2(\xi^2 - 1)\tilde{b}}{B}, \quad h = \frac{2\xi^2\tilde{b}}{B}, \\ \tilde{a} &= \frac{1 - \nu}{(1 + \nu)(1 - 2\nu)}, \quad \tilde{b} = \frac{1}{2(1 + \nu)}, \\ A &= -\frac{2\xi^2 \ln \xi}{\xi^2 - 1} + \frac{1 + \xi^2}{2}, \quad B = \frac{\xi^4 \ln \xi}{\xi^2 - 1} + \frac{1 - 3\xi^2}{4}, \\ C_1 &= \frac{2\xi^2 \ln \xi}{\xi^2 - 1} - 1, \quad C_2 = -\frac{2\xi^2 \ln \xi}{\xi^2 - 1} - 1 + 2\xi^2. \end{aligned} \quad (4.14)$$

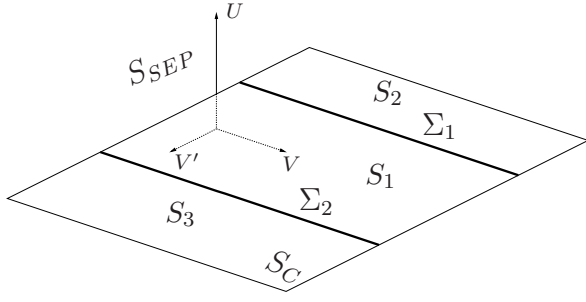


Figure 4.2: Topology of the phase space. See Figure 4.8 for an example of a trajectory in the phase space.

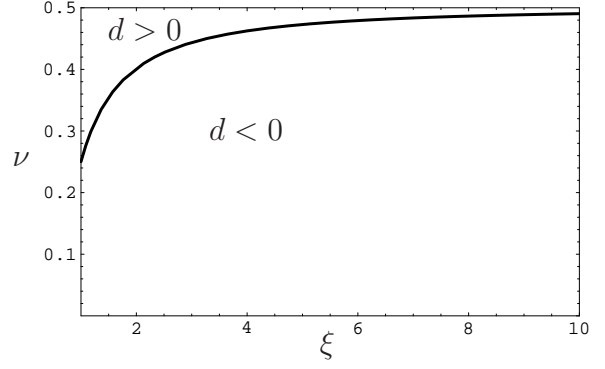


Figure 4.3: Sign of the parameter d depending on the Poisson number ν and the radial ratio ξ

It is remarked that all problem constants are positive except d . Next we look for travelling wave solutions of (4.13) which propagate at constant (non-dimensional) wave speed c . This permits to introduce a phase ϕ given by

$$\phi = \theta - ct \quad (4.15)$$

whereby the dependencies of U and V are reduced to

$$U = U(\phi), \quad V = V(\phi), \quad \dot{U} = -cU', \quad \dot{V} = -cV'. \quad (4.16)$$

The prime indicates differentiation with respect to ϕ now and U, V are periodic functions of period $2\pi/k$, k being the wave number of the considered solution. Recalling the scalings (4.2) the associated physical wave speed becomes $c\sqrt{E/\rho}$ m/s. Consequently, periodic waves are governed by a non-smooth system of o.d.e's depending on whether the contact pressure, given by (cf. (4.13))

$$P = g\delta - dV', \quad (4.17)$$

is zero or positive, i. e.

$$V'' = \left. \begin{array}{l} U = \delta, \quad U' = 0 \\ 0 \quad \text{if } |hV| \leq \mu(0)P \text{ and } V' = -\Omega/c \\ \frac{1}{c^2 - a} (-hV + \mu(\Omega + cV')P) \quad \text{otherwise} \end{array} \right\} \quad \text{if } P > 0 \quad (4.18a)$$

$$\left. \begin{array}{l} (c^2 - b)U'' - dV' + gU = 0 \\ (c^2 - a)V'' + dU' + hV = 0 \end{array} \right\} \quad \text{if } P = 0. \quad (4.18b)$$

Equations (4.18) possess a 4-dimensional phase space with elements $\mathbf{x} = (U, U', V, V')$. If the shaft is in contact with the bush the dynamics is governed by (4.18a) and restricted to the 2-dimensional manifold

$$S_C = \{\mathbf{x} \in \mathbb{R}^4 : U = \delta, U' = 0\}.$$

This *plane of contact* S_C can be regarded as a discontinuity in the complete 4-dimensional system (4.18) (see Figure 4.2). The vector field defined by (4.18b) is not only non-smooth

with respect to S_C but also discontinuous since U' will experience a jump if contact is reestablished and a trajectory hits S_C . The vector field in S_C is given by (4.18a) and therefore a 4-dimensional Filippov construction of the solutions in S_C is not applicable. Furthermore, S_C may not be pierced by a trajectory since $U \geq \delta$ must always hold. This defines a permissible 4-dimensional half-space for separated states, i. e.

$$S_{SEP} = \{\mathbf{x} \in \mathbb{R}^4 : U > \delta\}.$$

Inside S_C , however, there exist two 1-dimensional sub-boundaries Σ_1 and Σ_2 for vanishing relative velocity and vanishing normal pressure, respectively, given by

$$\Sigma_1 = \{\mathbf{x} \in S_c : \Omega + cV' = 0\}, \quad \Sigma_2 = \{\mathbf{x} \in S_c : g\delta - dV' = 0\}.$$

With respect to the boundary Σ_1 the 2-dimensional sub-system (4.18a) is of Filippov-type and gives rise to stick-slip solutions as explained in Section 3.1.1. It comprises the *sticking domain* $\Sigma_S = |hV| \leq \mu(0)P$. The boundary Σ_2 indicates the onset of a separation zone between the shaft and the bush and thus plays the role of a “window” into \mathbb{R}^4 . As soon as a trajectory in S_C hits Σ_2 , the governing equations switch to (4.18b) and the trajectory exits to S_{SEP} . Σ_2 is not of Filippov type since the adjacent vector fields are non-smooth, though, but continuous which is easily seen from letting $P = 0$ in (4.18). The plane S_c is sub-partitioned by Σ_1 and Σ_2 into three domains S_1, S_2 and S_3 (Figure 4.6), defined by

$$\begin{aligned} S_1 &= \{\mathbf{x} \in S_c : g\delta - dV' > 0 \wedge \Omega + cV' > 0\}, \\ S_2 &= \{\mathbf{x} \in S_c : g\delta - dV' > 0 \wedge \Omega + cV' < 0\}, \\ S_3 &= \{\mathbf{x} \in S_c : g\delta - dV' < 0\}. \end{aligned}$$

The domains S_1 and S_2 thus contain all admissible states of contact with positive normal pressure. We will call S_1 the *domain of positive slip*, since it contains slip states with positive relative velocity. Likewise, S_2 will be referred to as *overshooting domain*, since its elements correspond to a motion where the bush is locally faster than the shaft. Obviously, the domain S_3 is forbidden. We will in the following refer to a slip motion with positive (resp. negative) relative velocity simply as *positive slip* (resp. *negative slip* or *overshooting*). The system (4.18a) is a friction oscillator of the form discussed in Section 3.1.2 where the normal pressure P now depends on V' via (4.17). However, due to the presence of the second discontinuity Σ_2 we furthermore expect more complicated periodic solutions with separation zones.

4.5 Non-smooth solutions and bifurcations of travelling waves

4.5.1 Equilibria and tangent points

We start with the investigation of non-smooth solutions and bifurcations of the planar system (4.18a). As explained in Section 3.2.2 system (4.18a) has two tangent points with respect to Σ_1 where $V'' = 0$ and $V' = -\Omega/c$, given by

$$T_1 = \left(\frac{\alpha}{h} \left(g\delta + d\frac{\Omega}{c} \right), -\frac{\Omega}{c} \right), \quad T_2 = \left(-\frac{\alpha}{h} \left(g\delta + d\frac{\Omega}{c} \right), -\frac{\Omega}{c} \right), \quad (4.19)$$

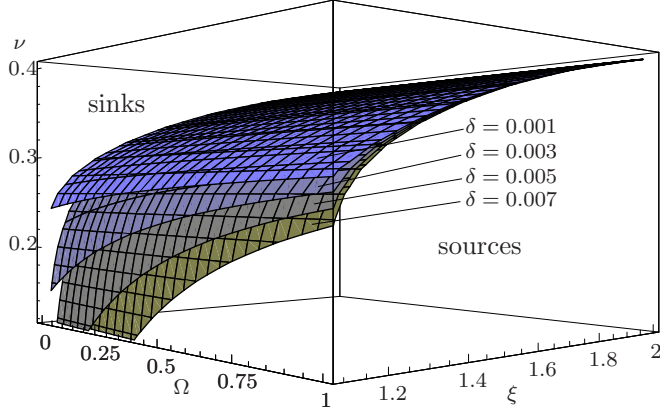


Figure 4.4: Surfaces of Hopf-bifurcations in the (Ω, ξ, ν) -parameter space for $\beta = 0.2$, $\gamma = 0.0615$, $k = 1$, $c > 0$ and $c\mu'(\Omega) < 0$

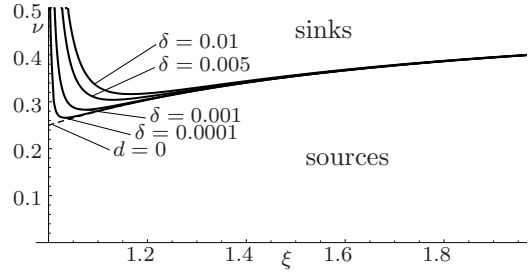


Figure 4.5: Hopf-bifurcations in the (ξ, ν) -parameter plane for $\Omega = 1$, $\beta = 0.2$, $\gamma = 0.0615$, $k = 1$, $c < 0$ and $c\mu'(\Omega) > 0$

where, as for the simple friction oscillator, T_1 is visible and T_2 is invisible.

The fixed point at $V = \mu(\Omega)g\delta/h$ corresponds to the stationary slipping solution discussed in Section 4.3. With respect to the original p.d.e. (4.3) this solution has been shown to be always unstable in Proposition 4.1. Nevertheless, the equilibrium may change its nature from a source to a sink within the approximated system (4.18a). Applying formula (3.12) we find that the term

$$K = c\mu'(\Omega)g\delta - d\mu(\Omega) \quad (4.20)$$

governs the stability of the equilibrium. If $K < 0$ it is a sink², if $K > 0$ it is a source and if $K = 0$ there is a Hopf-bifurcation. Observing (4.20) we recognize that in contrast to the simple friction oscillator (Section 3.2) the occurrence of a Hopf bifurcation is mainly determined by the parameter d here. Since $\mu'(\Omega)\delta$ will be small and $\mu(\Omega)$ is always positive K will only vanish if d is sufficiently small. From (4.14) the change in the sign of d is easily found by evaluating $d = 0$, which yields

$$\nu = \frac{1 + \xi^2 - 2\xi^4 + 6\xi^2 \ln \xi}{4\xi^2(1 - \xi^2 + 2 \ln \xi)}. \quad (4.21)$$

The graph of (4.21) is plotted in Figure 4.3. The wave speed $c = c_H$ at a Hopf bifurcation has to be determined such that the bifurcating limit cycle has a period $2\pi/k$. Since the frequency of the bifurcating cycle at the bifurcation value is given by the natural frequency $\sqrt{h/(c^2 - a)}$ of the oscillator (4.18a) we find that

$$c_H = \pm \sqrt{\frac{h}{k^2} + a}.$$

The sign of the wave speed indicates the direction of the considered wave (waves with positive wave speed propagate in the same sense as the applied rotation Ω). Using the

²We try to avoid the terms *stable* and *unstable* here since stability (instability) w.r.t. the approximation (4.18a) does not necessarily mean that the solution is indeed physically stable (unstable).

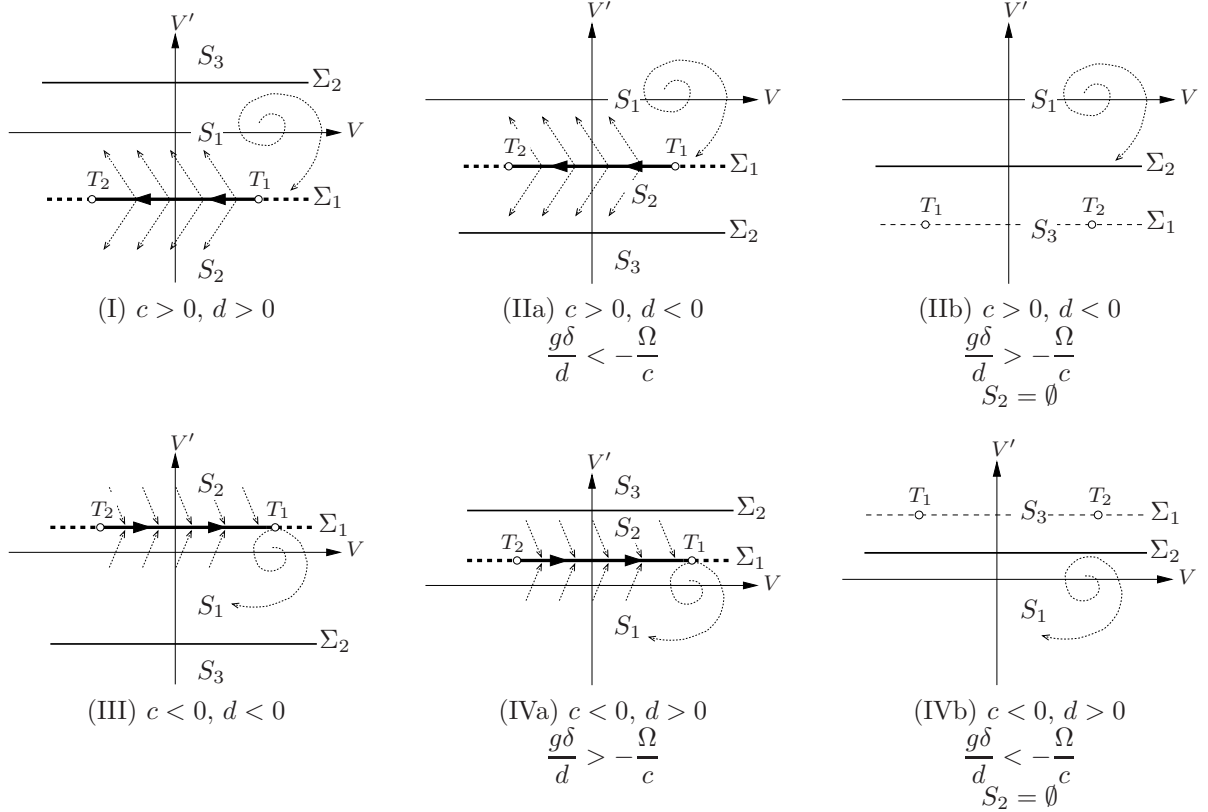


Figure 4.6: Possible lay-outs of the contact plane S_C and the corresponding arrangement of the domains S_1 , S_2 and S_3 . The tangent points and the sticking domain on Σ_1 are sketched. The equilibria are depicted as sources, which is the most significant case.

representations (4.14) for g and d we can compute numerically the loci of Hopf bifurcations in the parameter space for a given friction characteristic. Figure 4.4 shows the surfaces $K = 0$ in the (Ω, ξ, ν) -space if a forward rotating wave is bifurcating in mode 1 (i. e. $c_H > 0, k = 1$). A typical configuration of the friction characteristic which will also be used in the remainder of this chapter has been chosen ($\beta = 0.2, \gamma = 0.0615$) and Ω is small enough that everywhere $\mu'(\Omega) < 0$ is fulfilled. For waves rotating against the sense of the shaft ($c_H < 0$) the situation is depicted in Figure 4.5 where $\Omega = 1$ is kept fixed, since the influence of Ω would be visually indiscernible. We conclude from Figures 4.3, 4.4 and 4.4 that $d < 0$ covers most of the cases that are physically relevant³. Hopf bifurcations occur either for rather small radial ratios ξ or high Poisson numbers ν close to an incompressible material. Both cases can be regarded as physically not typical for the problem under consideration, hence we may argue that the emergence of travelling waves due to a Hopf bifurcation plays a minor role in the present example. However, we will see in Section 4.5.4 that waves with positive wave-speed are solely found in these exceptional cases.

For large Ω where $\mu'(\Omega) > 0$ we only have to swap figures 4.4 and 4.5 since the occurrence of Hopf bifurcation depends only on the sign of the product $c\mu'$ which shall be clarified by the following table:

³Choosing e. g. $\nu = 0.3$ and $\xi = 2$ yields $d = -8.865 \cdot 10^{-1}$.

	$d > 0$	$d < 0$
$c\mu' < 0$ (Fig. 4.4)	sinks	possibility of Hopf-bifurcations for $ \delta \ll 1$
$c\mu' > 0$ (Fig. 4.5)	possibility of Hopf-bifurcations for $ \delta \ll 1$	sources

Finally, note that the Hopf bifurcation is independent of the static friction coefficient α . Furthermore we know from numerical tests that the influence of the remaining parameters in the friction law on the loci of Hopf bifurcations is negligible.

Looking now at the plane of contact S_C in the phase space we distinguish six different lay-outs (see Figure 4.6) depending on the placement of Σ_1 and Σ_2 and the signs of the wave speed c and the parameter d . In order to find possible non-smooth waveforms we have to find periodic solutions with fixed period $2\pi/k$ of (4.18) numerically. Observing the possible topologies of S_C depicted in Figure 4.6 we expect stick, slip (including overshooting) and separated solutions in cases (I), (IIa), (III) and (IVa) while cases (IIb) and (IVb) only permit positive slip and separated solutions.

It is important to remark that due to the travelling wave reduction (4.15) and (4.16)_{3,4} a solution of (4.18) with $c > 0$ corresponds to a solution in negative time of the original p.d.e. (4.13). For forward waves the orientation of a phase curve in ϕ therefore is reversed if it is transferred to the time t . This fact will have important consequences on the different formulation of boundary conditions for $c < 0$ and $c > 0$ (Sections 4.5.3, 4.5.4). Moreover, system (4.18a) is invariant with respect to the transformation

$$c \rightarrow -c, \quad d \rightarrow -d, \quad \phi \rightarrow -\phi. \quad (4.22)$$

This means that once a travelling backward wave with, say, $c < 0$, $d < 0$ is found there exists an identical forward wave for $c > 0$ and $d > 0$. We will scrutinize this point when we reconsider forward travelling waves in Section 4.5.4 (Figure 4.9). Although, physically, the parameter d is linked via ξ and ν to a, b, g and h we expect that a solution that corresponds to an ‘artificial’ value of d will be close to a physically correct solution. In view of (4.22) we thus conjecture that solutions in the cases (I) and (II) in Figure 4.6 are similar to cases (III) and (IV) and in a first approach it shall suffice to consider one example out of each group in order to reduce the complexity of the problem.

4.5.2 Numerical Procedure

In order to cope with the non-smoothness of (4.18) a composite system of smooth equations is constructed similar to Section 3.2.2 each accounting for a different type of contact between the shaft and the bush. Introducing the variables $W(\phi) = V'(\phi)$ and $Y(\phi) = U'(\phi)$ and rescaling the respective integration variables with the periods Φ we divide a non-smooth limit cycle of (4.18) into the sticking segment on Σ_1 , m positive slipping segments in S_1 , n overshooting segments in S_2 and a separated segment in S_{SEP} . New variables are appended to the state space for each type of shaft-bush contact in the following fashion:

Type of contact	Rel. velocity	State variables	Period	Eqn.
Sticking	$\Omega + cW = 0$	V_0, W_0	Φ_0	(4.18a)
m slipping	$\Omega + cW > 0$	$V_{11}, W_{11}, \dots, V_{1m}, W_{1m}$	$\Phi_{11}, \dots, \Phi_{1m}$	(4.18a)
n overshooting	$\Omega + cW < 0$	$V_{21}, W_{21}, \dots, V_{1n}, W_{2n}$	$\Phi_{21}, \dots, \Phi_{2n}$	(4.18a)
Separating	$v_{rel} \geq 0 \vee v_{rel} < 0$	U_3, Y_3, V_3, W_3	Φ_3	(4.18b)

The first order system of o.d.e's that has to be integrated subject to appropriate boundary and transition conditions reads

$$\begin{aligned}
 V'_0 &= -\Phi_0 \frac{\Omega}{c} & W'_0 &= 0 & (V_0, W_0) &\in \Sigma_1 \\
 V'_{11} &= \Phi_{11} W_{11} & W'_{11} &= \Phi_{11} \frac{1}{c^2 - a} f_1(V_{11}, W_{11}) & (V_{11}, W_{11}) &\in S_1 \\
 &\vdots & &\vdots & & \\
 V'_{1m} &= \Phi_{1m} W_{1m} & W'_{1m} &= \Phi_{1m} \frac{1}{c^2 - a} f_1(V_{1k}, W_{1m}) & (V_{1m}, W_{1m}) &\in S_1 \\
 V'_{21} &= \Phi_{21} W_{21} & W'_{21} &= \Phi_{21} \frac{1}{c^2 - a} f_2(V_{21}, W_{21}) & (V_{21}, W_{21}) &\in S_2 \\
 &\vdots & &\vdots & & \\
 V'_{2n} &= \Phi_{2n} W_{2n} & W'_{2n} &= \Phi_{2n} \frac{1}{c^2 - a} f_2(V_{2n}, W_{2n}) & (V_{2n}, W_{2n}) &\in S_2 \\
 U'_3 &= \Phi_3 Y_3 & Y'_3 &= \Phi_3 \frac{1}{c^2 - b} (dW_3 - gU_3) \\
 V'_3 &= \Phi_3 W_3 & W'_3 &= \Phi_3 \frac{1}{c^2 - a} (-dY_3 - hV_3) & (U_3, Y_3, V_3, W_3) &\in S_{SEP} \\
 & & \Phi'_0 &= \Phi'_{11} = \dots = \Phi'_{1m} = \Phi'_2 = \Phi'_3 = 0
 \end{aligned} \tag{4.23}$$

where

$$\begin{aligned}
 f_1(V, W) &= -hV + \alpha \left[1 - \hat{\beta} \left(1 - \frac{1}{1 + \Omega - cW} \right) + \gamma(\Omega - cW) \right] (g\delta - dW), \\
 f_2(V, W) &= -hV + \alpha \left[-1 + \hat{\beta} \left(1 - \frac{1}{1 - \Omega + cW} \right) + \gamma(\Omega - cW) \right] (g\delta - dW).
 \end{aligned} \tag{4.24}$$

Above all we have to add the boundary condition that the overall period sums up to $2\pi/k$ in order to ensure the periodicity of the wave, i. e.

$$\Phi_0 + \Phi_{11} + \dots + \Phi_{1m} + \Phi_{21} \dots + \Phi_{1n} + \Phi_3 = \frac{2\pi}{k}, \tag{4.25}$$

which permits to determine the unknown wave speed c . In (4.23) the possibility of multiple slip segments has been incorporated, since typically slipping regimes precede and succeed a separation zone (i. e. usually $m = 2$). The solution and continuation of b.v.p's for (4.23) including (4.25) is performed numerically by a collocation method implemented in the continuation software AUTO (DOEDEL ET AL. [1998]). Use will also be made of the standard continuation routines for Folds and Hopf bifurcations that

are available in AUTO. The problem parameters suitable for continuation are collected in the parameter vector

$$\boldsymbol{\lambda} = (\alpha, \beta, \gamma, \delta, \xi, \nu, \Omega). \quad (4.26)$$

As a matter of fact, a complete stratification of the parameter space given by (4.26) is cumbersome and we have to restrict ourselves to a meaningful choice of continuation parameters for the numerical calculations. The b.v.p's (4.27)-(4.55) each describing a specific type of travelling wave are laid down in Tables 4.1 and 4.2.

4.5.3 The case $c < 0$

The case being most similar to the friction oscillator with one degree of freedom is case (III) in Figure 4.6. Hence, in view of the numerical results that will be presented in Section 4.6.1 we start with a listing of the different types of waves travelling on the shaft-bush interface and their bifurcations for $c < 0$, i. e. for waves propagating in the opposite direction than the rotation of the shaft.

(Overshooting) Stick-slip waves

Consider waves of mode k that exhibit k stick and slip zones with positive relative velocity on the circumference of the shaft. The waveform of a stick-slip wave with positive slip obeys the boundary value problem (4.27). A switching bifurcation produces overshooting stick-slip waves which exhibit slipping with negative relative velocity.

(Overshooting) Stick-slip-separation waves

Stick-slip-separation waves are born by a *separating bifurcation* (explained below) either of a stick-slip or an overshooting stick-slip wave. Thus, they feature k stick zones and $2k$ slip zones, which may as well exhibit overshooting behavior. The corresponding boundary value problems are given by (4.31) for a standard stick-slip-separation wave and (4.32) for its overshooting counterpart. A trajectory starts separating if $P = 0$ and exits smoothly into the separation space S_{SEP} , i. e. for the separated segment $U_3(0) = \delta$ and $Y_3(0) = U_3'(0) = 0$ holds. When contact is reestablished U_3' and P experience a jump at the connection between the separated and the slipping segment, which corresponds to a jump in the tangential and normal contact forces.

Crossing slip waves

A crossing slip wave is created by a crossing bifurcation. A crossing wave of mode k is composed of k positive slipping segments and k overshooting slipping segments. The sticking domain in Σ_1 is completely encircled.

Crossing slip-separation waves

Crossing slip-separation waves, accordingly, result from a separating bifurcation of a crossing cycle or from a crossing bifurcation of an overshooting stick-slip-separation cycle. The wave runs k times through the regimes: positive slip – separation – positive slip – overshooting slip. The corresponding b.v.p. is given in (4.33).

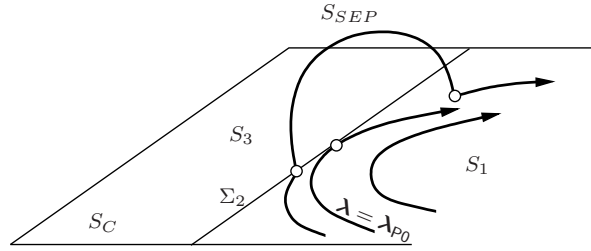


Figure 4.7: Separating bifurcation: upon the variation of a parameter a trajectory is tangent to Σ_2 and consequently exits to S_{SEP} .

Slip-separation waves

Pure Slip-separation waves without overshooting appear by the grazing bifurcation of a stick-slip-separation wave (4.47). The b.v.p. suitable for the 1-parameter continuation of slip-separation waves is given in (4.30). The cycle is composed of a positive slip segment in S_1 and a separation segment in S_{SEP} .

Separating bifurcations

Separating bifurcations are an essential feature of the model under consideration. The onset of a separation zone between the shaft and the bush is determined by a tangency of a trajectory in S_C with Σ_2 (Figure 4.7) for a certain parameter value $\lambda = \lambda_{P0}$. In DI BERNARDO ET AL. [2002] this event would be called a *multisliding bifurcation*. Upon the variation of a parameter a separated trajectory in S_{SEP} builds up governed by (4.18b). It may appear in all kinds of non-separated waveforms, i. e. stick-slip waves, overshooting stick-slip waves and crossing slip waves. The loci of separating bifurcations in the parameter space are calculated from boundary value problems (4.36)-(4.38).

Grazing bifurcations

Grazing bifurcations may appear for stick-slip as well as stick-slip-separation waves and are characterized in the phase space by a tangency of the considered limit cycle with Σ_1 . Either a stick-slip wave merges with a smooth slip wave or a stick-slip-separation cycle merges with a slip-separation cycle. The corresponding b.v.p's for the continuation of grazing bifurcations in the parameter space are given by (4.46) and (4.47).

Switching bifurcations

As it is the case for the simple friction oscillator in Section 3.2 switching bifurcations are characterized by a trajectory connecting the two tangent points T_1 and T_2 given in (4.19). Both, stick-slip as well as stick-slip-separation waves may undergo a switching bifurcation and consequently exhibit an overshooting segment. In order to continue the loci of switching bifurcations in the parameter space we have to solve the boundary value problems (4.39) for switching bifurcations of stick-slip waves and correspondingly (4.40) for stick-slip-separation waves.

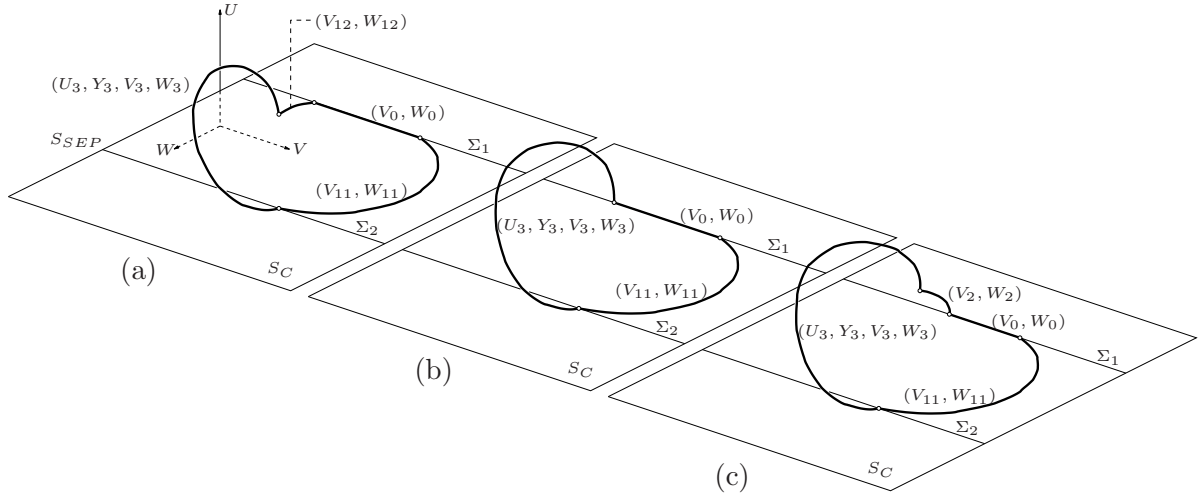


Figure 4.8: Fly-over bifurcation: (a) Stick-slip-separation cycle projected into the (U, V, W) -space. (b) *Fly-over* bifurcation at $\lambda = \lambda_{FO}$: the separated segment ends at Σ_1 . (c) Overshooting stick-slip-separation wave with *separated switching*.

Crossing bifurcations

If a limit cycle has a segment in S_2 which ends up in the tangent point T_1 we are facing a crossing bifurcation similar to the simple friction oscillator. The associated b.v.p's are (4.41) for the crossing bifurcation of an overshooting stick-slip cycle and (4.42) for the crossing bifurcation of an overshooting stick-slip-separation cycle. Upon the variation of a problem parameter, the considered wave loses its stick-regime and we observe crossing slip waves or crossing slip-separation waves, respectively.

Separated switching – “Fly Over” bifurcations

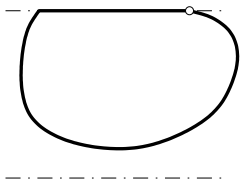
Imagine the case that the separated trajectory of a stick-slip-separation cycle (Figure 4.8a, b.v.p. (4.31)) ends up at the discontinuity Σ_1 for a certain constellation of parameter values, $\lambda = \lambda_{FO}$, say (Figure 4.8b). Physically, at λ_{FO} a separation regime is followed immediately by a stick regime. In the vicinity of λ_{FO} the separated trajectory may *fly over* the discontinuity Σ_1 in S_{SEP} (Figure 4.8c) and an overshooting stick-slip-separation wave is created, where the relative velocity changes its sign during separation. That's why we shall call this event a *fly-over bifurcation*. Since the projection of the phase portrait onto the (V, W) -Plane resembles the switching bifurcation we will analogously use the term *separated switching* to address this phenomenon. The boundary value problem suitable for the continuation of “fly-over” bifurcations is given by (4.43). System (4.34) finally shows the b.v.p. necessary for the continuation of the resulting overshooting stick-slip-separation waves that exhibit separated switching.

The same type of bifurcation may occur if an overshooting stick-slip-separation wave is considered with slip-segments in S_1 as well as in S_2 (b.v.p. (4.32)). The separated segment (U_3, Y_3, V_3, W_3) may grow large enough such that the second slip-segment (V_2, W_2) vanishes and S_2 is entered via S_{SEP} (see e.g. Figures 4.19-4.20). The loci of “fly-over”-bifurcations of an overshooting stick-slip-separation wave are calculated from b.v.p. (4.44).

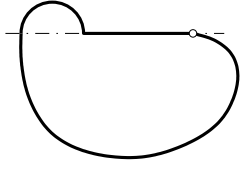
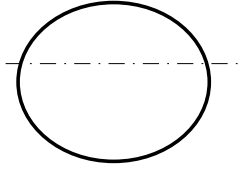
Furthermore, the same mechanism may cause Σ_1 to be flown over twice by a separated trajectory in S_{SEP} , i. e. a separation zone with *negative* relative velocity leads directly to a sticking segment. Upon the variation of a parameter the relative velocity of the separating trajectory may change from positive to negative to positive again and contact is reestablished when the trajectory hits S_C in S_1 (see the result in Figure 4.15). A secondary fly-over bifurcation can be continued using the same b.v.p. valid for the primary fly-over bifurcation given by (4.45). An appropriate overshooting stick-slip-separation solution with separated switching close to the secondary fly-over bifurcation must be provided as a starting solution.

Table 4.1: Boundary value problems corresponding to backward rotating waves ($c < 0$) and their non-smooth bifurcations.

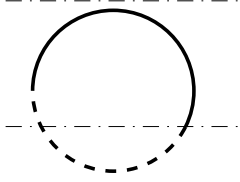
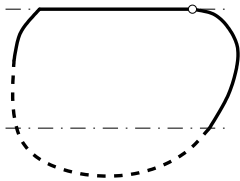
- discontinuity
- trajectory in S_C
- separated trajectory in S_{SEP}
- tangent point

<p>Stick-slip wave</p> $ \begin{aligned} V_0' &= -\Phi_0 \frac{\Omega}{c} & V_0(0) &= V_{11}(1) \\ V_{11}' &= \Phi_{11} W_{11} & V_0(1) &= V_{11}(0) \\ W_{11}' &= \Phi_{11} f_1(V_{11}, W_{11}) & V_{11}(0) &= \frac{\alpha}{h} \left(g\delta + d \frac{\Omega}{c} \right) \\ \Phi_0' &= 0 & W_{11}(0) &= -\frac{\Omega}{c} \\ \Phi_{11}' &= 0 & W_{11}(1) &= -\frac{\Omega}{c} \\ c' &= 0 & \frac{2\pi}{k} &= \Phi_0 + \Phi_{11} \end{aligned} \tag{4.27} $	<p>ODEs: 6 BCs: 6 Cont. par.: 1 Wave-form:</p> 
--	---

continued on next page

<p>Overshooting Stick-slip wave</p> $ \begin{aligned} V_0' &= -\Phi_0 \frac{\Omega}{c} & V_0(0) &= V_2(1) \\ V_{11}' &= \Phi_{11} W_{11} & V_0(1) &= V_{11}(0) \\ W_{11}' &= \Phi_{11} f_1(V_{11}, W_{11}) & V_{11}(0) &= \frac{\alpha}{h} \left(g\delta + d \frac{\Omega}{c} \right) \\ V_2' &= \Phi_2 W_2 & W_{11}(0) &= -\frac{\Omega}{c} \\ W_2' &= \Phi_2 \frac{1}{c^2 - a} f_2(V_2, W_2) & W_{11}(1) &= -\frac{\Omega}{c} \\ \Phi_0' &= 0 & V_2(0) &= V_{11}(1) \\ \Phi_{11}' &= 0 & W_2(0) &= W_{11}(1) \\ \Phi_2 &= 0 & W_2(1) &= -\frac{\Omega}{c} \\ c' &= 0 & \frac{2\pi}{k} &= \Phi_0 + \Phi_{11} + \Phi_2 \end{aligned} \tag{4.28} $	<p>ODEs: 9 BCs: 9 Cont. par.: 1 Wave-form:</p> 
<p>Crossing slip wave</p> $ \begin{aligned} V_{11}' &= \Phi_{11} W_{11} & V_{11}(0) &= V_2(1) \\ W_{11}' &= \Phi_{11} f_1(V_{11}, W_{11}) & W_{11}(0) &= -\frac{\Omega}{c} \\ V_2' &= \Phi_2 W_2 & W_{11}(1) &= -\frac{\Omega}{c} \\ W_2' &= \Phi_2 \frac{1}{c^2 - a} f_2(V_2, W_2) & V_2(0) &= V_{11}(1) \\ \Phi_{11}' &= 0 & W_2(0) &= W_{11}(1) \\ \Phi_2 &= 0 & W_2(1) &= W_{11}(0) \\ c' &= 0 & \frac{2\pi}{k} &= \Phi_{11} + \Phi_2 \end{aligned} \tag{4.29} $	<p>ODEs: 7 BCs: 7 Cont. par.: 1 Wave-form:</p> 

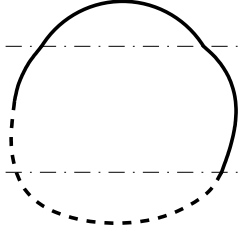
continued on next page

<p>Slip-separation wave</p> $ \begin{aligned} V'_{11} &= \Phi_{11} W_{11} & V_{11}(0) &= V_3(1) \\ W'_{11} &= \Phi_{11} \frac{1}{c^2 - a} f_1(V_{11}, W_{11}) & W_{11}(0) &= W_3(1) \\ U'_3 &= \Phi_3 Y_3 & W_{11}(1) &= \frac{g\delta}{d} \\ Y'_3 &= \Phi_3 \frac{1}{c^2 - b} (dW_3 - gU_3) & U_3(0) &= \delta \\ V'_3 &= \Phi_3 W_3 & Y_3(0) &= 0 \\ W'_3 &= \Phi_3 \frac{1}{c^2 - a} (-dY_3 - hV_3) & V_3(0) &= V_{11}(1) \\ \Phi'_{11} &= 0 & W_3(0) &= \frac{g\delta}{d} \\ \Phi'_3 &= 0 & U_3(1) &= \delta \\ c' &= 0 & \frac{2\pi}{k} &= \Phi_{11} + \Phi_3 \end{aligned} \tag{4.30} $	<p>ODEs: 9 BCs: 9 Cont. par.: 1 Wave-form:</p> 
<p>Stick-slip-separation wave</p> $ \begin{aligned} V'_0 &= -\Phi_0 \frac{\Omega}{c} & V_0(0) &= V_{12}(1) \\ V'_{11} &= \Phi_{11} W_{11} & V_0(1) &= V_{11}(0) \\ W'_{11} &= \Phi_{11} \frac{1}{c^2 - a} f_1(V_{11}, W_{11}) & V_{11}(0) &= \frac{\alpha}{h} \left(g\delta + d \frac{\Omega}{c} \right) \\ V'_{12} &= \Phi_{11} W_{12} & W_{11}(0) &= -\frac{\Omega}{c} \\ W'_{12} &= \Phi_{11} \frac{1}{c^2 - a} f_1(V_{12}, W_{12}) & W_{11}(1) &= \frac{g\delta}{d} \\ U'_3 &= \Phi_3 Y_3 & U_3(0) &= \delta \\ Y'_3 &= \Phi_3 \frac{1}{c^2 - b} (dW_3 - gU_3) & Y_3(0) &= 0 \\ V'_3 &= \Phi_3 W_3 & V_3(0) &= V_{11}(1) \\ W'_3 &= \Phi_3 \frac{1}{c^2 - a} (-dY_3 - hV_3) & W_3(0) &= \frac{g\delta}{d} \\ \Phi'_0 &= 0 & U_3(1) &= \delta \\ \Phi'_{11} &= 0 & V_{12}(0) &= V_3(1) \\ \Phi'_{12} &= 0 & W_{12}(0) &= W_3(1) \\ \Phi'_3 &= 0 & W_{12}(1) &= -\frac{\Omega}{c} \\ c' &= 0 & \frac{2\pi}{k} &= \Phi_0 + \Phi_{11} + \Phi_{12} + \Phi_3 \end{aligned} \tag{4.31} $	<p>ODEs: 14 BCs: 14 Cont. par.: 1 Wave-form:</p> 

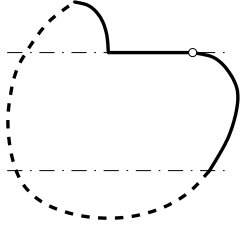
continued on next page

Overshooting stick-slip-separation wave		ODEs: 17 BCs: 17 Cont. par.: 1 Wave-form:	
$V'_0 = -\Phi_0 \frac{\Omega}{c}$	$V_0(0) = V_2(1)$		
$V'_{11} = \Phi_{11} W_{11}$	$V_0(1) = V_{11}(0)$		
$W'_{11} = \Phi_{11} \frac{1}{c^2 - a} f_1(V_{11}, W_{11})$	$V_{11}(0) = \frac{\alpha}{h} \left(g\delta + d \frac{\Omega}{c} \right)$		
$V'_{12} = \Phi_{11} W_{12}$	$W_{11}(0) = -\frac{\Omega}{c}$		
$W'_{12} = \Phi_{11} \frac{1}{c^2 - a} f_1(V_{12}, W_{12})$	$W_{11}(1) = \frac{g\delta}{d}$		
$V'_2 = \Phi_2 W_2$	$V_2(0) = V_{12}(1)$		
$W'_2 = \Phi_2 \frac{1}{c^2 - a} f_2(V_2, W_2)$	$W_2(0) = W_{12}(1)$		
$U'_3 = \Phi_3 Y_3$	$W_2(1) = -\frac{\Omega}{c}$		(4.32)
$Y'_3 = \Phi_3 \frac{1}{c^2 - b} (dW_3 - gU_3)$	$U_3(0) = \delta$		
$V'_3 = \Phi_3 W_3$	$Y_3(0) = 0$		
$W'_3 = \Phi_3 \frac{1}{c^2 - a} (-dY_3 - hV_3)$	$V_3(0) = V_{11}(1)$		
$\Phi'_0 = 0$	$W_3(0) = \frac{g\delta}{d}$		
$\Phi'_{11} = 0$	$U_3(1) = \delta$		
$\Phi'_{12} = 0$	$V_{12}(0) = V_3(1)$		
$\Phi'_2 = 0$	$W_{12}(0) = W_3(1)$		
$\Phi'_3 = 0$	$W_{12}(1) = -\frac{\Omega}{c}$		
$c' = 0$	$\frac{2\pi}{k} = \Phi_0 + \Phi_{11} + \Phi_{12} + \Phi_2 + \Phi_3$		

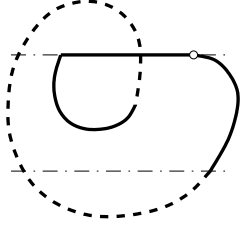
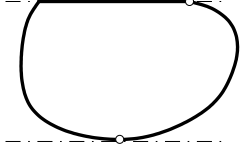
continued on next page

Crossing slip-separation wave		ODEs: 15 BCs: 15 Cont. par.: 1 Wave-form:
$V'_{11} = \Phi_{11}W_{11}$	$V_{11}(0) = V_2(1)$	
$W'_{11} = \Phi_{11}\frac{1}{c^2 - a}f_1(V_{11}, W_{11})$	$W_{11}(0) = -\frac{\Omega}{c}$	
$V'_{12} = \Phi_{11}W_{12}$	$W_{11}(1) = \frac{g\delta}{d}$	
$W'_{12} = \Phi_{11}\frac{1}{c^2 - a}f_1(V_{12}, W_{12})$	$V_2(0) = V_{12}(1)$	
$V'_2 = \Phi_2W_2$	$W_2(0) = -\frac{\Omega}{c}$	
$W'_2 = \Phi_2\frac{1}{c^2 - a}f_2(V_2, W_2)$	$W_2(1) = -\frac{\Omega}{c}$	
$U'_3 = \Phi_3Y_3$	$U_3(0) = \delta$	
$Y'_3 = \Phi_3\frac{1}{c^2 - b}(dW_3 - gU_3)$	$Y_3(0) = 0$	
$V'_3 = \Phi_3W_3$	$V_3(0) = V_{11}(1)$	
$W'_3 = \Phi_3\frac{1}{c^2 - a}(-dY_3 - hV_3)$	$W_3(0) = \frac{g\delta}{d}$	
$\Phi'_{11} = 0$	$U_3(1) = \delta$	
$\Phi'_{12} = 0$	$V_{12}(0) = V_3(1)$	
$\Phi'_2 = 0$	$W_{12}(0) = W_3(1)$	
$\Phi'_3 = 0$	$W_{12}(1) = -\frac{\Omega}{c}$	
$c' = 0$	$\frac{2\pi}{k} = \Phi_{11} + \Phi_{12} + \Phi_2 + \Phi_3$	

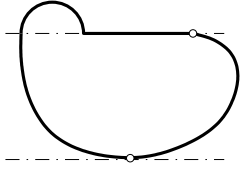
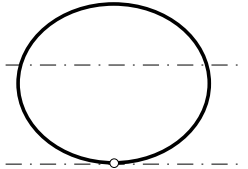
continued on next page

<p>Overshooting stick-slip-separation wave with separated switching.</p> $ \begin{aligned} V_0' &= -\Phi_0 \frac{\Omega}{c} & V_0(0) &= V_2(1) \\ V_{11}' &= \Phi_{11} W_{11} & V_0(1) &= V_{11}(0) \\ W_{11}' &= \Phi_{11} \frac{1}{c^2 - a} f_1(V_{11}, W_{11}) & V_{11}(0) &= \frac{\alpha}{h} \left(g\delta + d \frac{\Omega}{c} \right) \\ V_2' &= \Phi_2 W_2 & W_{11}(0) &= -\frac{\Omega}{c} \\ W_2' &= \Phi_2 \frac{1}{c^2 - a} f_2(V_2, W_2) & W_{11}(1) &= \frac{g\delta}{d} \\ U_3' &= \Phi_3 Y_3 & V_2(0) &= V_3(1) \\ Y_3' &= \Phi_3 \frac{1}{c^2 - b} (dW_3 - gU_3) & W_2(0) &= W_3(1) \\ V_3' &= \Phi_3 W_3 & W_2(1) &= -\frac{\Omega}{c} \\ W_3' &= \Phi_3 \frac{1}{c^2 - a} (-dY_3 - hV_3) & U_3(0) &= \delta \\ \Phi_0' &= 0 & Y_3(0) &= 0 \\ \Phi_{11}' &= 0 & V_3(0) &= V_{11}(1) \\ \Phi_2' &= 0 & W_3(0) &= \frac{g\delta}{d} \\ \Phi_3' &= 0 & U_3(1) &= \delta \\ c' &= 0 & \frac{2\pi}{k} &= \Phi_0 + \Phi_{11} + \Phi_2 + \Phi_3 \end{aligned} \tag{4.34} $	<p>ODEs: 14 BCs: 14 Cont. par.: 1 Wave-form:</p> 
--	--

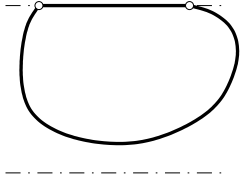
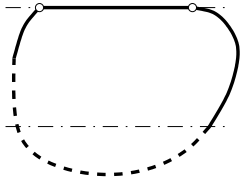
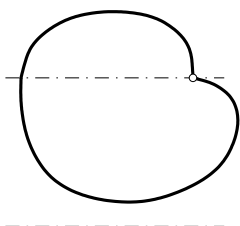
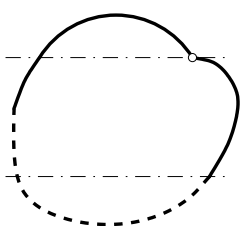
continued on next page

<p>Overshooting stick-slip-separation wave with <i>double</i> separated switching.</p> $ \begin{aligned} V'_0 &= -\Phi_0 \frac{\Omega}{c} & V_0(0) &= V_{12}(1) \\ V'_{11} &= \Phi_{11} W_{11} & V_0(1) &= V_{11}(0) \\ W'_{11} &= \Phi_{11} \frac{1}{c^2 - a} f_1(V_{11}, W_{11}) & V_{11}(0) &= \frac{\alpha}{h} \left(g\delta + d \frac{\Omega}{c} \right) \\ V'_{12} &= \Phi_{11} W_{12} & W_{11}(0) &= -\frac{\Omega}{c} \\ W'_{12} &= \Phi_{11} \frac{1}{c^2 - a} f_1(V_{12}, W_{12}) & W_{11}(1) &= \frac{g\delta}{d} \\ U'_3 &= \Phi_3 Y_3 & V_{12}(0) &= V_3(1) \\ Y'_3 &= \Phi_3 \frac{1}{c^2 - b} (dW_3 - gU_3) & W_{12}(0) &= W_3(1) \\ V'_3 &= \Phi_3 W_3 & W_{12}(1) &= -\frac{\Omega}{c} \\ W'_3 &= \Phi_3 \frac{1}{c^2 - a} (-dY_3 - hV_3) & U_3(0) &= \delta \\ \Phi'_0 &= 0 & Y_3(0) &= 0 \\ \Phi'_{11} &= 0 & V_3(0) &= V_{11}(1) \\ \Phi'_{12} &= 0 & W_3(0) &= \frac{g\delta}{d} \\ \Phi'_3 &= 0 & U_3(1) &= \delta \\ c' &= 0 & \frac{2\pi}{k} &= \Phi_0 + \Phi_{11} + \Phi_{12} + \Phi_3 \end{aligned} \tag{4.35} $	<p>ODEs: 14 BCs: 14 Cont. par.: 1 Wave-form:</p> 
<p>Separating bifurcation of a stick-slip wave</p> $ \begin{aligned} V'_0 &= -\Phi_0 \frac{\Omega}{c} & V_{11}(0) &= \frac{\alpha}{h} \left(g\delta + d \frac{\Omega}{c} \right) \\ V'_{11} &= \Phi_{11} W_{11} & W_{11}(0) &= -\frac{\Omega}{c} \\ W'_{11} &= \Phi_{11} f_1(V_{11}, W_{11}) & W_{11}(1) &= \frac{g\delta}{d} \\ V'_{12} &= \Phi_{12} W_{12} & 0 &= f_1(V_{11}(1), W_{11}(1)) \\ W'_{12} &= \Phi_{12} \frac{1}{c^2 - a} f_1(V_{12}, W_{12}) & V_0(0) &= V_{12}(1) \\ \Phi'_0 &= 0 & V_0(1) &= V_{12}(0) \\ \Phi'_{11} &= 0 & W_{12}(1) &= -\frac{\Omega}{c} \\ \Phi'_{12} &= 0 & V_{12}(0) &= V_{11}(1) \\ c' &= 0 & W_{12}(0) &= W_{11}(1) \\ & & \frac{2\pi}{k} &= \Phi_0 + \Phi_{11} + \Phi_{12} \end{aligned} \tag{4.36} $	<p>ODEs: 9 BCs: 10 Cont. par.: 2 Label: P0 Wave-form:</p> 

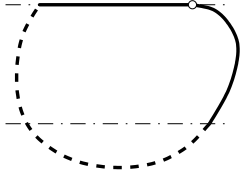
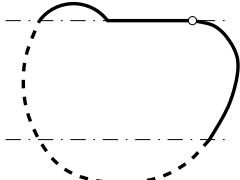

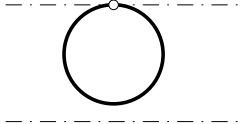
continued on next page

<p>Separating bifurcation of an overshooting stick-slip wave</p> $ \begin{aligned} V_0' &= -\Phi_0 \frac{\Omega}{c} & V_0(0) &= V_2(1) \\ V_{11}' &= \Phi_{11} W_{11} & V_0(1) &= V_{11}(0) \\ W_{11}' &= \Phi_{11} \frac{1}{c^2 - a} f_1(V_{11}, W_{11}) & V_{11}(0) &= \frac{\alpha}{h} \left(g\delta + d \frac{\Omega}{c} \right) \\ V_{12}' &= \Phi_{12} W_{12} & W_{11}(0) &= -\frac{\Omega}{c} \\ W_{12}' &= \Phi_{12} \frac{1}{c^2 - a} f_1(V_{12}, W_{12}) & W_{11}(1) &= \frac{g\delta}{d} \\ V_2' &= \Phi_2 W_2 & 0 &= f_1(V_{11}(1), W_{11}(1)) \\ W_2' &= \Phi_2 \frac{1}{c^2 - a} f_2(V_2, W_2) & V_{12}(0) &= V_{11}(1) \\ \Phi_0' &= 0 & W_{12}(0) &= W_{11}(1) \\ \Phi_{11}' &= 0 & W_{12}(1) &= -\frac{\Omega}{c} \\ \Phi_{12}' &= 0 & V_2(0) &= V_{12}(1) \\ \Phi_2 &= 0 & W_2(0) &= W_{12}(1) \\ c' &= 0 & W_2(1) &= -\frac{\Omega}{c} \\ & & \frac{2\pi}{k} &= \Phi_0 + \Phi_{11} + \Phi_2 \end{aligned} \tag{4.37} $	<p>ODEs: 12 BCs: 13 Cont. par.: 1 Label: P0 Wave-form:</p> 
<p>Separating bifurcation of a crossing slip wave</p> $ \begin{aligned} V_{11}' &= \Phi_{11} W_{11} & V_{11}(0) &= V_2(1) \\ W_{11}' &= \Phi_{11} \frac{1}{c^2 - a} f_1(V_{11}, W_{11}) & W_{11}(0) &= -\frac{\Omega}{c} \\ V_{12}' &= \Phi_{12} W_{12} & W_{11}(1) &= \frac{g\delta}{d} \\ W_{12}' &= \Phi_{12} \frac{1}{c^2 - a} f_1(V_{12}, W_{12}) & 0 &= f_1(V_{11}(1), W_{11}(1)) \\ V_2' &= \Phi_2 W_2 & V_{12}(0) &= V_{11}(1) \\ W_2' &= \Phi_2 \frac{1}{c^2 - a} f_2(V_2, W_2) & W_{12}(0) &= W_{11}(1) \\ \Phi_{11}' &= 0 & W_{12}(1) &= -\frac{\Omega}{c} \\ \Phi_{12}' &= 0 & V_2(0) &= V_{12}(1) \\ \Phi_2 &= 0 & W_2(0) &= W_{12}(1) \\ c' &= 0 & W_2(1) &= -\frac{\Omega}{c} \\ & & \frac{2\pi}{k} &= \Phi_0 + \Phi_{11} + \Phi_2 \end{aligned} \tag{4.38} $	<p>ODEs: 12 BCs: 13 Cont. par.: 1 Label: P0 Wave-form:</p> 

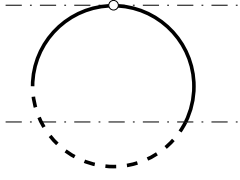
continued on next page

<p>Switching bifurcation of a stick-slip wave</p> <p>BVP (4.27) augmented by the boundary condition</p> $V_{11}(1) = -\frac{\alpha}{h} \left(g\delta + d\frac{\Omega}{c} \right) \quad (4.39)$	<p>ODEs: 6 BCs: 7 Cont. par.: 2 Label: SW Wave-form:</p> 
<p>Switching bifurcation of a stick-slip-separation wave</p> <p>BVP (4.31) augmented by the boundary condition</p> $V_{12}(1) = -\frac{\alpha}{h} \left(g\delta + d\frac{\Omega}{c} \right) \quad (4.40)$	<p>ODEs: 14 BCs: 15 Cont. par.: 2 Label: SW Wave-form:</p> 
<p>Crossing bifurcation of an overshooting stick-slip wave</p> <p>BVP (4.28) augmented by the boundary condition</p> $V_2(1) = \frac{\alpha}{h} \left(g\delta + d\frac{\Omega}{c} \right) \quad (4.41)$	<p>ODEs: 6 BCs: 7 Cont. par.: 2 Label: CR Wave-form:</p> 
<p>Crossing bifurcation of an overshooting stick-slip-separation wave</p> <p>BVP (4.32) augmented by the boundary condition</p> $V_2(1) = \frac{\alpha}{h} \left(g\delta + d\frac{\Omega}{c} \right) \quad (4.42)$	<p>ODEs: 6 BCs: 7 Cont. par.: 2 Label: CR Wave-form:</p> 

continued on next page

<p>Fly-over bifurcation of a stick-slip-separation wave</p> <p>BVP (4.31) augmented by the boundary condition</p> $W_3(1) = -\frac{\Omega}{c} \quad (4.43)$	<p>ODEs: 15 BCs: 16 Cont. par.: 2 Labels: FO1 Wave-form:</p> 
<p>Fly-over bifurcation of an overshooting stick-slip-separation wave</p> <p>BVP (4.32) augmented by the boundary condition</p> $W_3(1) = -\frac{\Omega}{c} \quad (4.44)$	<p>ODEs: 17 BCs: 18 Cont. par.: 2 Label: FO1 Wave-form:</p> 
<p>Secondary fly-over bifurcation of an overshooting stick-slip-separation wave with separated switching</p> <p>BVP (4.31) augmented by the boundary condition</p> $W_3(1) = -\frac{\Omega}{c} \quad (4.45)$	<p>ODEs: 15 BCs: 16 Cont. par.: 2 Labels: FO2 Wave-form:</p> 
<p>Grazing bifurcation of a stick-slip wave</p> <p>BVP (4.27) augmented by the boundary condition</p> $\Phi_0 = 0 \quad (4.46)$	<p>ODEs: 6 BCs: 7 Cont. par.: 2 Label: GR Wave-form:</p> 

continued on next page

<p>Grazing bifurcation of a stick-slip-separation wave</p> <p>BVP (4.31) augmented by the boundary condition</p> $\Phi_0 = 0 \quad (4.47)$	<p>ODEs: 14 BCs: 15 Cont. par.: 2 Label: GR Wave-form:</p> 
--	--

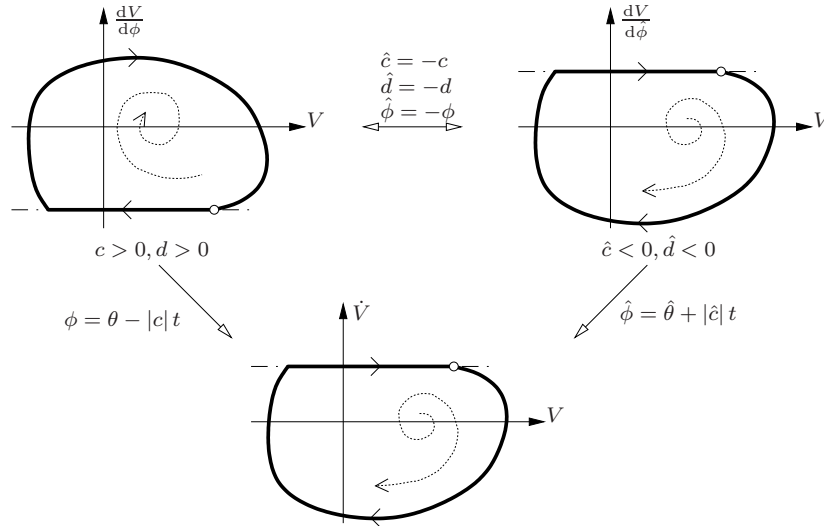


Figure 4.9: Construction of forward and backward waves in time changing the signs of d and c .

4.5.4 The case $c > 0$

Considering forward waves with $c > 0$ we always have to bear in mind that the orientation of the wave in time t is opposite to the orientation in the phase ϕ . Observing again cases (I)-(IIb) in Figure 4.6 we expect periodic solutions only if the equilibrium is a sink w.r.t. ϕ which corresponds to a source w.r.t. t . Otherwise, a phase curve starting at the sicking domain would spiral towards the equilibrium in time. Thus, periodic solutions are expected in the neighborhood of the Hopf bifurcation discussed in Section 4.5.1, so we have to consider small values of the radial ratio ξ . Indeed, the bifurcating smooth periodic orbit at the Hopf-Bifurcation will be continued numerically until it hits the discontinuity at a grazing bifurcation. Thus we will find smooth pure slip waves in the present case. The following mechanism of successive switching, crossing and separating bifurcations has already been exhaustively explained in Section 3.2 and Section 4.5.3 and we will only provide a listing of the boundary value problems that have been continued numerically in Table 4.2 here.

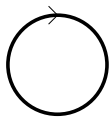
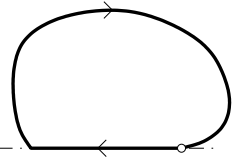
Another method to obtain forward waves has already been mentioned in Section 4.5.1 which is due to the invariance relation (4.22). However, such a solution requires the isolated change of the sign of d leaving the remaining parameters constant, which is physically not consistent. It makes sense, though, for a deeper understanding of the problem to give some thought to this issue. Consider a forward wave, say $V(\phi)$, with $c > 0$ and $d > 0$. By (4.22) this corresponds to a backward wave $V(\hat{\phi})$ where $\hat{\phi} = -\phi$, $\hat{c} = -c$ and $\hat{d} = -d$ the phase portrait of which is obtained by a reflection at the V -axis and a reversal of the orientation (Figure 4.9). If we transform both solutions back from the $(\phi, \hat{\phi})$ -domains to the time domain we obtain equal waveforms, which are rotating in opposite directions on the shaft-bush interface.

Next, the formulation of boundary conditions deserves closer attention. Again, due to the inversion of the orientation in time (see again Figure 4.9) the boundary conditions on the right and left ends of certain segments of a cycle have to be swapped compared

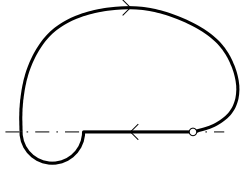
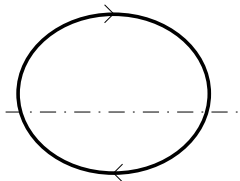
4 Non-smooth bifurcations of travelling waves

with the backward waves described before in Section 4.5.3. This shall become clear in Table 4.2. The solutions are discussed in Section 4.6. We will find pure slip (b.v.p. (4.48)), stick-slip (b.v.p. (4.49)), overshooting stick-slip (b.v.p. (4.50)), crossing slip (b.v.p. (4.51)) waves in the cases (I) and (IIa) and additionally crossing slip-separation waves (b.v.p. (4.52)) only in case (I) where $d > 0$. For the time being no periodic solutions have been found in case (IIb).

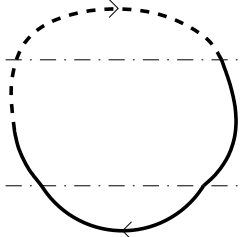
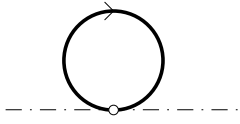
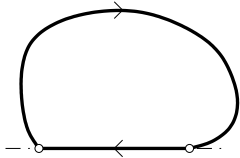
Table 4.2: Boundary value problems corresponding to forward rotating waves ($c > 0$) and their non-smooth bifurcations. The indicated sense of rotation corresponds to the orientation of ϕ .

<p>Pure slip waves</p> $\begin{aligned} V'_{11} &= \Phi_{11} W_{11} & V_{11}(0) &= V_{22}(1) \\ W'_{11} &= \Phi_{11} \frac{1}{c^2 - a} f_1(V_{11}, W_{11}) & W_{11}(0) &= W_{22}(1) \\ \Phi'_{11} &= 0 & f_1(V_{11}(0), W_{11}(0)) &= 0 \\ c' &= 0 & \frac{2\pi}{k} &= \Phi_{11} \end{aligned} \quad (4.48)$	<p>ODEs: 4 BCs: 45 Cont. par.: 1 Wave-form:</p> 
<p>Stick-slip waves</p> $\begin{aligned} V'_0 &= -\Phi_0 \frac{\Omega}{c} & V_0(0) &= V_{11}(1) \\ V'_{11} &= \Phi_{11} W_{11} & V_0(1) &= V_{11}(0) \\ W'_{11} &= \Phi_{11} f_1(V_{11}, W_{11}) & V_{11}(1) &= \frac{\alpha}{h} \left(g\delta + d \frac{\Omega}{c} \right) \\ \Phi'_0 &= 0 & W_{11}(0) &= -\frac{\Omega}{c} \\ \Phi'_{11} &= 0 & W_{11}(1) &= -\frac{\Omega}{c} \\ c' &= 0 & \frac{2\pi}{k} &= \Phi_0 + \Phi_{11} \end{aligned} \quad (4.49)$	<p>ODEs: 6 BCs: 6 Cont. par.: 1 Wave-form:</p> 

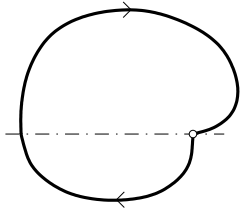
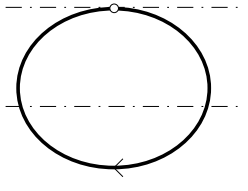
continued on next page

<p>Overshooting Stick-slip wave</p> $ \begin{aligned} V_0' &= -\Phi_0 \frac{\Omega}{c} & V_0(0) &= V_{11}(1) \\ V_{11}' &= \Phi_{11} W_{11} & V_0(1) &= V_2(0) \\ W_{11}' &= \Phi_{11} f_1(V_{11}, W_{11}) & V_{11}(1) &= \frac{\alpha}{h} \left(g\delta + d \frac{\Omega}{c} \right) \\ V_2' &= \Phi_2 W_2 & W_{11}(0) &= -\frac{\Omega}{c} \\ W_2' &= \Phi_2 \frac{1}{c^2 - a} f_2(V_2, W_2) & W_{11}(1) &= -\frac{\Omega}{c} \\ \Phi_0' &= 0 & V_2(0) &= V_0(1) \\ \Phi_{11}' &= 0 & W_2(0) &= -\frac{\Omega}{c} \\ \Phi_2 &= 0 & W_2(1) &= W_{11}(0) \\ c' &= 0 & \frac{2\pi}{k} &= \Phi_0 + \Phi_{11} + \Phi_2 \end{aligned} $ <p style="text-align: right;">(4.50)</p>	<p>ODEs: 9 BCs: 9 Cont. par.: 1 Wave-form:</p> 
<p>Crossing slip wave</p> <p style="text-align: center;">Equivalent to (4.29)</p> <p style="text-align: right;">(4.51)</p>	<p>ODEs: 7 BCs: 7 Cont. par.: 1 Wave-form:</p> 

continued on next page

<p>Crossing slip-separation wave (only for $d > 0$)</p> $ \begin{aligned} V'_{11} &= \Phi_{11} W_{11} & V_{11}(0) &= V_2(1) \\ W'_{11} &= \Phi_{11} \frac{1}{c^2 - a} f_1(V_{11}, W_{11}) & W_{11}(0) &= -\frac{\Omega}{c} \\ V'_{12} &= \Phi_{11} W_{12} & W_{11}(1) &= \frac{g\delta}{d} \\ W'_{12} &= \Phi_{11} \frac{1}{c^2 - a} f_1(V_{12}, W_{12}) & V_2(0) &= V_{12}(1) \\ V'_2 &= \Phi_2 W_2 & W_2(0) &= -\frac{\Omega}{c} \\ W'_2 &= \Phi_2 \frac{1}{c^2 - a} f_2(V_2, W_2) & W_2(1) &= -\frac{\Omega}{c} \\ U'_3 &= \Phi_3 Y_3 & U_3(0) &= \delta \\ Y'_3 &= \Phi_3 \frac{1}{c^2 - b} (dW_3 - gU_3) & Y_3(1) &= 0 \\ V'_3 &= \Phi_3 W_3 & V_3(0) &= V_{11}(1) \\ W'_3 &= \Phi_3 \frac{1}{c^2 - a} (-dY_3 - hV_3) & W_3(1) &= \frac{g\delta}{d} \\ \Phi'_{11} &= 0 & U_3(1) &= \delta \\ \Phi'_{12} &= 0 & V_{12}(0) &= V_3(1) \\ \Phi'_2 &= 0 & W_{12}(0) &= W_3(1) \\ \Phi'_3 &= 0 & W_{12}(1) &= -\frac{\Omega}{c} \\ c' &= 0 & \frac{2\pi}{k} &= \Phi_{11} + \Phi_{12} + \Phi_2 + \Phi_3 \end{aligned} \tag{4.52} $	<p>ODEs: 15 BCs: 15 Cont. par.: 1 Wave-form:</p> 
<p>Grazing bifurcation of a pure slip wave</p> <p>BVP (4.48) augmented by the boundary condition</p> $ W_{11}(1) = -\frac{\Omega}{c} \tag{4.53} $	<p>ODEs: 6 BCs: 7 Cont. par.: 2 Label: GR Wave-form:</p> 
<p>Switching bifurcation of a stick-slip wave</p> <p>BVP (4.49) augmented by the boundary condition</p> $ V_{11}(0) = -\frac{\alpha}{h} \left(g\delta + d\frac{\Omega}{c} \right) \tag{4.54} $	<p>ODEs: 6 BCs: 7 Cont. par.: 2 Label: SW Wave-form:</p> 

continued on next page

<p>Crossing bifurcation of an overshooting stick-slip wave</p> <p>BVP (4.50) augmented by the boundary condition</p> $V_2(0) = \frac{\alpha}{h} \left(g\delta + d\frac{\Omega}{c} \right) \quad (4.55)$	<p>ODEs: 6 BCs: 7 Cont. par.: 2 Label: CR Wave-form:</p> 
<p>Separating bifurcation of a crossing slip wave (only for $d > 0$)</p> <p>Equivalent to (4.38)</p>	<p>ODEs: 12 BCs: 13 Cont. par.: 1 Label: P0 Wave-form:</p> 

4.6 Numerical Results

4.6.1 Backward waves ($c < 0$)

In a first approach we choose the static coefficient of friction α and the rotation velocity Ω as continuation parameters and present a stratification of the parameter space (α, Ω, c) in Figure 4.10 for waves with wave-number $k = 1$ and $c < 0$. Throughout the depicted plots we use the black color for bifurcations of non-separated solutions and accordingly the blue color for separated solutions. Note that Figure 4.10 is a projection of the parameter space into the (α, Ω) -plane, i. e. all true intersections of solution paths are explicitly indicated by dots. We find the loci of switching and crossing bifurcations of non-separated stick-slip cycles, indicated by SW and CR, respectively and plotted in black color. The remaining bifurcations occur for separation waves which appear by separating bifurcations shown in red labeled P0. There are two branches of switching bifurcations of separated stick-slip cycles, labeled SW in blue color: one appears for small values of α and $\Omega > 6 \cdot 10^{-2}$ (Figures 4.26-4.27), another near $\alpha \approx 1.5$ and $\Omega \approx 10^{-2}$ (Figure 4.16 and 4.18). A curve of crossing bifurcations of overshooting stick-slip-separation cycles (blue-colored label CR) connects to the curve of crossing bifurcations of non-separated cycles. Furthermore two curves of fly-over bifurcations are found indicating single (FO1) and double (FO2) crossings of Σ_1 via S_{SEP} as described in Section 4.5.3. Moreover we observe three bifurcation points of codimension 2 located at B_1, B_2 and B_3 . At B_1 a crossing and a separating event appear simultaneously and at B_2 switching and separating occur together. At B_3 the switching bifurcation of a separated

stick-slip cycle coincides with a fly-over bifurcation, which means that the separated part of the wave ends up in the tangent point T_2 . In the following all possible sequences of bifurcations are explained by considering three typical examples.

Example 1. Bifurcations for constant α

Figures 4.11-4.15 illustrate the sequence of bifurcations for given $\alpha = 0.42$. Figure 4.11 shows the corresponding solution path in the (Ω, c) -domain. Interestingly, there are two solution branches, yielding two different rotating waves with wave speeds near $c \approx -1$ and $c \approx -2$.⁴

Consider first the “fast” wave. It starts as a stick-slip wave if the rotation velocity Ω is increased from zero (Figure 4.12). It suffers a switching bifurcation, starts overshooting and afterwards exhibits a separating segment beyond the red bifurcation curve labeled P0. Immediately, a crossing bifurcation of the overshooting stick-slip-separation circle follows at CR. In the interval⁵ $0.053 < \Omega < 0.122$ we hence observe crossing slip-separation cycles lacking a stick-regime. A stick-regime appears again after a second crossing bifurcation (CR) at $\Omega \cong 0.122$ (Figure 4.13) and grows until a second switching bifurcation at $\Omega \cong 2.871$ terminates the overshooting motion (cf. Figure 4.10). Physically, the separated gap, however, has become too large to be meaningful.

The “slow” wave coexisting with the previously described one departs at $\Omega = 0$ with $c \cong -0.9732$. It likewise emanates as a stick-slip wave which starts separating instead of switching. When the solution branch hits the bifurcation curve FO1 (see enlargement A in Figure 4.11) the separating segment ends up at the discontinuity and a variation of Ω leads to separated switching solutions, i. e. the separating segment terminates in the overshooting domain (Figure 4.14). A wave of this kind is also shown in Figure 4.24 where the radial displacements are plotted around the circumference of the shaft in order to show the different contact zones. We observe a large sticking region and a quite small circulating zone of slip, separation and overshooting.

A second fly-over happens at FO2 after which the separated trajectory crosses Σ_1 a second time and reenters the domain of positive slip (Figure 4.15). Although it is still uncertain, whether these solution will occur physically, the corresponding radial displacements describing the separated gap seem small enough to be feasible (Figure 4.21). Considering the S-shaped continuation path of these waves we perceive the coexistence of four waves in an interval of Ω , three of which are “slow” and one of which is “fast”. The continuation had to be terminated as a second separation area would build up at P02 because the simple numerical method described in Section 4.5.2 becomes too cumbersome. It is conjectured that the formation of novel separation zones and fly-overs continues and that consequently this second branch of solutions exists for all pairs (α, Ω) . However, this issue has to remain an open question for the time being. A single solution shortly after the point PO2 in Figure 4.11 is still presented in Figure 4.25. It was obtained by direct integration using the algorithm in LEINE [2000]. The boundary

⁴Selecting steel as the material of the bush the physical wave speed is about $5000 \times c$ m/s!

⁵For steel and an inner radius of $R_i = 0.1$ m the number of rotations per second may be approximated by $8000 \times \Omega$!

conditions were fulfilled by trial and error. However, this issue has to remain an open question for the time being.

Example 2. Bifurcations for intermediate Ω

We choose next a fixed value of $\Omega = 1.19 \cdot 10^{-2}$ (Figure 4.10). Increasing α from zero we start with a crossing slip wave which obtains a stick zone after the crossing bifurcation at **CR** in Figure 4.10. The resulting overshooting stick-slip wave suffers a switching bifurcation at **SW** which annihilates the overshooting segment. For a relatively large interval of α we observe stick-slip waves. Near $\alpha \approx 1.5$ the bifurcations become more complicated again and Figure 4.16 shows the corresponding detailed bifurcation diagram in the (α, c) -plane. The stick slip cycle starts separating at **P0** (Figure 4.17). However, considering Figure 4.16 the separation effect acts as a non-smooth fold bifurcation, where a stick-slip wave merges with a stick-slip separation wave (Figure 4.18). The separated wave starts overshooting beyond **SW** (Figure 4.19), the overshooting amplitude, however, being very small (detail in Figure 4.19). The period on the circumference, however, is quite considerable as it is seen in Figure 4.23.

Again, due to the turning points of the continuation path, we observe an interval of α where multiple waveforms coexist. After **SW** the separating segment grows large enough to generate two fly-over bifurcations, successively (**FO1** and **FO2** in Figures 4.19-4.20). In this case however, the displacements during separation are too large to be practically meaningful (see Figure 4.22).

Example 3. Bifurcations for large Ω

Choosing $\Omega = 1$ we obtain the bifurcation diagram shown in Figure 4.26 for increasing α . At $\alpha = 0$ (i. e. no friction) we obtain a pure slip wave with non-zero amplitude (Figure 4.27). For $\alpha > 0$ immediately a separation zone is established and the slip-separation cycle grows until it touches the discontinuity Σ_1 at **GR**. The continuation path of the slip-separation solution has a limit point which can itself be continued in the parameter space yielding the curve labeled **LP** in Figures 4.10 and 4.26. At the grazing bifurcation **GR** a slip-separation wave merges with a stick-slip-separation wave. The latter starts overshooting at **SW** and exhibits a fly-over at $\alpha = 1.65$ (Figure 4.27). Again, the displacements during separation grow too large quite rapidly.

4.6.2 Forward waves ($c > 0$)

Hopf-bifurcations for small ξ

As already announced in Section 4.5.4 we start with a continuation of Hopf bifurcations of the equilibrium given by the analytic relation (4.20) varying the radial ratio ξ and the rotation velocity Ω . We choose again a representative friction law where $\alpha = 0.1$, $\beta = 0.2$ and $\gamma = 0.0615$. The diameter mismatch and the Poisson ratio are kept fixed ($\delta = 0.005, \nu = 0.3$) and we more or less arbitrarily selected mode-4 waves for a closer investigation. The static friction coefficient was chosen sufficiently small that the computed bifurcations occur at reasonably low rotation velocities. In Figure 4.28 the obtained continuation path is shown in the parameter plane as the curve labeled **Ho**.

As expected, Hopf bifurcations occur for small ratios ξ i. e. for small rings around the shaft. Figure 4.29 provides a closer look to the Hopf bifurcation for a fixed $\xi = 1.22$ ($d < 0$). The equilibrium is stable⁶ for low rotation velocities. At the critical value a stable supercritical cycle branches off which exists only within a very small interval of rotation velocities. The bifurcating periodic orbit corresponds to a smooth mode-4 pure-slip wave. At a grazing bifurcation the stable smooth cycle merges with an unstable stick-slip cycle that has developed in parallel. Beyond this grazing bifurcations no limit cycles have been found so far. The continuation path of the grazing bifurcation using b.v.p. (4.53) is inserted in Figure 4.28 as a bold curve labeled GR. The aforementioned (unstable) stick slip cycle may suffer a sequence of switching, crossing and separating bifurcations that will be explained in the following.

Non-smooth bifurcations of mode-4 waves

In addition to the grazing bifurcation Figure 4.28 contains the continuation paths of switching (SW), crossing (CR) and separating (P0) bifurcations obtained from b.v.p.'s (4.54), (4.55) and (4.38). Below the switching line SW stick slip cycles exist that vanish in the grazing bifurcation. Figure 4.30 shows the evolution of stick-slip waves in the phase plane for constant $\Omega = 0.1^7$ increasing the ratio ξ . The amplitude of the cycle increases with the diameter of the bush while the wave speed decreases.

Figure 4.31 shows overshooting stick-slip waves in the phase plane that build up after a switching bifurcation (SW) of a stick-slip wave. In the example $\xi = 1.122$ has been chosen and Ω has been increased quasi-statically starting from the cycle labeled $\xi = 1.12$ in Figure 4.30. It is remarked that increasing the shaft velocity for fixed ξ recovers practically the same bifurcation sequence as in the simple friction oscillator for rising band speeds. For a critical rotation velocity ($\Omega = 1.78$) the overshooting part ends up in the visible tangent point, which produces crossing slip waves if Ω is increased further (see Figure 4.32). The phase curves in Figure 4.32 are obtained for $\xi = 1.14, \alpha = 0.1$. A larger value of $\alpha = 1$ has been chosen in Figures 4.30-4.31 in order to ensure a better visibility of sticking and overshooting domains. The wave speed of the crossing cycles settles at the almost constant value $c = 2.388$. For larger shaft velocities the grazing, switching and crossing bifurcations virtually coincide such that a crossing slip wave emerges almost immediately after the grazing bifurcation.

For huge rotation velocities a separation zone builds up after a separating bifurcation. Figure 4.33 shows some solutions in the vicinity of the separating bifurcation projected into the (U, V, W) -phase space. The separated segment grows very fast, the wave speed remains practically constant. Figure 4.34 finally demonstrates the propagation of an overshooting slip-separation wave from Figure 4.33 (those, with the largest radial displacements) on the shaft-bush interface. While the radial displacements had to be scaled by a factor 8000 for better visibility the periods of the slip, separation and overshooting segments agree with the values computed numerically. Separated solutions appear only if $d > 0$. For $d < 0$ all periodic solutions terminate at a finite rotation velocity in a

⁶Note again, that 'stability' here means stability with respect to the phase ϕ . In time t the stability properties are reversed but still are confined to the reduced system (4.18)!

⁷Note that due to the scaling (4.2)₆ rotation velocities beyond $\Omega = 1$ are hardly feasible.

grazing bifurcation.

The stratification of the parameter plane presented in Figure 4.28 fortifies the assertion that the behavior of forward waves with $d > 0$ is similar to backward waves with $d < 0$. Take for example $\alpha = 0.1$ in Figure 4.10 and follow the bifurcations for increasing Ω . The value of $d = -0.88$ used there was obtained for $\xi = 2$ and $\nu = 0.3$. Accordingly, $d = +0.88$ yields $\xi = 1.11$. The sequences of bifurcations are equal in Figure 4.28 for $\xi = 1.11$ and in Figure 4.10 for $\alpha = 0.1$ albeit shifted towards larger shaft velocities for forward waves.

4.6.3 A note on stability investigations

Certainly, the first question that one is tempted to ask observing the numerical results in Section 4.6 is, whether the obtained solutions are mechanically stable or not. For the time being an answer that is satisfactory can unfortunately not be given. First steps towards stability considerations for a travelling stick-slip wave (excluding separation!) using just Coulomb's law of friction (i. e. $\beta = \gamma = 0$ here) were published by STEINDL [2006], TEUFEL ET AL. [2006a] and NGUYEN ET AL. [2007] and shall in the following be briefly explained.

In order to investigate the stability of a travelling stick-slip wave solution, say $V_{TW}(\phi)$, two approaches have been proposed. The first is to smooth the sign function by $\tanh(v_{rel}/\epsilon)$ where ϵ is a sufficiently small parameter, next to replace the spacial derivatives in (4.13) by finite differences and finally to formulate a large boundary value problem for the components $V_i(t)$, each describing one segment of the travelling wave, connecting a grid point to the next one. The eigenvalues of a permutation map that takes the solution at one grid point to the previous one are used as a first estimate for the eigenvalues of the travelling wave. However, these eigenvalues are not very accurate and numerical difficulties arise because of the stiffness caused by the smoothed sign function. Next, the paths of critical eigenvalues λ found by the previous idea have been continued by formulating a boundary value problem for the eigenfunctions $\psi(\theta)$ using an ansatz $V = V_{TW} + V_L$ where $V_L = \exp(\lambda t)\psi(\theta)$ in (4.13). Recent advances suggest that e. g. a stick-slip wave of mode 4 loses stability by a Hopf bifurcation which creates a motion on a non-smooth torus. Parameter regions which at first glance produce an irregular motion are found as well (NGUYEN ET AL. [2007]).

Let us summarize that the stability calculations start to be successful for *one* type of stick-slip wave with considerable numerical effort. In view of the more complicated solutions presented here incorporating a more sophisticated friction law the development of a numerical procedure that reliably allows for the prediction of the stability of a travelling wave is still an open task. Moreover, it has to be mentioned that even the calculations of A. STEINDL outlined above are based upon the one-mode Galerkin reduction (4.13) introduced in Section 4.4.

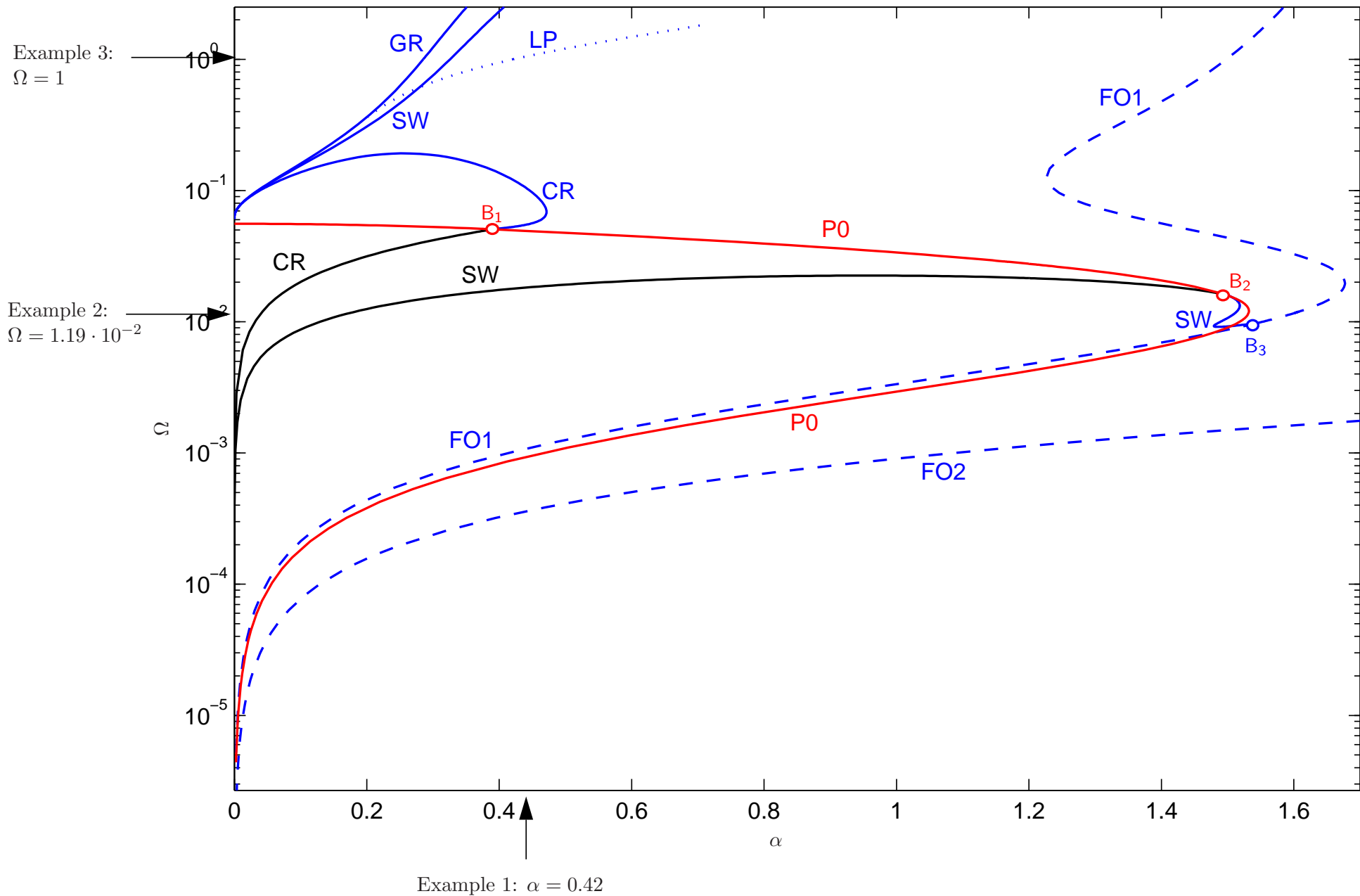


Figure 4.10: Stratification of the parameter space projected into the (α, Ω) -plane for mode $k = 1$, $c < 0$ and $\beta = 0.2$, $\gamma = 0.0615$, $\delta = 0.005$, $\xi = 2$, $\nu = 0.3$ showing the loci of grazing (GR), switching (SW), crossing (CR), separating (P0), fly-over (FO1) and double fly-over (FO2) bifurcations as well as the continuation path of limit points of slip-separation solutions (LP). The blue color is used for bifurcations of separated cycles. The sequences of bifurcations in Examples 1-3 are shown in Figures 4.11-4.27. Bifurcations of codimension 2 occur at B_1 - B_3 .

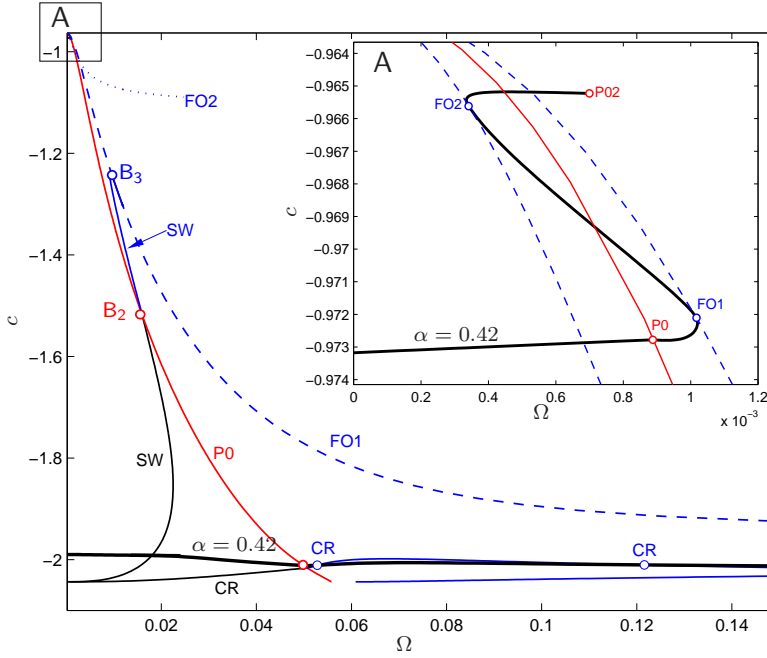


Figure 4.11: Stratification of the parameter space projected into the (Ω, c) -plane. The solution paths of waveforms for $\alpha = 0.42$ as the rotation velocity Ω is increased are shown as black bold curves. Two solution paths are found at $c \approx -2$ (phase portraits in Figures 4.12-4.13) and $c \approx -1$ (enlargement A, phase portraits Figures 4.14-4.15).

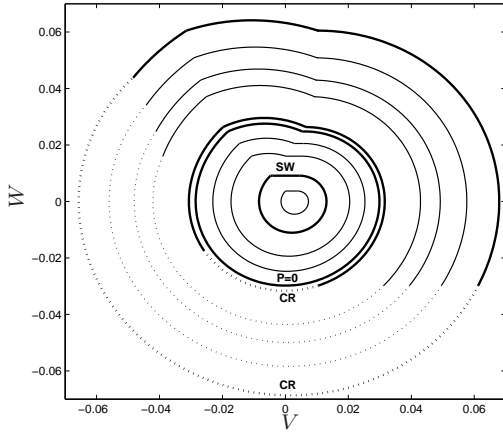


Figure 4.12: Evolution of a stick-slip wave in the phase plane for $c \approx -2$. The bifurcating cycles are highlighted. Separation is indicated by a dotted line.

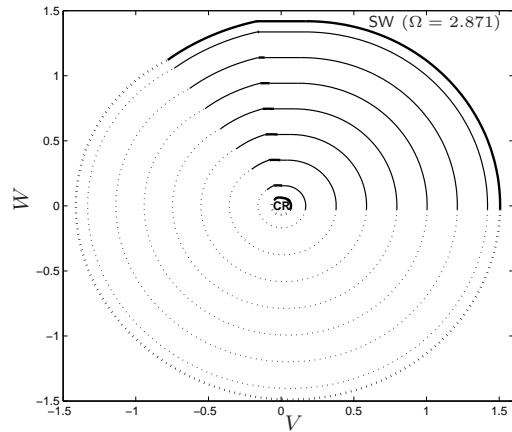


Figure 4.13: Further evolution towards stick-slip-separation waves of higher amplitude for large Ω beyond the second crossing bifurcation. The overshooting segments are barely visible.

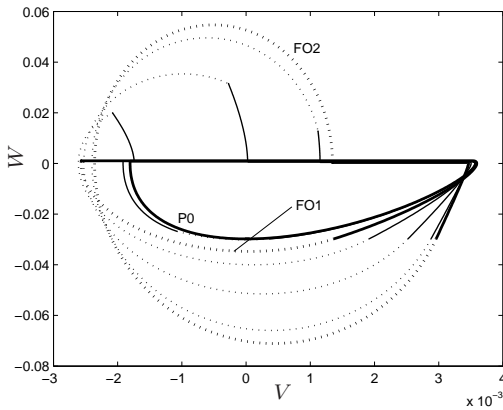


Figure 4.14: Evolution of a stick-slip wave for $c \approx -1$. After separation (P0) two fly-over bifurcations (FO1, FO2) can be observed.

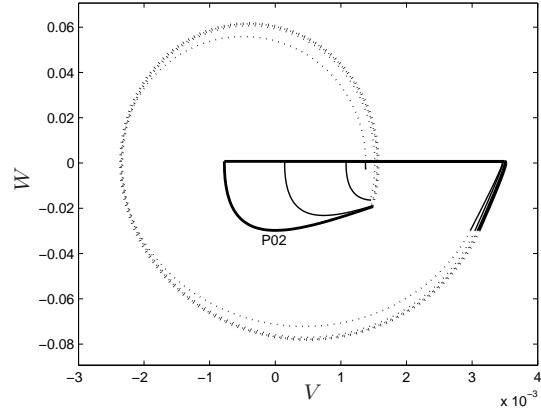


Figure 4.15: Cycles with double separated switching beyond the second fly-over (FO2). At P02 a second separation zone starts to build up.

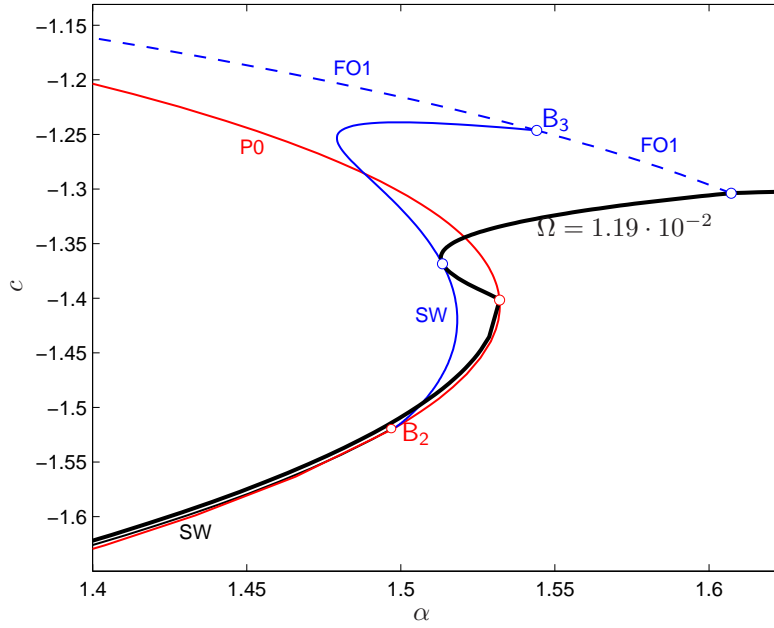


Figure 4.16: Stratification of the parameter space projected into the (α, c) -plane. The black bold curve shows the solution path for $\Omega = 1.19 \cdot 10^{-2}$ as the static coefficient of friction α is increased. B_3 indicates a bifurcation point of codimension 2. The corresponding phase portraits are depicted in Figures 4.17-4.20.

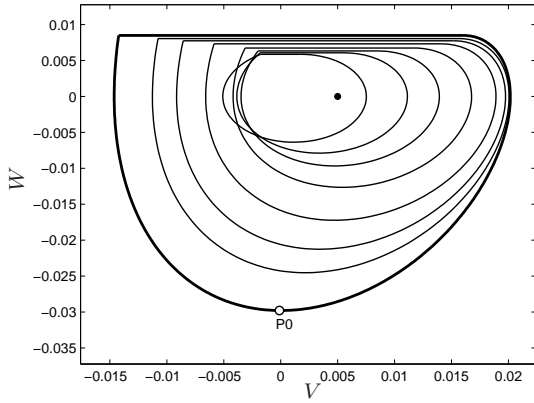


Figure 4.17: Evolution of stick-slip waves in the phase plane for increasing α until separation occurs at P_0 .

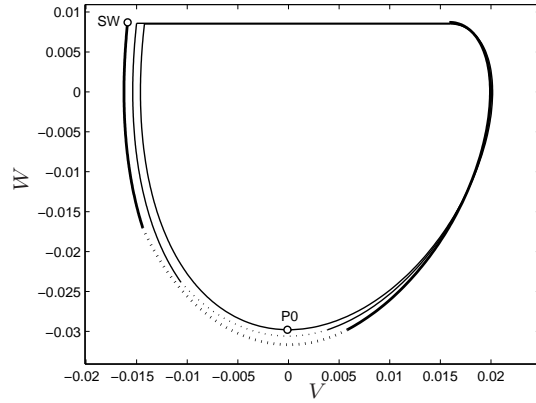


Figure 4.18: Passage from separating (P_0) to the switching bifurcation of the separated cycle (SW) close-by.

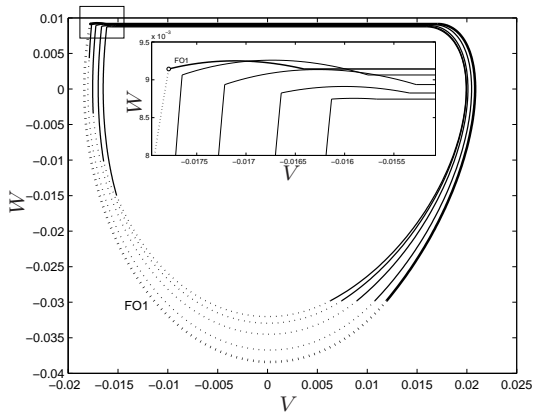


Figure 4.19: Overshooting stick-slip-separation cycles for increasing α until a fly-over happens at FO_1 . The overshooting segments are enlarged.

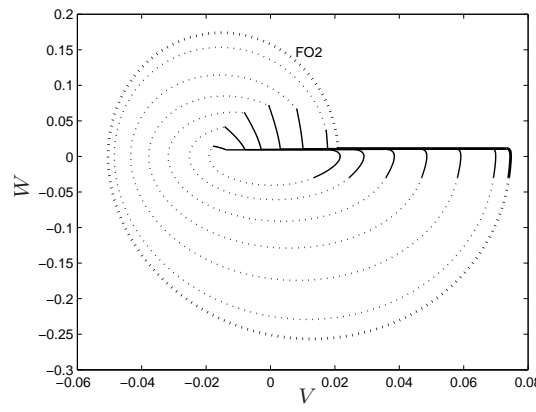


Figure 4.20: Evolution of overshooting stick-slip-separation waves with separated switching up to a second fly-over (FO_2). The result becomes physically infeasible (see Figure 4.22)!

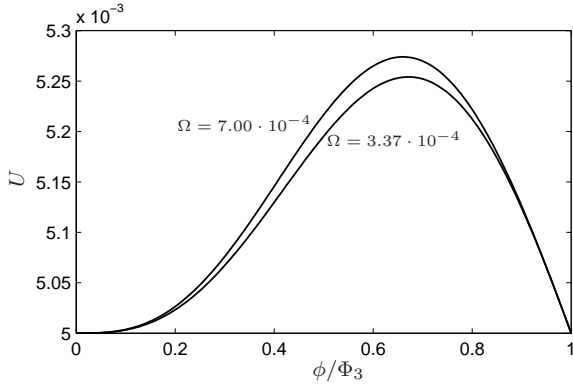


Figure 4.21: Radial displacement U corresponding to Figure 4.15 during separation.

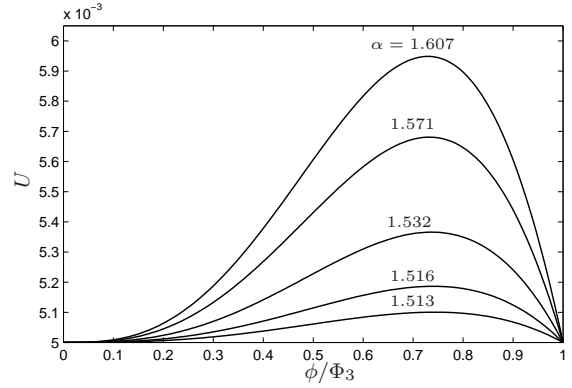


Figure 4.22: Radial displacement U corresponding to Figure 4.20 during separation.

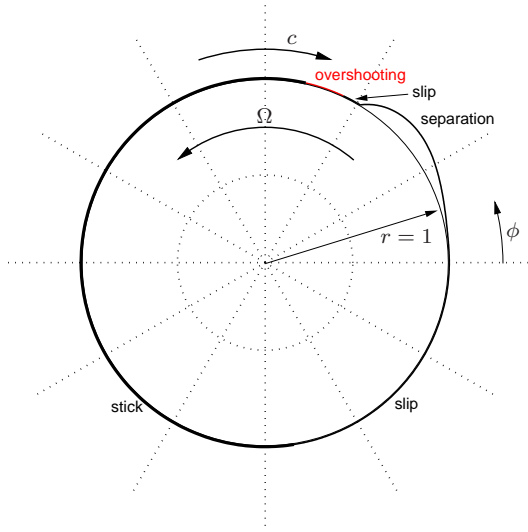


Figure 4.23: Distribution of the radial displacement (scaled!) around the circumference of the shaft showing the different contact zones for an overshooting stick-slip-separation wave corresponding to Figure 4.19 ($\alpha = 1.52$, $\Omega = 0.012$).

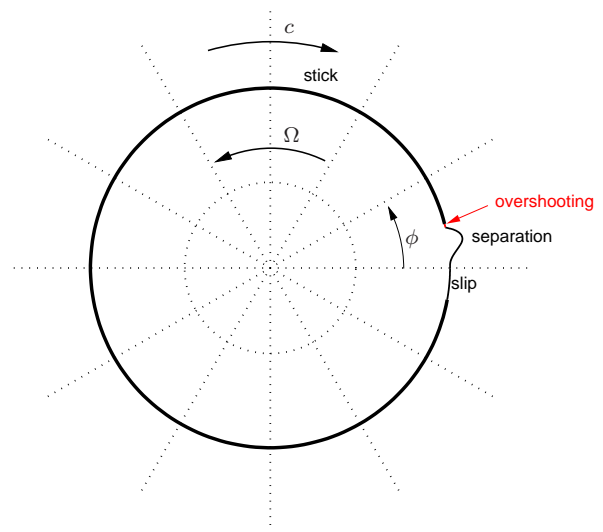


Figure 4.24: Contact zones for an overshooting stick-slip-separation wave with separated switching after a fly-over corresponding to a solution in Figure 4.14 ($\alpha = 0.42$, $\Omega = 5.71 \cdot 10^{-4}$). Bold lines indicate a stick segment.

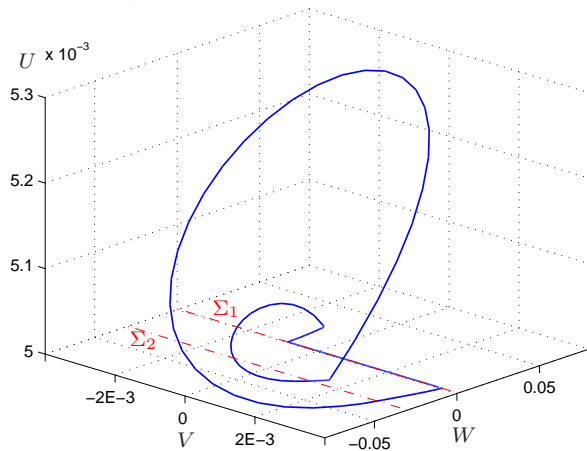


Figure 4.25: Emergence of a secondary separation zone shortly beyond the point PO2 in Figure 4.11 obtained by direct forward integration in the phase space.

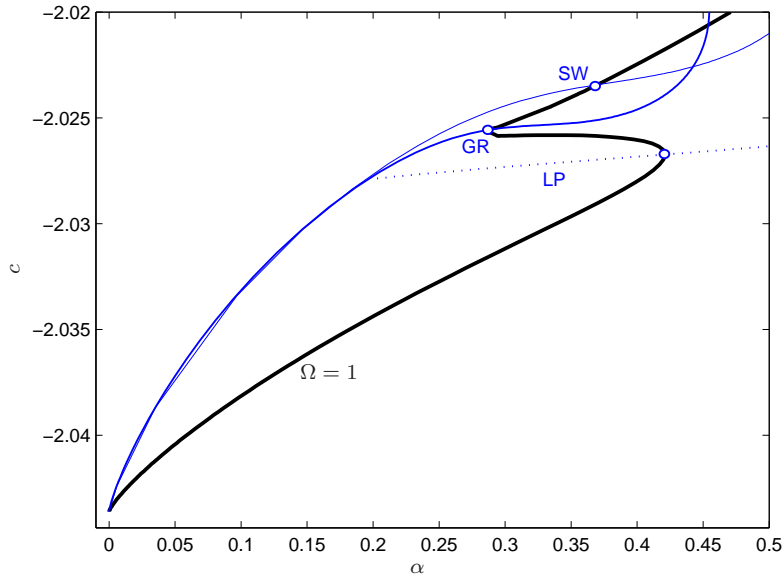


Figure 4.26: Stratification of the parameter space projected into the (α, c) -plane near the grazing bifurcations (GR). The bold curve shows the path of bifurcating slip-separation waves for $\Omega = 1$ depending on α .

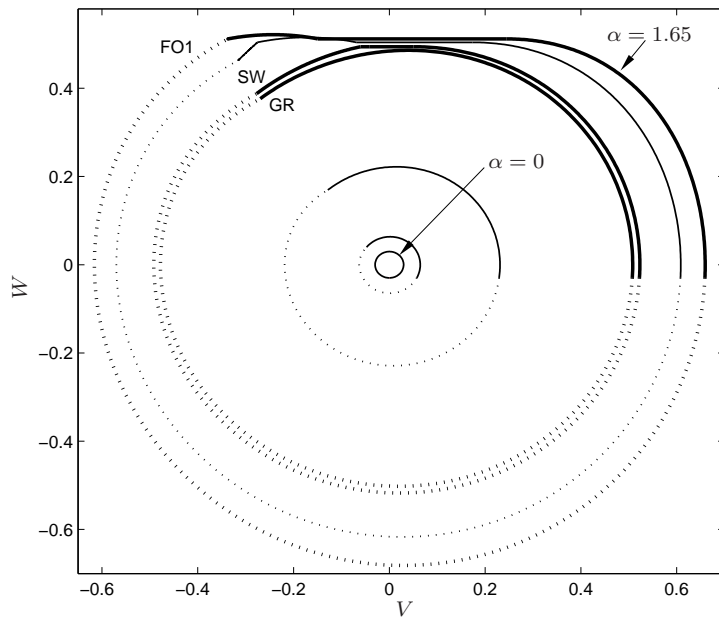
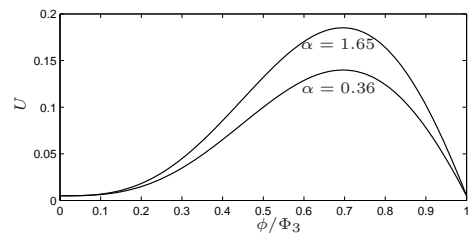


Figure 4.27: Evolution of a slip-separation wave in the phase plane. The grazing (GR), switching (SW), and fly-over (FO1) cycles are highlighted. However, the radial displacements are by far too large (below)!



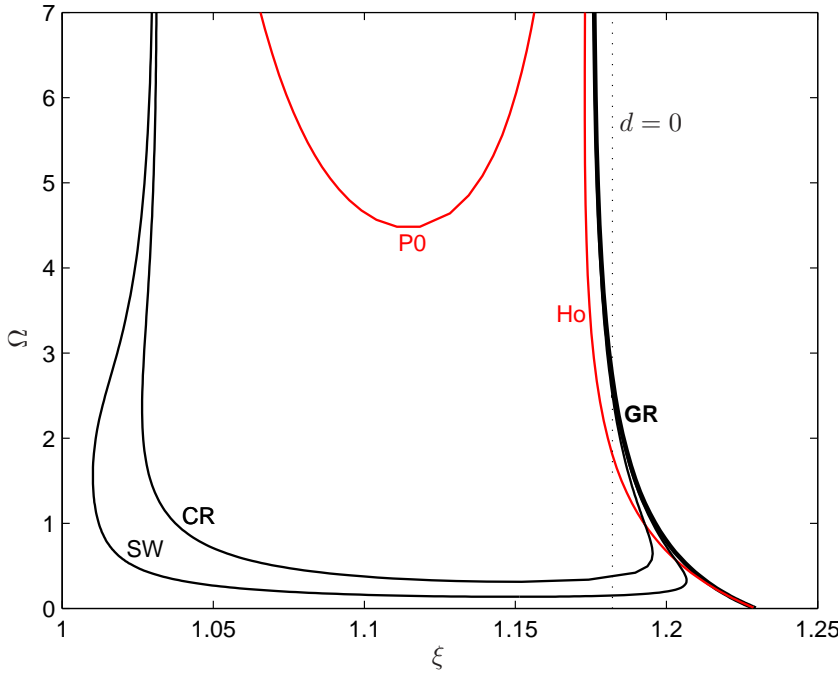


Figure 4.28: Stratification of the parameter space projected into the (ξ, Ω) -plane for $c > 0$, mode 4 and $\alpha = 0.1, \beta = 0.2, \gamma = 0.0615, \delta = 0.005, \nu = 0.3$ showing the loci of Hopf (Ho), grazing (GR), switching (SW), crossing (CR) and separating (P0) bifurcations. The line where $d = 0$ is dotted. Some examples of corresponding solutions are depicted in Figures 4.29-4.34

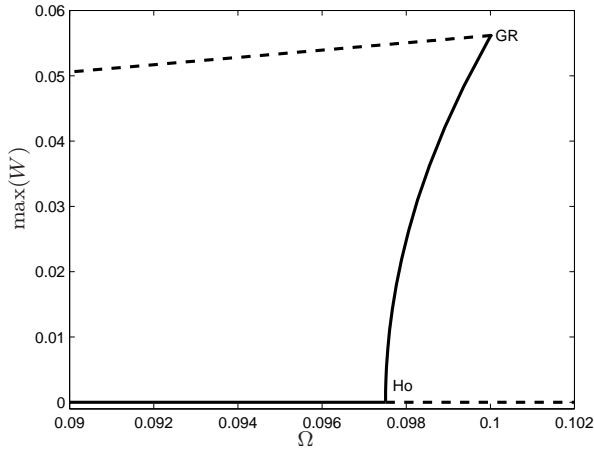


Figure 4.29: Bifurcation diagram of the supercritical Hopf-bifurcation (Ho) and the adjacent grazing bifurcation (GR) in Figure 4.28 at $\xi = 1.22$. Dotted lines indicate instability w.r.t. the phase ϕ .

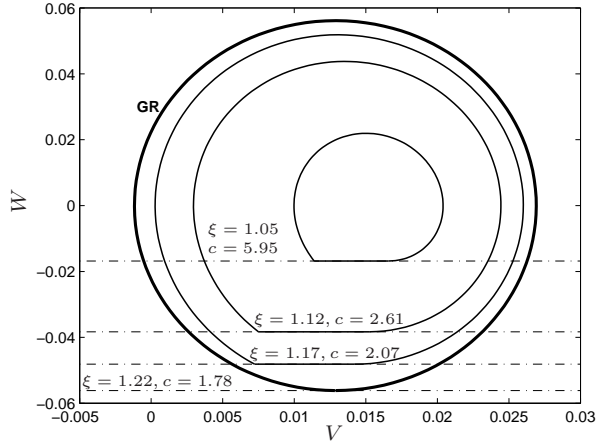


Figure 4.30: Evolution of stick-slip cycles for $\Omega = 0.1, \alpha = 1, c > 0$ for increasing ξ up to the grazing bifurcation at GR.

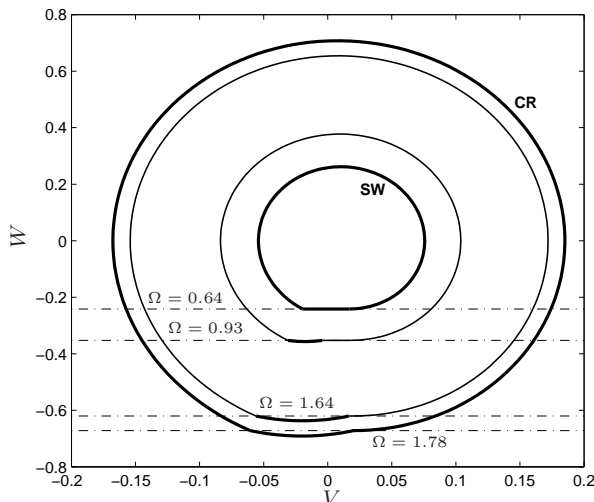


Figure 4.31: Evolution of overshooting stick slip cycles at $\xi = 1.122, \alpha = 1$. The corresponding wave speeds are $c = 2.633, 2.637, 2.643$ and 2.644 for increasing Ω . Bold lines indicate bifurcating solutions and overshooting segments.

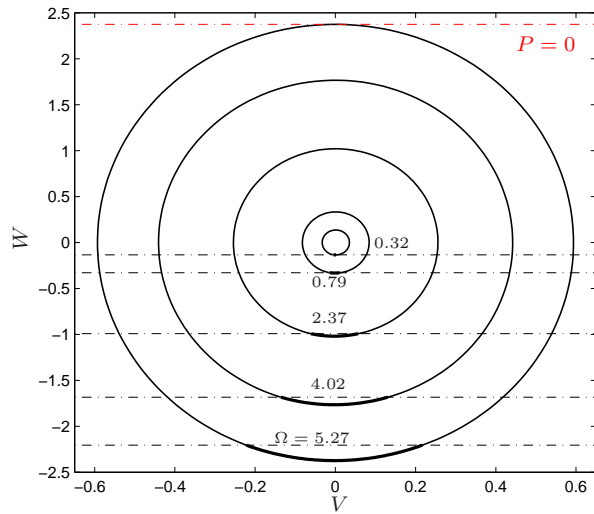


Figure 4.32: Evolution of crossing cycles for $\xi = 1.14, \alpha = 0.1$ increasing Ω . The wave speed remains almost constant at $c \approx 2.388$. Since $d > 0$ the discontinuity where $P = 0$ touches the limit cycle from above.

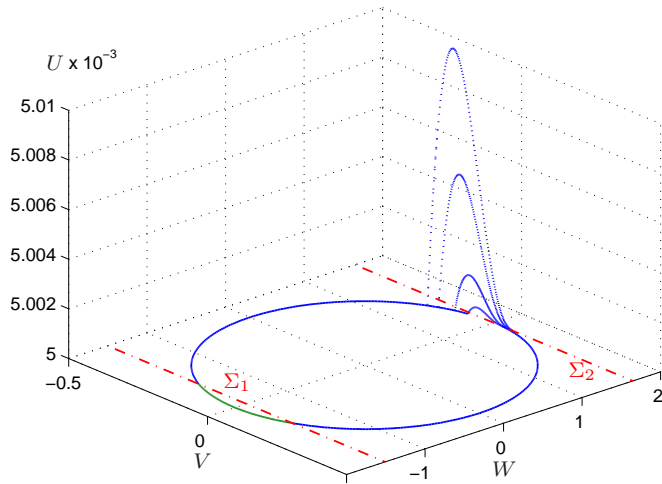


Figure 4.33: Crossing slip-separation cycles emerging after the separating bifurcation (P_0) in Figure 4.28 for $\xi = 1.1$ ($d > 0$) projected into the (U, V, W) phase space. Ω ranges from 4.66 to 4.90, c remains virtually constant at $c \approx 3.097$. The separated segment is dotted, the overshooting part is plotted in green color.

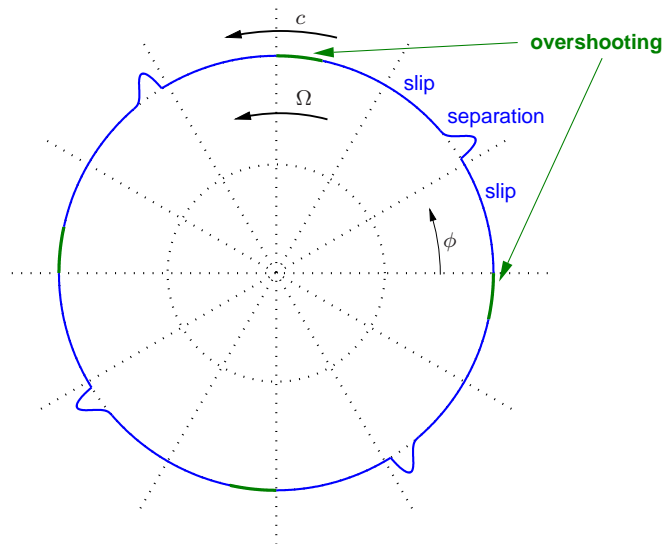


Figure 4.34: Radial displacement of a mode-4 crossing slip-separation wave at $\Omega = 4.9, \xi = 1.1$ corresponding to Figure 4.33 illustrated on the circumference of the shaft. The different contact regimes are indicated by different colors. The displacements during separation are scaled for better visibility.

4.7 Conclusions and Outlook

Originating from KUZNETSOV's classification of non-smooth 1-parameter bifurcations in planar Filippov systems Chapters 3 and 4 were concerned with the application of KUZNETSOV's findings to mechanical systems. Due to the mathematical properties of oscillation equations, where a discontinuity is introduced by friction effects, it could be shown that bifurcations of non-smooth cycles constitute the main mechanism of non-smooth bifurcations in friction oscillators. The simple friction oscillator consisting of an elastically mounted mass on a driving belt served as a descriptive example which exhibits all major types of non-smooth bifurcations that are expected in mechanical 1-degree-of-freedom-systems once it is equipped with a friction law that has decreasing and increasing branches with respect to the relative velocity. Moreover, a concise bifurcation analysis of the simple friction oscillator is still a topic which is treated rather scarcely.

The simple friction oscillator provided a basis for the investigation of an infinite dimensional system, namely a rigid shaft, rotating inside an elastic bush where a diameter mismatch causes a contact pressure. This system – besides friction – includes a second discontinuity due to the possibility of local separation between the shaft and the bush. It has been studied in a 1-mode Galerkin approximation of travelling waves rotating with constant wave speed on the shaft-bush interface. The concept of non-smooth bifurcations allowed an unconventional insight into the formation of different wave forms with varying contact regimes, such as sticking, slipping and separation. We have shown that the existence of pure slip, stick-slip, slip-separation and stick-slip-separation waves, both for negative and positive wave speeds, depends on main system parameters such as the rotation velocity of the shaft, the static coefficient of friction or the size of the bush. The appearance of different types of contact between the shaft and the bush upon the variation of a system parameter constitutes a vivid mechanical interpretation of the concept of non-smooth bifurcations. Although the numerical computations already showed a rich diversity of different solution types, the approximated model was still simple enough to permit theoretical considerations and fortifications of the results.

However, we have not in the least calculated all major modes of travelling waves that may appear. Nevertheless, we take the liberty to conjecture that the basic mechanisms of non-smooth bifurcations of travelling waves have been found so far if we restrict ourselves to the applied approximation. The computation of further bifurcation diagrams for higher modes remains a matter of time and diligence but the solutions are expected to be qualitatively similar to those presented here. It still seems promising to sleuth the solution branch of slow backward mode-1 waves that produced a secondary separation segment in Figures 4.11 and 4.25. To this end, a more refined numerical routine would be necessary since the rather crude method to add new equations for each new segment sooner or later becomes too expensive.

As already mentioned in Section 4.6.3 the major drawback of the preceding calculations is the lack of a reliable method to check the stability of the computed solutions with respect to the original p.d.e. It is felt that further research on this shaft-bush problem has to focus on the question of stability. In connection with stability calculations one would expect to get hold of further bifurcations that have not appeared in the present

analysis, such as Hopf or torus bifurcations of non-smooth waves. First steps have been made in this direction by A. STEINDL, however, the numerical procedure is still too cumbersome to cope with a bigger load of qualitatively different solutions.

Another approach would be to refine the Galerkin approximation and include higher modes, both for the calculation of new solutions and the analysis of their stability. Clearly this would be accompanied by a loss of simplicity of the model but probably this would be the only way to obtain more trustworthy results.

In view of the long-term objective to explain squealing noises let us finally recall the rich bifurcating behavior for backward mode-1 waves in Section 4.6.1 occurring at small rotation velocities, in particular again the branch of solutions near $c = -1$, which means that the waves propagate approximately with the speed of sound in the material. Being imaginative we could think of these solutions having something to do with the occurrence of squealing noises, since it is known from common sense that these noises appear particularly at low velocities, e. g. if we listen to a breaking train in the railway station. However, lots of trains will still have to arrive squealing and squeaking in railway stations before we will definitely know why they squeal and squeak...

Bibliography

- ABADI (2003). *Nonlinear dynamics of self-excitation in autoparametric systems*. ISBN 90-393-3496-X. Phd.-thesis.
- ANDRONOV, A. A., A. A. VITT & S. E. KHAIKIN (1966). *Theory of oscillators*. Dover Publications, New York.
- ARNOLD, V. I. (1978). *Mathematical Methods of Classical Mechanics*. Springer, New York Heidelberg Berlin.
- ARNOLD, V. I. (1983). *Geometrical Methods in the Theory of Ordinary Differential Equations*. Springer, New York Heidelberg Berlin.
- ARONSON, D. G., E. J. DOEDEL & H. G. OTHMER (1987). ‘An analytical and numerical study of the bifurcations in a system of linearly coupled oscillators’. *Physica D* **25**, 20–104.
- ARONSON, D. G., G. B. ERMENTROUT & N. KOPELL (1990). ‘Amplitude response of coupled oscillators’. *Physica D* **41**, 403–449.
- AWREJCEWICZ, J. & C. H. LAMARQUE (2003). *Bifurcation and chaos in nonsmooth mechanical systems*. Number A, Vol. 45 in ‘Nonlinear Science’. World Scientific, New Jersey London Singapore Hong Kong.
- BLEKHMANN, I. I. (1988). *Synchronization in Science and Technology*. ASME Press, New York.
- BLEKHMANN, I. I. (2000). *Vibrational Mechanics*. World Scientific, Singapore New-Jersey Hong-Kong.
- BLEKHMANN, I. I., A. L. FRADOV, H. NIJMEIJER & A. Y. POGROMSKY (1997). ‘On self-synchronization and controlled synchronization’. *Systems & Control Letters* **31**, 299–305.
- BLEVINS, R. D. (1977). *Flow-induced vibration*. Van Nostrand Reinhold Company, London Toronto Melbourne.
- CHAKRABORTY, T. & R. H. RAND (1988). ‘The transition from phase locking to drift in a system of two weakly coupled Van-der-Pol oscillators’. *Int. J. Non-Linear Mechanics* **23**, 369–376.
- CHANDRASEKHAR, S. (1970). *Hydrodynamic and Hydromagnetic Stability*. Dover Publications Inc., New York.

Bibliography

- DERECOLE, F. & Y. KUZNETSOV (2004). *User guide to SlideCont 2.0*. Dept. of Electronics and Information, Politecnico di Milano, Italy; Dept. of Mathematics, Utrecht University, Netherlands.
- DI BERNARDO, M., P. KOWALCZYK & A. NORDMARK (2002). ‘Sliding bifurcations: a novel mechanism for the sudden onset of chaos in dry friction oscillators’. *International Journal of Bifurcation and Chaos* **13**(10), 2935–2948.
- DOEDEL, E. J., A. R. CHAMPNEYS, T. F. FAIRGRIEVE, Y. A. KUZNETSOV, B. SANDSTEDE & X. WANG (1998). *Auto 97: Continuation and bifurcation software for ordinary differential equations*. Concordia University Montreal, Canada.
- ELMER, F. J. (1997). ‘Nonlinear dynamics of dry friction’. *J. Phys. A: Math. Gen.* **30**, 6057–6063.
- FILIPPOV, A. F. (1988). *Differential equations with discontinuous right-hand side*. Kluwer Academic, Dordrecht.
- GALVANETTO, U. & S. BISHOP (1999). ‘Dynamics of a simple damped oscillator undergoing stick-slip vibrations’. *Meccanica* **34**, 337–347.
- GUCKENHEIMER, J. & P. HOLMES (1983). *Nonlinear Oscillations, Dynamical Systems and Bifurcation of Vector Fields*. Springer, New York Heidelberg Berlin.
- HETZLER, H., D. SCHWARZER & W. SEEMANN (2007). ‘Analytical investigation of steady-state stability and Hopf-bifurcations occurring in sliding friction oscillators with application’. *Communications in Nonlinear Science and Numerical Simulation* **12**, 83–99.
- HOLMES, P. J. (1980). Unfolding a degenerate nonlinear oscillator: a codimension two bifurcation. In R. H. G. HELLEMAN (Ed.). ‘Nonlinear Dynamics’. New York Academy of Sciences, New York. pp. 473–488.
- HOLMES, P. J. & D. A. RAND (1978). ‘Bifurcations of the forced Van-der-Pol oscillator’. *Quart. Appl. Math.* **35**, 495–509.
- IBRAHIM, R. A. (1994). ‘Friction-induced vibration, chatter, squeal and chaos. part 1: Mechanics of contact and friction’. *Appl. Mech. Rev.* **47**(7), 209–253.
- KAUDERER, H. (1958). *Nichtlineare Mechanik*. Springer, Berlin Göttingen Heidelberg.
- KERN, G. & A. MAITZ (1998). ‘Self-excited wind induced vibrations and limit cycles in bundled conductors’. *Meccanica* **33**, 243–253.
- KIRCHGRABER, U. & E. STIEFEL (1978). *Methoden der analytischen Störungsrechnung und ihre Anwendungen*. B. G. Teubner, Stuttgart. in German.
- KUNZE, M. & T. KÜPPER (1997). ‘Qualitative bifurcation analysis of a non-smooth friction-oscillator model’. *Z. angew. Math. Phys.* **48**, 87–101.
- KUZNETSOV, Y. A. (1995). *Elements of Applied Bifurcation Theory*. Number 112 in ‘Applied Mathematical Sciences’. Springer, New York Berlin Heidelberg.

Bibliography

- KUZNETSOV, Y. A., S. RINALDI & A. GRAGNANI (2003). ‘One-parameter bifurcations in planar Filippov systems’. *International Journal of Bifurcation and Chaos* **13**(8), 2157–2188.
- LANDA, P. S. (2001). *Regular and Chaotic Oscillations*. Foundations of Engineering Mechanics. Springer, Berlin Heidelberg.
- LEINE, R. I. (2000). Bifurcations in discontinuous mechanical systems of Filippov-type. Ph.D.-thesis. Technische Universiteit Eindhoven. ISBN 90-386-2911-7.
- LEINE, R. I., D. H. VAN CAMPEN, A. DE KRAKER & L. VAN DEN STEEN (1998). ‘Stick-slip vibrations induced by alternate friction models’. *Nonlinear Dynamics* **16**, 41–54.
- LI, Y. & Z. C. FENG (2004). ‘Bifurcation and chaos in friction-induced vibration’. *Communications in Nonlinear Science and Numerical Simulation* **9**(6), 571–581.
- LOW, L. A., P. G. REINHALL & D. W. STORTI (2003). ‘An investigation of coupled Van-der-Pol oscillators’. *J. of Vibration and Acoustics* **125**, 162–169.
- LUO, A. C. J. (2004). ‘A theory for non-smooth dynamic systems on the connectable domains’. *Communications in Nonlinear Science and Numerical Simulation* **10**, 1–55.
- LUO, A. C. J. (2007). ‘On flow switching bifurcations in discontinuous dynamical systems’. *Communications in Nonlinear Science and Numerical Simulation* **12**(1), 100–116.
- MAGNUS, K. & K. POPP (2002). *Schwingungen*. 6 ed. Teubner, Stuttgart Leipzig Wiesbaden.
- MOIROT, F. & Q. S. NGUYEN (2002). Some examples of friction-induced vibrations and instabilities. In J. A. C. MARTINIS & M. RAOUS (Eds.). ‘Friction and Instabilities’. Springer, Wien New York. pp. 137–178.
- MOIROT, F., Q.-S. NGUYEN & A. OUESLATI (2002). ‘An example of stick-slip and stick-slip-separation waves’. *European Journal of Mechanics A/Solids* **22**, 107–118.
- NGUYEN, Q.-S. (2003). ‘Instability and friction’. *C. R. Mecanique* **331**, 99–112.
- NGUYEN, Q. S., A. OUESLATI, A. STEINDL, A. TEUFEL & H. TROGER (2007). ‘Travelling interface waves in a brake-like system under unilateral contact and Coulomb’s friction’. *Compte Rendus Mecanique* **333**, to appear.
- OBERLE, H. H., W. GRIMM & E. BERGER (1985). *BNDSCO, Rechenprogramm zur Lösung beschränkter optimaler Steuerungsprobleme, User Manual, TUM-M8509*. Math. Inst. TU-München.
- PIKOVSKY, A., M. ROSENBLUM & J. KURTHS (2001). *Synchronization*. Number 12 in ‘Cambridge Nonlinear Science Series’. Cambridge University Press.

Bibliography

- RAND, R. H. & P. J. HOLMES (1980). ‘Bifurcation of periodic motions in two weakly coupled Van-der-Pol oscillators’. *Int. J. Non-Linear Mechanics* **15**, 387–399.
- SANDERS, J. A. & F. VERHULST (1985). *Averaging Methods in Nonlinear Dynamical Systems*. Springer, New York Berlin Heidelberg Tokyo.
- SETHNA, P. R. (1967). ‘An extension of the method of averaging’. *Quarterly of Applied Mathematics* **XXV**(2), 205–211.
- SETHNA, P. R. (1995). ‘On averaged and normal form equations’. *Nonlinear Dynamics* **7**, 1–10.
- SEYDEL, R. (1994). *Practical bifurcation and stability analysis*. Springer, New York Berlin Heidelberg.
- SHILNIKOV, L. P., A. L. SHILNIKOV, D. V. TURAEV & L. O. CHUA (1998). *Methods of Qualitative Theory in Nonlinear Dynamics*. Vol. 1. World Scientific, Singapore New-Jersey Hong-Kong.
- SHILNIKOV, L. P., A. L. SHILNIKOV, D. V. TURAEV & L. O. CHUA (2001). *Methods of Qualitative Theory in Nonlinear Dynamics*. Vol. 2. World Scientific, Singapore New-Jersey Hong-Kong.
- SMIRNOW, W. I. (1967). *Lehrgang der höheren Mathematik*. Vol. III, 2. VEB Detuscher Verlag der Wissenschaften, Berlin.
- STEINDL, A. (2006). ‘Bifurcations of stick-slip-separation waves in a brake-like system’. *Proc. Appl. Math. Mech.* **6**, 337–338.
- STORTI, D. W. & R. H. RAND (1982). ‘Dynamics of two strongly coupled Van-der-Pol oscillators’. *Int. J. Non-Linear Mechanics* **17**, 143–152.
- STRIBERSKY, A. & H. TROGER (1987). ‘Stabilitätsverlust einer Gleichgewichtslage eines gedämpften Schwingungssystems mit zwei Paaren rein imaginärer Eigenwerte’. *ZAMM* **67**, 151–153.
- TAKENS, F. (1974). ‘Singularities of vector fields’. *Publ. Math. IHES* **43**, 47–100.
- TEUFEL, A., A. STEINDL & H. TROGER (2003). Synchronization of two flow excited pendula. In J. AWREJCEWICS, A. OWCZAREK & J. MROZOWSKI (Eds.). ‘Proceedings of the 7th conference on dynamical systems, theory and applications’. Vol. 1. Lodz, Poland. pp. 239–246.
- TEUFEL, A., A. STEINDL & H. TROGER (2006a). Rotating slip stick separation waves. In ‘IUTAM Symposium on dynamics and control of nonlinear systems with uncertainty’. Springer. pp. 257–267.
- TEUFEL, A., A. STEINDL & H. TROGER (2006b). ‘Synchronization of two flow excited pendula’. *Communications in Nonlinear Science and Numerical Simulation* **11**, 577–594.

Bibliography

- TROGER, H. & A. STEINDL (1991). *Nonlinear Stability and Bifurcation Theory*. Springer, Wien New York.
- VERHULST, F. (1990). *Nonlinear Differential Equations and Dynamical Systems*. Springer, Berlin Heidelberg.